Radio Science Bulletin

ISSN 1024-4530

INTERNATIONAL
UNION OF
RADIO SCIENCE

UNION
RADIO-SCIENTIFIQUE
INTERNATIONALE

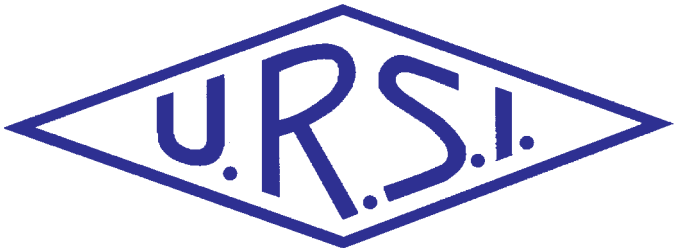

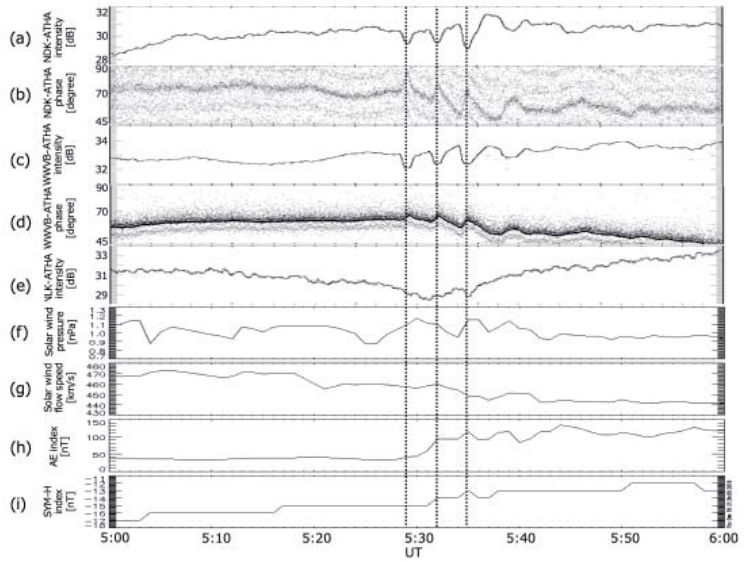

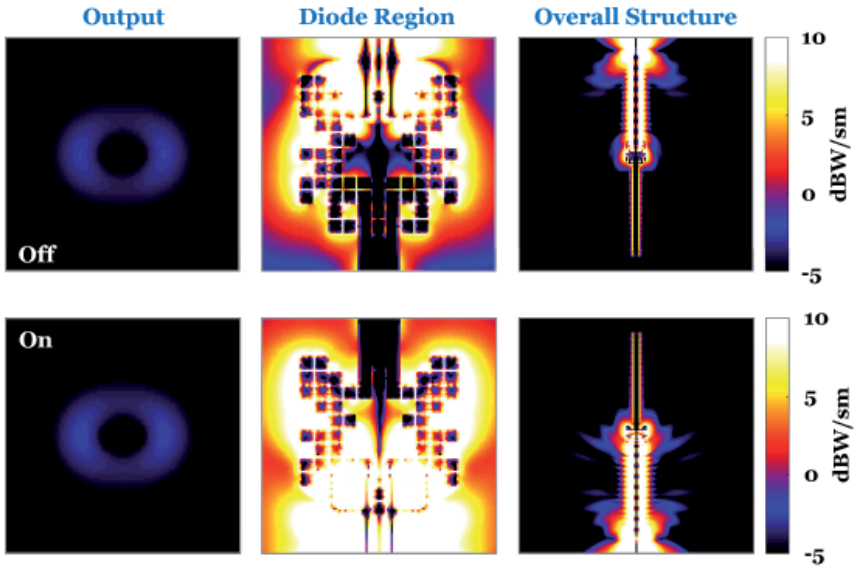

Vol. 2020, No. 372
March 2020

URSI, c/o Ghent University (INTEC)
Technologiepark - Zwijnaarde 126, B-9052 Gent (Belgium)

Contents

Radio Science Bulletin Staff 3
URSI Officers and Secretariat 6
Editor's Comments 8
Introduction to the URSI-JRSM 2019 SPC Special Issue 10
ASIC Waveform Receiver with Improved Environmental Tolerance for Probing Space Plasma Waves in Environments with High Radiation and Wide Temperature Variation 12
Performance Improvement of Resonator-Coupled Wireless Power Transfer System Using Dual-Spiral Resonator with Angular Misalignments 22
ULF Modulation of Energetic Electron Precipitation Observed by VLF/LF Radio Propagation 29
Et Cetera 41
Book Review 42
Solution Box 43
Announcement of a Commission E corner in the Radio Science Bulletin 49
Ethically Speaking 50
Historical Corner Column 52
Telecommunications Health and Safety 56
European School of Antennas 2021 60
Women in Radio Science 61
IEEE RADIO 2019 64
URSI Accounts 2019 66
EUCAP 2021 70
URSI Conference Calendar 72
Information for Authors 74
Become An Individual Member of URSI 75

Cover: (top) The first observational evidence of ULF modulation of VLF/LF radio-frequency waves propagating through the D region of the ionosphere. Periodic oscillations in intensities and phase of the VLF/LF transmitter signals in North America during the substorm of June 4, 2017: (a) NDK-ATHA intensity, (b) NDK-ATHA phase, (c) WWVB-ATHA intensity, (d) WWVB-ATHA phase, (e) NLK-ATHA intensity, (f) solar wind speed, (g) solar wind dynamic pressure, (h) AE index, and (i) SYM-H index. See the paper by Takuya Miyashita et al. (bottom) The results of an optimization to obtain unidirectional transmission characteristics in a structure involving nano-particles with a diode. Vertical-line asymmetry was enforced in the diode design. The structure consisted of 61 nano-cubes. See the paper in the Solution Box column by Gökhan Karaova, Tuna Atmaz, and Özgür Ergül.

The International Union of Radio Science (URSI) is a foundation Union (1919) of the International Council of Scientific Unions as direct and immediate successor of the Commission Internationale de Télégraphie Sans Fil which dates from 1914.

Radio Science Bulletin Staff

Editor

W. R. Stone
Stoneware Limited
840 Armada Terrace
San Diego, CA 92106, USA
Tel: +1-619 222 1915, Fax: +1-619 222 1606
E-mail: r.stone@ieee.org

Editor-in-Chief

P. Van Daele
URSI Secretariat
Ghent University - INTEC
Technologiepark - Zwijnaarde 126
B-9052 Gent, BELGIUM
Tel: +32 9-264 33 20, Fax: +32 9-264 42 88
E-mail: Pet.VanDaele@UGent.be

Production Editor

I. Lievens
URSI Secretariat / Ghent University - INTEC
Technologiepark - Zwijnaarde 126
B-9052 Gent, BELGIUM
Tel: +32 9-264.33.20, Fax: +32 9-264.42.88
E-mail: ingeursi@ugent.be, info@ursi.org

Senior Associate Editors

A. Pellinen-Wannberg
Department of Physics
Umea University
BOX 812
SE-90187 Umea, SWEDEN
Tel: +46 90 786 74 92, Fax: +46 90 786 66 76
E-mail: asta.pellinen-wannberg@umu.se

O. Santolik
Institute of Atmospheric Physics
Academy of Sciences of the Czech Republic
Bocni II
1401, 141 31 Prague 4, CZECH REPUBLIC
Tel: +420 267 103 083, Fax +420 272 762 528
E-mail os@ufa.cas.cz, santolik@gmail.com

Associate Editors, Commissions

Commission A

Nuno Borges Carvalho
Instituto de Telecomunicaçoes
Universidade de Aveiro, Campus Universitario
3810-193 Aveiro, Portugal
Tel: +351 234377900, Fax: +351 234377901
E-mail: nbcarvalho@ua.pt

Pedro Miguel Cruz
Rua Sao Sebastiao
n34 Hab 33
4520-250 Santa Maria da Feira, Aveiro, PORTUGAL
Tel: +351 225898410
E-mail: pedro.cruz@controlar.pt

Tian Hong Loh
National Physical Laboratory
Hampton Road
Teddington TW11 0LW, United Kingdom
Tel: +44 020 8943 6508
E-mail: tian.loh@npl.co.uk

Nosherwan Shoaib
School of Electrical Engineering and Computer Science (SEECS)
National University of Sciences and Technology (NUST)
NUST Campus H-12, Islamabad, Pakistan
Tel: 051 90852561
E-mail: nosherwan.shoaib@seccs.edu.pk

Commission B

Andrea Michel
Department of Information Engineering
Università di Pisa
Pisa, Italy
E-mail: andrea.michel@iet.unipi.it

John Volakis
College of Engineering and Computing
Florida International University
10555 W. Flagler Street, EC2477
Miami, FL 33174, USA
Tel: +1 305 348 2807
E-mail: jvolakis@fiu.edu

Commission C

Yves Louet
CS 47601, SUPELEC
Avenue de Boulaie
F-35576 Cesson-Sévigné, France
Tel: +33 2 99 84 45 34, Fax: +33 2 99 84 45 99
E-mail: yves.louet@supelec.fr

Commission D

Naoki Shinohara
RISH
Kyoto University
Uji 611-0011, Japan
Tel: +81 774 38 3807 Fax: +81 774 31 8463
E-mail: shino@rish.kyoto-u.ac.jp

Commission E

Virginie Deniau
IFSTTAR
20. rue Elisée Reclus BP 70317
F-59666 Villeneuve d'Ascq Cedex, France
Tel: +33 03 20438991
E-mail: virginie.deniau@ifsttar.fr

Commission F

Haonan Chen
Earth System Research lab, Physical Sciences Division
NOAA
325 Broadway, Boulder, CO 80305, USA
Tel: +1 303 497 4616
E-mail: haonan.chen@noaa.gov

Tullio Tanzi
Télécom ParisTech - LabSoC, c/o EURECOM
Campus SophiaTech Les Templiers
450 route des Chappes 06410 Biot, FRANCE
Tel: +33 0 4 93008411, Fax: 33 0 493008200
E-mail: tullio.tanzi@telecom-paristech.fr

Commission G

Giorgiana De Franceschi
Dept. Arenonomy, Istituto Nazionale di Geofi sica e Vulcanology
Via di Vigna, Murata 605
00 143 Roma, Italy
Tel: +39 06 51860307, Fax: +39 06 51860397
E-mail: giorgiana.defranceschi@ingv.it

Commission H

Jyrki Manninen
Sodankylä Geophysical Observatory
Tähteläntie 62
FIN-99600 Sodanskylä, Finland
Tel: +358 400 151503, Fax +358 16 610248
E-mail: Jyrki.Manninen@oulo.fi

Commission J

Jacob W. Baars
Max Planck Institute for Radio Astronomy
Auf dem Hügel 69
53121 Bonn, Germany
Tel: +49 228 525303
E-mail: jacobbaars@arcor.de

Commission K

Kensuke Sasaki
Applied EM Research Institute
NICT
Koganei, Tokyo, Japan
E-mail: k_sasaki@nict.go.jp

Associate Editors, Columns

Book Reviews

G. Trichopoulos
Electrical, Computer & Energy Engineering ISTB4 555D
Arizona State University
781 E Terrace Road, Tempe, AZ, 85287 USA
Tel: +1 (614) 364-2090
E-mail: gtrichop@asu.edu

Historical Papers

J. D. Mathews
Communications and Space Sciences Lab (CSSL)
The Pennsylvania State University
323A, EE East
University Park, PA 16802-2707, USA
Tel: +1(814) 777-5875, Fax: +1 814 863 8457
E-mail: JDMathews@psu.edu

Et Cetera

T. Akgül
Dept. of Electronics and Communications Engineering
Telecommunications Division
Istanbul Technical University
80626 Maslak Istanbul, TURKEY
Tel: +90 212 285 3605, Fax: +90 212 285 3565
E-mail: tayfunakgul@itu.edu.tr.

Women in Radio Science

A. Pellinen-Wannberg
Department of Physics and Swedish Institute of Space Physics
Umeå University
S-90187 Umeå, Sweden
Tel: +46 90 786 7492
E-mail: asta.pellinen-wannberg@umu.se

Ethically Speaking

R. L. Haupt
Colorado School of Mines
Brown Building 249
1510 Illinois Street, Golden, CO 80401 USA
Tel: +1 (303) 273 3721
E-mail: rhaupt@mines.edu

A. J. Shockley
E-mail: aj4317@gmail.com

Solution Box

Ö. Ergül
Department of Electrical and Electronics Engineering
Middle East Technical University
TR-06800, Ankara, Turkey
E-mail: ozgur.ergul@eee.metu.edu.tr

Telecommunications Health & Safety

J. C. Lin
University of Illinois at Chicago
851 South Morgan Street, M/C 154
Chicago, IL 60607-7053 USA
Tel: +1 312 413 1052, Fax: +1 312 996 6465
E-mail: lin@uic.edu

Historical Column

G. Pelosi
Department of Information Engineering
University of Florence
Via di S. Marta, 3, 50139 Florence, Italy
E-mail: giuseppe.pelosi@unifi.it

Early Career Representative Column

S. J. Wijnholds
Netherlands Institute for Radio Astronomy
Oude Hoogeveensedijk 4
7991 PD Dwingeloo, The Netherlands
E-mail: wijnholds@astron.nl

Education Column

Madhu Chandra
Microwave Engineering and Electromagnetic Theory
Technische Universität Chemnitz
Reichenhainerstrasse 70
09126 Germany
E-mail: madhu.chandra@etit.tu-chemnitz.de

URSI Officers and Secretariat

Current Officers triennium 2017-2020

President

M. Ando
Senior Executive Director
National Institute of Technology
701-2, Higashi Asakawa, Hachioji,
Tokyo 193-0834, Japan
Tel:+81-42-662-3123,
Fax: +81-42-662-3131
E-mail: ando@kosen-k.go.jp,
mando@antenna.ee.titech.ac.jp

Vice President

O. Santolik
Institute of Atmospheric Physics
Electrical Eng. Dept
Academy of Sciences of the Czech Republic
Bocni II, 1401
141 31 Prague 4, CZECH REPUBLIC
Tel: +420 267 103 083
Fax: 420 272 762 528
E-mail: os@ufa.cas.cz, santolik@gmail.com

Past President

P. S. Cannon
Gisbert Kapp Building
University of Birmingham
Edgbaston , Birmingham, B15 2TT,
UNITED KINGDOM
Tel: +44 (0) 7990 564772
Fax: +44 (0)121 414 4323
E-mail: p.cannon@bham.ac.uk

Vice President

A. Sihvola
Electronic Science Department
Aalto University
School of Electrical Engineering
PO Box 13000
FI-00076 AALTO
FINLAND
Tel: +358 50 5871286
E-mail: Ari.Sihvola@aalto.fi

Secretary General

P. Van Daele
URSI Secretariat
Ghent University - INTEC
Technologiepark - Zwijnaarde 126
B-9052 Gent
BELGIUM
Tel: +32 9-264 33 20
Fax: +32 9-264 42 88
E-mail: Pet.VanDaele@UGent.be

Vice President

P. L. E. Uslenghi
Dept. of ECE (MC 154)
University of Illinois at Chicago 851
S. Morgan Street
Chicago, IL 60607-7053
USA
Tel: +1 312 996-6059
Fax: +1 312 996 8664
E-mail: uslenghi@uic.edu

Vice President

W. Baan
Astron
Asserweg 45
9411 LP Beilen
THE NETHERLANDS
Tel: +31 521-595 773/100
Fax: +31 521-595 101
E-mail: baan@astron.nl

URSI Secretariat

Secretary General

P. Van Daele
URSI Secretariat
Ghent University - INTEC
Technologiepark - Zwijnaarde 126
B-9052 Gent
BELGIUM
Tel: +32 9-264 33 20
Fax: +32 9-264 42 88
E-mail: Pet.VanDaele@UGent.be

Assistant Secretary General AP-RASC

K. Kobayashi
Dept. of Electr and Commun. Eng,
Chuo University
1-13-27 Kasuga, Bunkyo-ku
Tokyo, 112-8551, JAPAN
Tel: +81 3 3817 1846/69
Fax: +81 3 3817 1847
E-mail: kazuya@tamacc.chuo-u.ac.jp

Assistant Secretary General

Stefan J. Wijnholds
Netherlands Institute for
Radio Astronomy
Oude Hoogeveensedijk 4
7991 PD Dwingeloo
The Netherlands
E-mail: wijnholds@astron.nl

Executive Secretary

I. Heleu
URSI Secretariat
Ghent University - INTEC
Technologiepark - Zwijnaarde 126
B-9052 Gent
BELGIUM
Tel. +32 9-264.33.20
Fax +32 9-264.42.88
E-mail info@ursi.org

Assistant Secretary General Publications & GASS

W. R. Stone
840 Armada Terrace
San Diego, CA 92106
USA
Tel: +1-619 222 1915
Fax: +1-619 222 1606
E-mail: r.stone@ieee.org

Administrative Secretary

I. Lievens
URSI Secretariat
Ghent University - INTEC
Technologiepark - Zwijnaarde 126
B-9052 Gent
BELGIUM
Tel: +32 9-264.33.20
Fax: +32 9-264.42.88
E-mail: ingeursi@ugent.be

Editor's Comments

W. Ross Stone
Stoneware Limited
840 Armada Terrace
San Diego, CA 92106, USA
Tel: +1-619 222 1915, Fax: +1-619 222 1606
E-mail: r.stone@ieee.org

Special Issue on the URSI-JRSM 2019 Student Paper Competition

This issue contains the three top prize-winning papers from the Student Paper Competition held as part of the 2019 URSI Japan Radio Science Meeting (URSI-JRSM 2019). The conference was held at the University of Electro-Communications (UEC), Tokyo, Japan, on September 5-6, 2019. The guest editors for this section of this issue were Satoshi Yagitani and Shinichiro Ohnuki, respectively the General Chair and the Technical Program Chair for URSI-JRSM 2019. Their efforts are greatly appreciated. They have provided a separate introduction to the special issue.

Observations of plasma waves in the Earth's ionosphere have to be made in an environment that has high radiation levels and a very wide range of temperatures. This presents significant challenges to the electronics used for such observations. The paper by Yuya Tokunaga, Mitsunori Ozaki, Satoshi Yagitani, Hiroki Koji, Daisuke Yonetoku, Takahiro Zushi, and Hirotsugu Kojima describes the design and implementation of a new application-specific integrated circuit (ASIC) waveform receiver tailored to meet these challenges. The paper describes how a conventional receiver circuit was modified to harden it against the space radiation levels and to provide compensation for the wide temperature variations. The paper is interesting not only for the quite useful design that was obtained, but also for the insight into how that design was developed.

Wireless power-transfer systems are used to couple power to and charge a variety of appliances and electronic devices. The paper by Nur Syafiera Azreen Norodin and Masashi Hotta considers a specific category of such systems, based on the use of coupled spiral resonators on the power source and the device receiving the power. Such resonator-coupled wireless power transfer systems have significant advantages, but quickly lose power-transfer efficiency if there is an angular misalignment between the resonators. The authors showed that adding an appropriate amount of axial displacement to the receiving unit can compensate for the losses due to such misalignments.

The paper by Takuya Miyashita, Hiroyo Ohya, Fuminori Tsuchiya, Asuka Hirai, Mitsunori Ozaki, Kazuo Shiokawa, Yoshizumi Miyoshi, Nozomu Nishitani, Mariko Teramoto, Martin Connors, Simon G. Shepherd, Yoshiya Kasahara, Atsushi Kumamoto, Masafumi Shoji, Iku Shinohara, Hiroyuki Nakata, and Toshiaki Takano reports the first observational evidence of ULF modulation of VLF/LF radio-frequency waves propagating through the D region of the ionosphere. Oscillations in intensities and phases of the signals from three transmitters in the US were observed at a location in Canada during a substorm in June 2017. Correlation of the observations with results from the SuperDARN HF radars suggested that energetic electron precipitation over two of the US-Canada paths was modulated by the ULF waves. The paper provides an in-depth analysis of the results and explores possible mechanisms for their cause.

Our Other Contributions

In the Book Review column, George Trichopoulos has provided us with a review of a book on the life of Elizabeth Alexander. She was a scientist and educator who lived and worked in India, Singapore, Malaysia, New Zealand, Australia, and Nigeria prior to and during the second World War. The review was written by Niru Nahar, who also provides her own personal observations on the social and political background of the book.

Tayfun Akgul supplies us with some timely perspectives on life in the pandemic in his Et Cetera column.

Randy Haupt and Amy Shockley take a look at the roles ethics and reprioritization play in our lives in their Ethically Speaking column. They raise some issues that are certainly appropriate to think about in these times of coronavirus.

In Giuseppe Pelosi's Historical Corner, Antonio Savini provides a fascinating look at the historical development of what is usually called the Seebeck Effect. This is thermoelectricity, in which a temperature difference across a circuit composed of two different metals (or other materials) produces an electric current. As the author points out, the effect was actually first observed by Alessandro Volta. I think you'll particularly enjoy the quotations from the original literature in the article.

Özgür Ergül's Solution Box column has considered the computational challenges of nano-optical structures in several previous columns. In the column in this issue, Gökhan Karaova, Tuna Atmaz, and Özgür Ergül look at nano-optical diodes. These are computationally designed using a grid of nano-particles and keeping or removing particles until the desired operating properties are obtained. Doing this for a design that involved a highly nonlinear structure such as a diode presented interesting computational challenges.

In his Telecommunications Health and Safety column, Jim Lin examines some strange reports that tried to link the coronavirus to 5G telecommunications. He also looks at some of the other possible health concerns related to 5G technology.

Hedy Lamarr is well known as an actress. What is perhaps less well know is that she and a show-business musician, George Antheil, invented and patented the concept of frequency-hopping spread spectrum communications. Karl-Arne Markström tells the story of this in Asta Pellinen Wannberg's Women in Radio Science column.

URSI XXXIVth GASS

The URSI XXXIVth General Assembly and Scientific Symposium will be held August 28 - September 4, 2021, at the Sapienza Faculty of Engineering, Sapienza University, Rome, Italy. The deadline for paper submission is January 31, 2021. Further details can be found at www.URSI2021.org.

I hope this finds you healthy and safe, and coping well with the coronavirus pandemic. My best wishes that you and your loved ones remain so.

Introduction to the URSI-JRSM 2019 Student Paper Competition Special Issue

This special issue is a collection of papers by university students who successfully applied for the Student Paper Competition organized at the 2019 URSI Japan Radio Science Meeting (URSI-JRSM 2019). The conference was held at the University of Electro-Communications (UEC), Tokyo, Japan, on September 5-6, 2019 (http://www.ursi.jp/jrsm2019/).

The URSI Japan Radio Science Meeting (URSI-JRSM) is the URSI conference organized by the Japan National Committee of URSI (JNC-URSI). The URSI-JRSM provides a regional scientific forum for radio scientists and engineers in Japan and the Asian region. The objective of the meeting is to review current research trends, present new discoveries, and make plans for future research and special projects in all areas of radio science. A particular emphasis is placed on enhancing the visibility of URSI in the Asian countries and encouraging young scientists to contribute to various URSI activities.

The first URSI-JRSM was successfully held in Tokyo, Japan, in September 2014. A one-day program was organized with keynote lectures and invited talks, including the topics covered by URSI Commissions A through K. The second URSI-JRSM was also held in Tokyo, Japan, September 3 and 4, 2015.The conference was successful, with 132 participants, and 74 papers (14 oral and 60 poster) being presented. The Student Paper Competition (SPC) was organized and the papers by the three SPC finalists, awarded the first, second, and third prizes, were published in the "Special Issue of the URSI-JRSM 2015 Student Paper Competition" in the March 2016 issue of the *Radio Science Bulletin*.

The 2019 URSI-Japan Radio Science Meeting (URSI-JRSM 2019) is the third URSI-JRSM. It had a scientific program consisting of keynote and invited lectures by outstanding scientists, and oral and poster sessions for contributed papers. This conference was sponsored by the Institute of Electronics, Information and Communication Engineers (IEICE), and technically supported by URSI. It was held in cooperation with the Science Council of Japan, Japan Geoscience Union, Society of Atmospheric Electricity of Japan, the Astronomical Society of Japan, the Institute of Electrical Engineers of Japan, the Laser Society of Japan, and the Remote Sensing Society of Japan. The subject areas of URSI-JRSM 2019 were broad, covering URSI Commissions A through K. Sessions consisted of a keynote lecture, ten invited lectures from the ten URSI Commissions, as well as 75 oral and 78 poster presentations. Part of the topics in the oral sessions treated the history and perspective of radio science research in Japan at this year's opportunity of the

Figure 1. The URSI-JRSM 2019 SPC finalists (l-r) Prof. Satoshi Yagitani, URSI-JRSM 2019 General Chair; Mr. Yuya Tokunaga, SPC First Prize winner; Ms. Nur Syafiera Azreen Norodin, SPC Second Prize winner; Mr. Takuya Miyashita, SPC Third Prize winner; Prof. Shinichiro Ohnuki, URSI-JRSM 2019 Technical Program Committee Chair.

centennial anniversary of URSI. A total of 232 scientists and engineers attended from three countries. A technical tour was organized for participants to explore the University of Electro-Communications (UEC) Communication Museum, where they got a better understanding of the history and development of radio science and technology through the exhibition of historical equipment and documents related to education and research at UEC.

The Student Paper Competition (SPC) was again organized in URSI-JRSM 2019 for full-time university students in a degree program, and was financially supported by URSI. A total of seven students applied for the SPC program. On the first day of the conference, September 5, 2019, the URSI-JRSM 2019 Technical Program Committee selected three SPC finalists based on the applicants' full-length papers and poster presentations. All of the three SPC finalists subsequently orally presented their papers at the SPC special session held on the second day of the conference, September 6, 2019. After careful consideration, the URSI-JRSM 2019 Technical Program Committee decided on the following ranking:

- First Prize: Yuya Tokunaga, Kanazawa University, Japan
- Second Prize: Nur Syafiera Azreen Norodin, Yamaguchi University, Japan
- Third Prize: Takuya Miyashita, Chiba University, Japan

These three winners received prizes (certificates and prize money) at the SPC Award Ceremony held during the URSI-JRSM 2019 Closing Ceremony on the second day of the conference. All the three SPC finalists are shown in Figure 1.

The following three papers by the SPC finalists appear in this special issue of the *Radio Science Bulletin*:

1. "ASIC Waveform Receiver with Improved Environmental Tolerance for Probing Space Plasma Waves in Environments with High Radiation and Wide Temperature Variation"
   Yuya Tokunaga, Mitsunori Ozaki, Satoshi Yagitani, Hiroki Koji, Daisuke Yonetoku, Takahiro Zushi, and Hirotsugu Kojima

2. "Performance Improvement of Resonator-Coupled Type Wireless Power Transfer System Using Dual-Spiral Resonator with Angular Misalignments"
   Nur Syafiera Azreen Norodin and Masashi Hotta

3. "ULF Modulation of Energetic Electron Precipitation Observed by VLF/LF Radio Propagation"
   Takuya Miyashita, Hiroyo Ohya, Fuminori Tsuchiya, Asuka Hirai, Mitsunori Ozaki, Kazuo Shiokawa, Yoshizumi Miyoshi, Nozomu Nishitani, Mariko Teramoto, Martin Connors, Simon G. Shepherd, Yoshiya Kasahara, Atsushi Kumamoto, Masafumi Shoji, Iku Shinohara, Hiroyuki Nakata, and Toshiaki Takano

We are happy that the SPC program at URSI-JRSM 2019 was successful. This success was mainly due to the efforts of the URSI-JRSM 2019 Technical Program Committee. We are very thankful to the members of the committee for their hard work during the selection process. Thanks are also extended to URSI for its financial support for running the program. Finally, we would like to express our appreciation to the SPC finalists who contributed to this special issue.

Guest Editors:
Satoshi Yagitani
URSI-JRSM 2019General Chair
E-mail: yagitani@is.t.kanazawa-u.ac.jp

Shinichiro Ohnuki
URSI-JRSM 2019Technical Program Committee Chair
E-mail: ohnuki.shinichiro@nihon-u.ac.jp

ASIC Waveform Receiver with Improved Environmental Tolerance for Probing Space Plasma Waves in Environments with High Radiation and Wide Temperature Variation

Yuya Tokunaga[1], Mitsunori Ozaki[1], Satoshi Yagitani[1], Hiroki Koji[1], Daisuke Yonetoku[1], Takahiro Zushi[2], and Hirotsugu Kojima[3]

[1]Kanazawa University, Ishikawa, Japan
Kakuma-machi, Kanazawa 920-1192, Japan
E-mail:ozaki@is.t.kanazawa-u.ac.jp

[2]Department of Electrical Engineering
National Institute of Technology, Nara College

[3]Research Institute for Sustainable Humanosphere
Kyoto University

Abstract

Plasma-wave observations are conducted under conditions of high radiation and wide temperature variation. The electrical characteristics of plasma-wave instruments should therefore be insensitive to these environmental factors. We have developed a new application-specific integrated circuit (ASIC) waveform receiver with a rad-hard [radiation-hardened] amplifier and a temperature-compensation circuit. The environmental tolerance of the conventional ASIC receiver is unsuitable for probing plasma waves in the range 1 Hz to 10 kHz in harsh space environments. Its weak radiation tolerance under 350 krad results in radiation-induced degradation in noise performance, such that weak plasma waves are lost in the noise floor. With an ambient temperature change of −40° C to +100° C, the gain response of the conventional ASIC receiver varies by more than ±1.0 dB, preventing accurate measurement of plasma waves around the cutoff frequency of 10 kHz. Our new ASIC receiver operates at a total dose rate of 350 krad without degradation in noise performance. Moreover, the temperature dependence of the gain response from −60° C to +100° C dramatically improved by ±0.05 dB due to the addition of a compensation circuit. Our new ASIC receiver can contribute to the measurement of plasma waves in challenging environmental conditions to further the understanding of magnetospheric dynamics.

1. Introduction

The Earth's radiation belts consist of relativistic particles trapped by geomagnetic fields [1]. Bombardment by high-energy relativistic particles affects the electrical systems within satellites (e.g., GPS) [2]. Plasma-wave observations are important for understanding the relationship between plasma waves and radiation-belt formation. Multipoint plasma-wave observations have been conducted using multi-satellites (e.g., Cluster [3], THEMIS [4], and MMS [5]). However, the spatial resolution of multi-satellite observations is too low for plasma-wave probing due to the insufficient number of satellites for the plasma wavelength. Poor spatial resolution could be improved by launching more satellites at lower cost. Application-specific integrated circuit (ASIC) technology has been applied to plasma-wave observations (e.g., dc [6] and ac [7-9] magnetic-field observations), providing dramatic reductions in mass, volume, and power.

This study deals with a plasma waveform receiver [10-12] connected to electromagnetic sensors (e.g., search-coil magnetometers [13] and wire-probe antennas [14]), and high-sensitivity preamplifiers. Fukuhara et al. [11] previously described an ASIC-based plasma waveform receiver. However, the output dynamic range, radiation tolerance, and temperature dependence of conventional

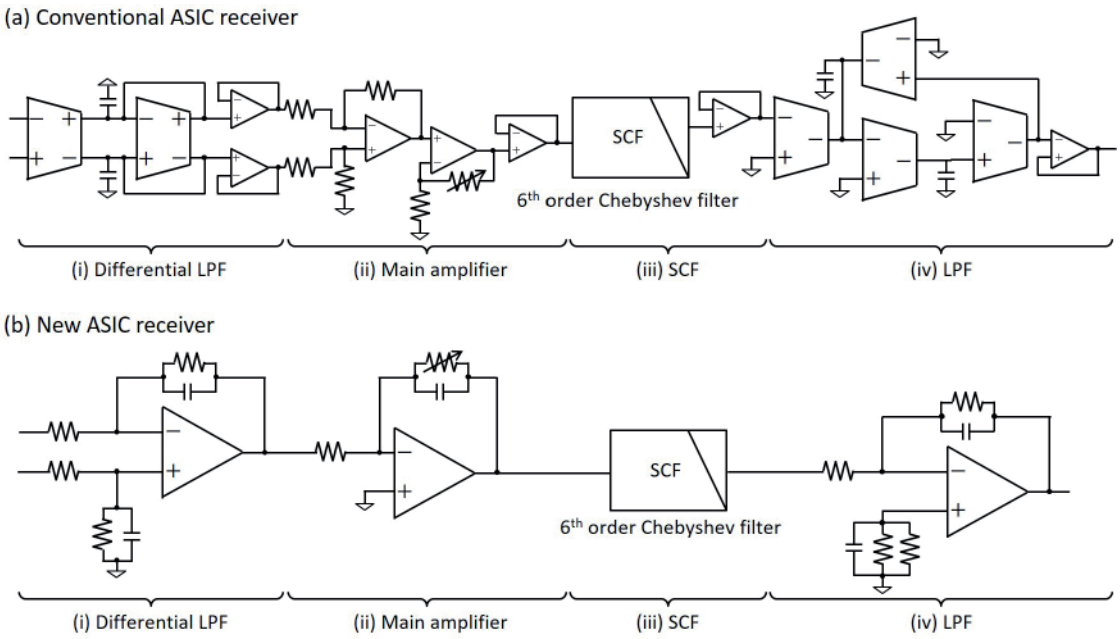

Figure 1. The schematic block diagrams of the conventional (a) and new (b) ASIC receivers.

ASIC receivers are inadequate for plasma-wave observations. These require a flat gain response from 1 Hz to 10 kHz with sharp cutoff characteristics and a wide dynamic range of 2.6 Vpp (approximately 80% of the 3.3 V supply voltage). The gain response of a conventional ASIC receiver is not flat, having a large ripple of 2.0 dB generated by the sharp cutoff of a sixth-order Chebyshev filter. The narrow output dynamic range of a conventional ASIC receiver is 45% of its 3.3 V supply voltage. The gain response of the conventional ASIC receiver can be smoothed by redesigning the transfer function, but without buffering to expand its dynamic range, the amplifier cannot output waveforms of amplitude greater than 45% of the 3.3 V supply voltage. Hence, the conventional ASIC receiver cannot deliver the required electrical performance. Furthermore, the ASIC receiver must be able to operate within harsh space environments to accurately capture plasma waves.

Ozaki et al. [9] developed an ASIC preamplifier for plasma-wave observations that could tolerate the extreme environments of space. Our target for environmental tolerance is almost identical to that of Ozaki et al. [9], to use the new ASIC receiver connected to a search-coil magnetometer via the ASIC preamplifier for probing plasma waves. We performed a radiation test for an experimental ASIC receiver. The SS520-3 sounding rocket used the experimental ASIC receiver. The SS520-3 sounding rocket will launch to detect in situ wave-particle interactions causing the ion outflow phenomena at the cusp. The observation targets are electric fields in the VLF range below 10 kHz. In this study, the receiver was used to estimate the radiation tolerance of a conventional ASIC receiver, which is discussed in Section 4. The noise performance of the experimental receiver was degraded following radiation tests with 350 krad total dose rate. From the radiation test results, the radiation tolerance of the conventional ASIC receiver was found to be inadequate. Testing the conventional ASIC receiver across the temperature range −40° C to +100° C, we confirmed it to have a large temperature-dependent gain response of over ±1.0 dB.

To improve the electrical performance and environmental tolerance of the conventional ASIC receiver, in this study we redesigned its transfer function and replaced the conventional amplifier with a new operational amplifier (OPA). We designed the new operational amplifier to be approximately twice the size of the conventional amplifier to improve its radiation tolerance, and we added a temperature-compensation circuit [9] to minimize temperature dependence.

Our new ASIC receiver achieved a flat gain response with a ripple of 0.8 dB or less, and a wide dynamic range of 2.7 Vpp: 82% of the 3.3 V supply voltage. The receiver demonstrated a radiation tolerance of 350 krad or more, and a gain response with an ultra-low temperature dependence of 0.05 dB or less.

2. ASIC Receiver

The schematic circuit diagrams of the conventional and new ASIC receivers are shown in Figure 1. In each design, stage (i) is a differential low-pass filter (LPF) to remove common-mode noise and to limit the bandwidth. Stage (ii) is a main amplifier to adjust the system gain. Stage (iii) is a sixth-order Chebyshev low-pass switched-capacitor filter (SCF) to prevent aliasing. The cutoff frequency of the switched-capacitor filter can be controlled by its clock frequency. In this study, we applied a 1 MHz clock signal

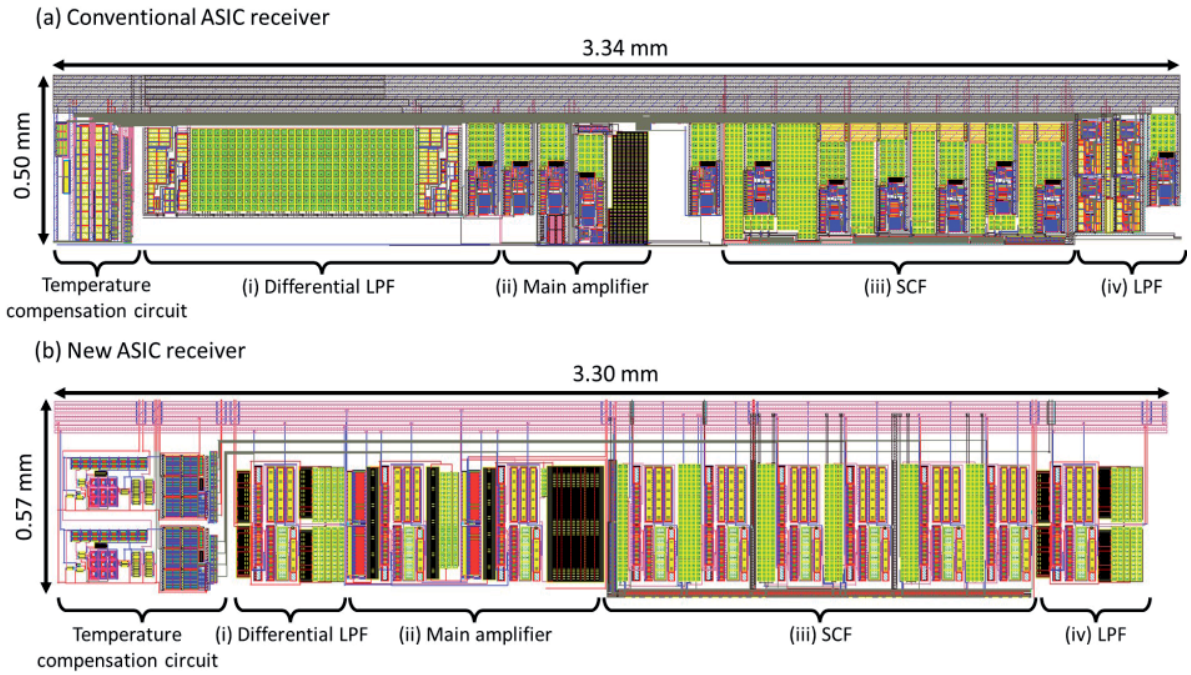

Figure 2. The layouts of the conventional (a) and new (b) ASIC receivers.

of 3.3 Vpp to the switched-capacitor filter to tune the cutoff frequency to 10 kHz. The final stage (iv) is a low-pass filter to reduce ringing from the switched-capacitor filter clock. Stages (i) and (iv) of the conventional ASIC receiver are Gm-C low-pass filters, based on operational transconductance amplifiers (OTAs). We replaced the Gm-C filters with active low-pass filters based on the new operational amplifier to improve the ASIC receiver's dynamic range. The existing operational transconductance amplifier, without output buffering, had a narrow dynamic range. Our new amplifier was two times larger than the conventional amplifier to reduce its radiation absorbed dose, which is discussed in Section 4.

As plasma waves propagate in three-dimensional space, plasma-wave measurements demand a three-axis electromagnetic sensor. The size of a three-channel ASIC receiver is limited to a bare die size of 5 mm × 5 mm. Figure 2 shows the layouts of the conventional and new ASIC receivers. Both green areas of stages (i) in Figure 2 show the metal-insulator-metal capacitors. The capacitor area of new stage (i) was smaller than the conventional are because of changing the cutoff frequencies from 170 kHz to 300 kHz. The size of the new ASIC receiver was 0.57 mm × 3.30 mm, which was close to that of the conventional ASIC receiver and within the acceptable range. Power consumption figures for the conventional and new ASIC receivers were 20 mW and 25 mW, respectively. The 5 mW increase was due to the addition of the new amplifiers and a temperature-compensation circuit. The conventional ASIC receiver had a temperature-compensation circuit different from that of the new receiver. However, the conventional switched-capacitor filter was supplied not by the compensation circuit but by an external resistance, which was not sufficient for supplying reference currents corresponding to ambient temperature.

3. Electrical Characteristics of ASIC Receiver

The ASIC receiver required a flat gain response between 1 Hz and 10 kHz, with a sharp cutoff at 10 kHz, and a low pass-band ripple of 1.0 dB or less, to capture plasma waves without aliasing. Figure 3 shows the gain response of the conventional and new ASIC receivers. Both simulations in Figure 3 were performed with a *Tanner EDA* circuit simulator [15]. In the gain simulations, we calculated both gains using the harmonic ratio between output and input waveforms when inputting a 100 Hz clock waveform. For each receiver, the gain response of the switched-capacitor filter clock was simulated using transient rather than ac analysis. Both sets of results were plotted from 100 Hz to 100 kHz to reduce the memory required for the circuit simulations. The conventional ASIC receiver exhibited significant pass-band ripple of 2.0 dB. The measurements in Figure 3a displayed a 2.5 dB difference between calculated and simulated values due to the output impedance of the conventional amplifier [11]. The large ripple could cause the conventional ASIC receiver's output to saturate. The new ASIC receiver displayed flat gain characteristics up to the cutoff frequency of 10 kHz, with a low ripple of 0.8 dB, as shown in Figure 3b.

Figure 4 shows the input-output characteristics of the conventional and new ASIC receivers. The conventional ASIC receiver had a narrow output dynamic range of 1.5 Vpp, which was 45% of the 3.3 V supply voltage.

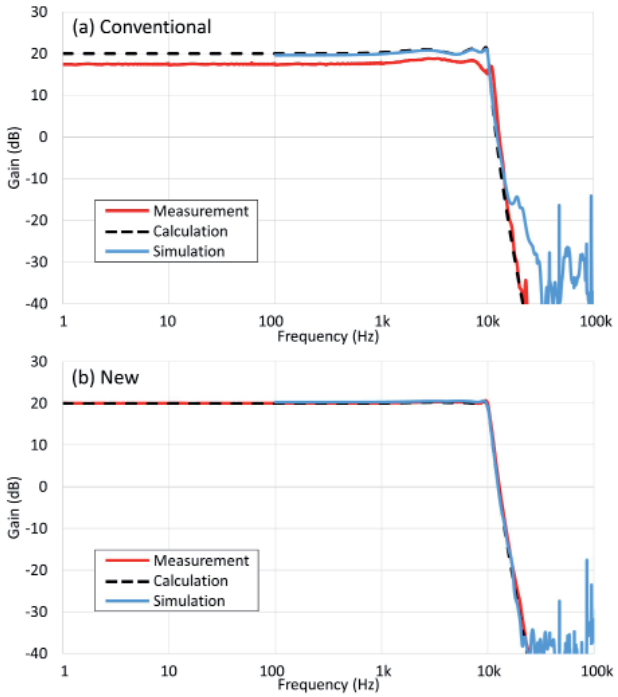

Figure 3. The measured (red solid lines), calculated (black dashed lines), and simulated (blue solid lines) gain-response results for the conventional (top) and new (bottom) ASIC receivers.

To improve this, we designed the new ASIC receiver to use operational amplifiers, increasing the dynamic range by 80% to 2.7 Vpp. Figure 5 shows the measured output waveforms for the conventional and new ASIC receivers for a 1 kHz 0.25 Vpp sine-wave input. The narrow dynamic range of the conventional ASIC receiver caused the output to saturate, but the new ASIC receiver sufficiently amplified the sine waves. The output voltage of the ideal operational transconductance amplifier and operational amplifier are given by [16]

$$V_{inp} - V_{ov1} < V_{OTA} < V_{power} - V_{ov2}, \quad (1)$$

$$V_{ov3} < V_{OPA} < V_{power} - V_{ov4}, \quad (2)$$

where V_{inp} is the positive input voltage of the operational transconductance amplifier; V_{ov1}, V_{ov2}, V_{ov3}, and V_{ov4} are the CMOS overdrive voltages; V_{OTA} is the output voltage; V_{power} is the ASIC receiver power supply voltage; and V_{OPA} is the operational amplifier output voltage. In both ASIC receivers, V_{inp}, V_{ov1}, V_{ov2}, V_{ov3}, V_{ov4}, and V_{power} are approximately 1.65 V, 0.1 V, 0.2 V, 0.2 V, 0.4 V, and 3.3 V, respectively. The input voltage, V_{inp}, was set at the common voltage of the conventional ASIC receiver to consist of the fourth stage (iv) based on the single-ended operational transconductance amplifier from Figure 1a. The voltages V_{OTA} and V_{OPA} in Equations (1) and (2) ranged from 1.55 V to 3.1 V and from 0.2 V to 2.9 V, respectively. An ideal output dynamic range for the operational transconductance amplifier was 1.55 Vpp, which was 4.82 dB lower than that of the operational amplifier. Moreover, as shown in Figure 1a, the operational transconductance amplifier needed a voltage follower due to its high output impedance of 300 kΩ, which could otherwise couple to stray capacitance and pick up noise. From Equation (2), the ideal output dynamic range of the new ASIC receiver was 2.7 Vpp, which was the same as the measurement shown in Figure 4. The low output impedance of the operational amplifier was 10 kΩ for driving the large output buffer current of 320 μA. We measured total harmonic distortion (THD) by inputting 5 kHz sine waves of 0.12 Vpp and 0.09 Vpp into the ASIC receivers, under which input conditions both receivers could output a 1.0 Vpp sine wave. Both ASIC receivers displayed total harmonic distortion degradation at 5 kHz due to the presence of ripple at 10 kHz, which was the second harmonic of a

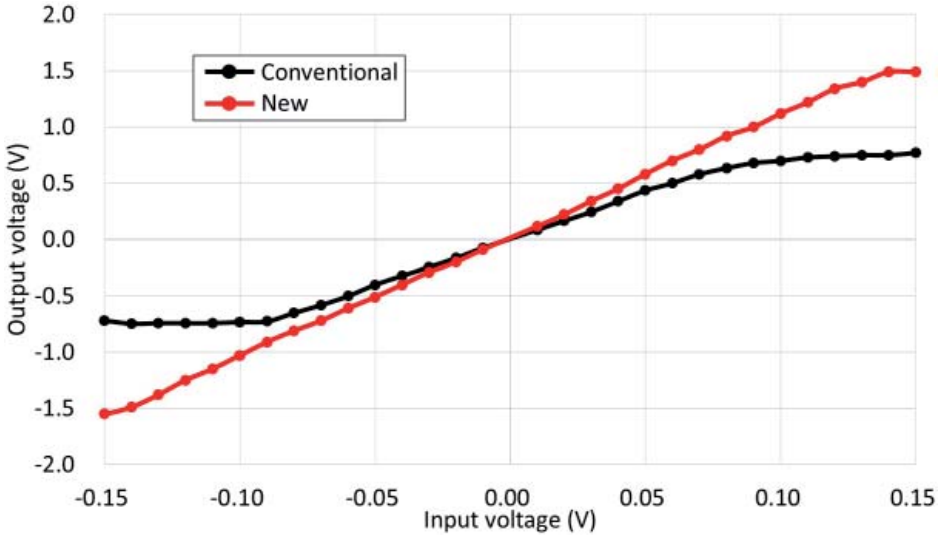

Figure 4. The input-output characteristics of the conventional (black line) and new (red line) ASIC receivers.

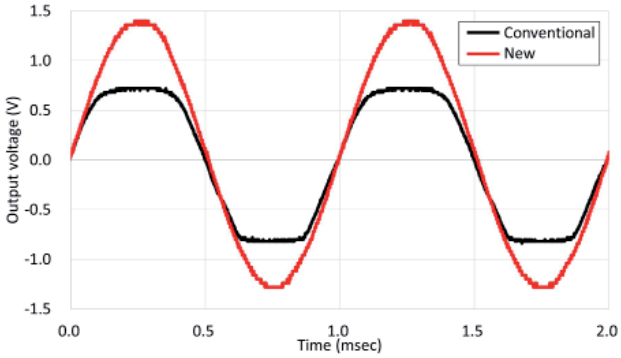

Figure 5. The output waveforms at 1 kHz for the conventional (black line) and new (red line) ASIC receivers.

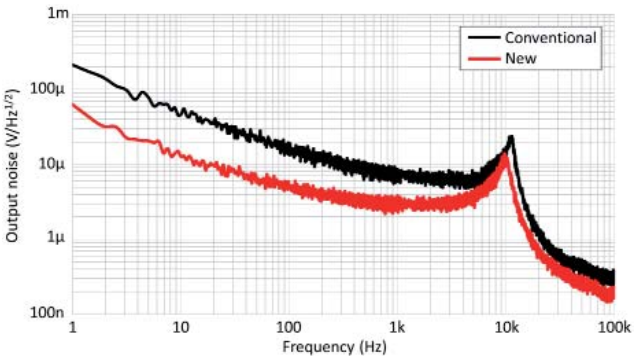

Figure 6. The output noise of the conventional (black line) and new (red line) ASIC receivers.

distorted 5 kHz sine wave. The total harmonic distortion of the conventional and new ASIC receivers was 20 dB and 42 dB, respectively. The measured slew rates of the conventional and new ASIC receivers were 0.01 V/µsec and 0.03 V/µsec, respectively.

As shown in Figure 1a, the conventional ASIC receiver includes several capacitors between signal and ground lines. We assumed charging and discharging of these to be responsible for the slow slew rate. When outputting a 1.0 Vpp sine wave, both receivers put out waveforms below 3.18 kHz and 9.55 kHz without the slew-rate limitation. The new ASIC receiver displayed reduced total harmonic distortion at 5 kHz due to the suppression of ripple between 2.0 dB and 0.8 dB and an improved slew rate. Figure 6 shows the output noise of both receivers. We evaluated their noise performance using output noise rather than equivalent input noise due to the switched-capacitor filters being the dominant noise source. Low output noise is preferable for probing weak plasma waves. The new receiver offered improved output-noise performance between 1 Hz and 10 kHz. In particular, its output noise at 1 Hz was 10 dB lower than that of the conventional ASIC receiver. The voltage noise spectral density of CMOS is described as per [17]

$$e_n = \sqrt{\frac{k_f}{2C_{ox}WLf}\frac{1}{f} + \frac{8}{3}kT\frac{1}{g_m}}, \quad (3)$$

where k_f is the flicker noise coefficient, C_{ox} is the gate capacitance per unit area, W and L are the gate width and length, f is the frequency, k is the Boltzmann constant, T is the absolute temperature, and g_m is the CMOS transconductance. The first and second terms in Equation (3) dominate in the frequency range of flicker noise from 1 Hz to 1 kHz and thermal noise over 1 kHz, respectively. Flicker noise is reduced by increasing the gate dimensions, WL WL ; the resulting amplifier design had a larger surface area and lower output noise than the original.

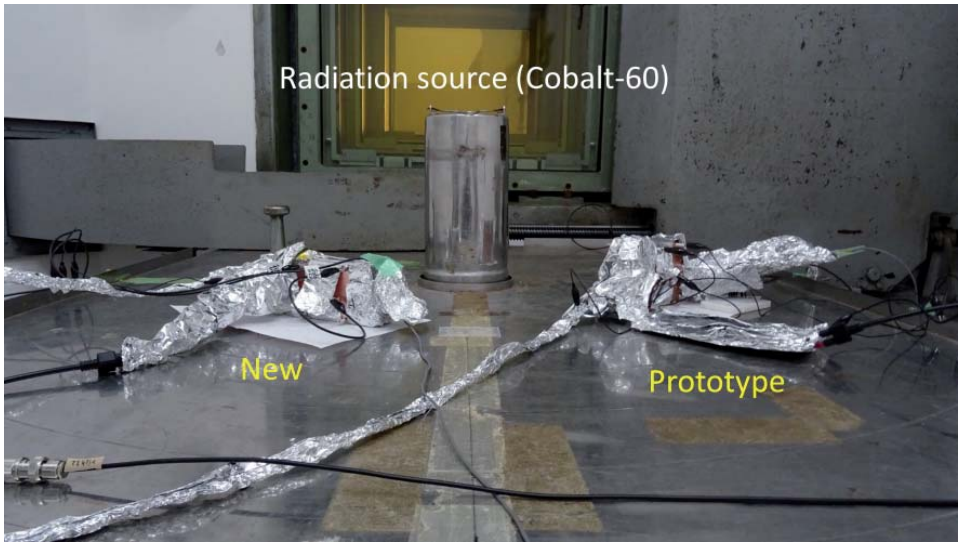

Figure 7. The radiation test setups for the conventional and new ASIC receivers.

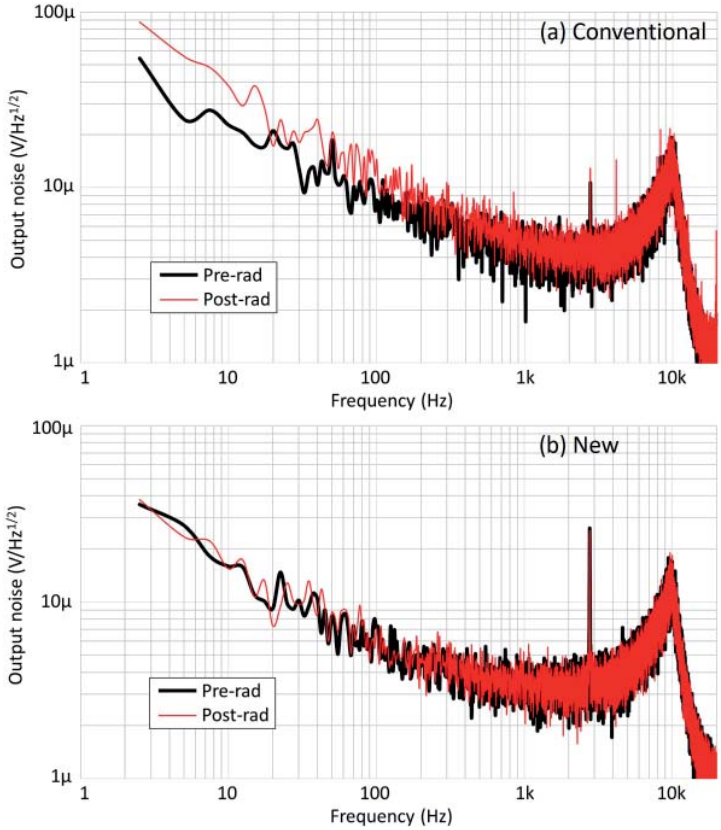

Figure 8. The radiation test results for the conventional (a) and new (b) ASIC receivers.

4. Radiation Tolerance

In space environments, plasma-wave instruments are exposed to high-energy particles of several hundred MeV [18]. The effects of radiation on the ASIC receiver degrade its noise characteristics. To design a rad-hard amplifier for the new ASIC receiver, we evaluated the relationship between amplifier surface area and radiation absorbed dose using a particle and heavy ion transport code system (*PHITS*) radiation simulator [19]. Radiation affects amplifiers by entering their gate oxide films (SiO_2) [20]. In the radiation simulation models, we used SiO_2 plates to model the two amplifier designs. Both simulation models had the same surface area as the CMOS area of the two amplifiers. The first model was 0.5 mm × 0.5 mm, and the second was 0.7 mm × 0.7 mm. The thickness of both models was assumed to be 10 nm. A pencil beam was used as a gamma radiation source.

From the simulation results, the total dose rate for the model with 0.7 mm × 0.7 mm surface area was approximately 0.5 times lower than that of the model with 0.5 mm × 0.5 mm surface area. The surface area ratio of 0.5 mm × 0.5 mm to 0.7 mm × 0.7 mm is approximately 0.5, which was the same ratio as the total dose rate between both simulation models. The total dose rate depends on the surface area of the SiO_2 plate: Increasing the SiO_2 surface area decreases the amplifier's total dose rate. The amplifier in the new ASIC receiver was designed to be approximately twice as large as that of the conventional ASIC receiver to provide improved radiation tolerance.

To evaluate the conventional receiver's radiation tolerance, the experimental ASIC receiver was exposed to gamma ray from cobalt-60 at the Radioisotope Research Center, Tokyo Institute of Technology. Figure 7 shows the radiation test setup for the new ASIC receiver and the experimental receiver. The switched-capacitor filter of the experimental ASIC receiver was similar to that of the conventional ASIC receiver. The noise of the switched-capacitor filter was dominant in both ASIC receivers.

Figure 8 shows the pre- and post-radiation output noise levels for the experimental receiver and new ASIC receivers. Both ASIC receivers were exposed to total dose rates of up to 350 krad. As shown in Figure 8a, the experimental receiver's output noise was degraded between 2.5 Hz and 1 kHz following the radiation tests. Output noise degradation was 4.0 dB at 2.5 Hz. The radiation test results can be described by the CMOS voltage noise density Equation (3). The degradation in output noise below 1 kHz in the conventional ASIC receiver was possibly due to the gate capacitance per unit area, C_{ox}, in Equation (3) having decreased by 0.4 times its pre-rad value as a result of charged particles from the gamma ray becoming trapped in the gate-oxide films. Conversely, we theorized that the output noise of the new ASIC receiver

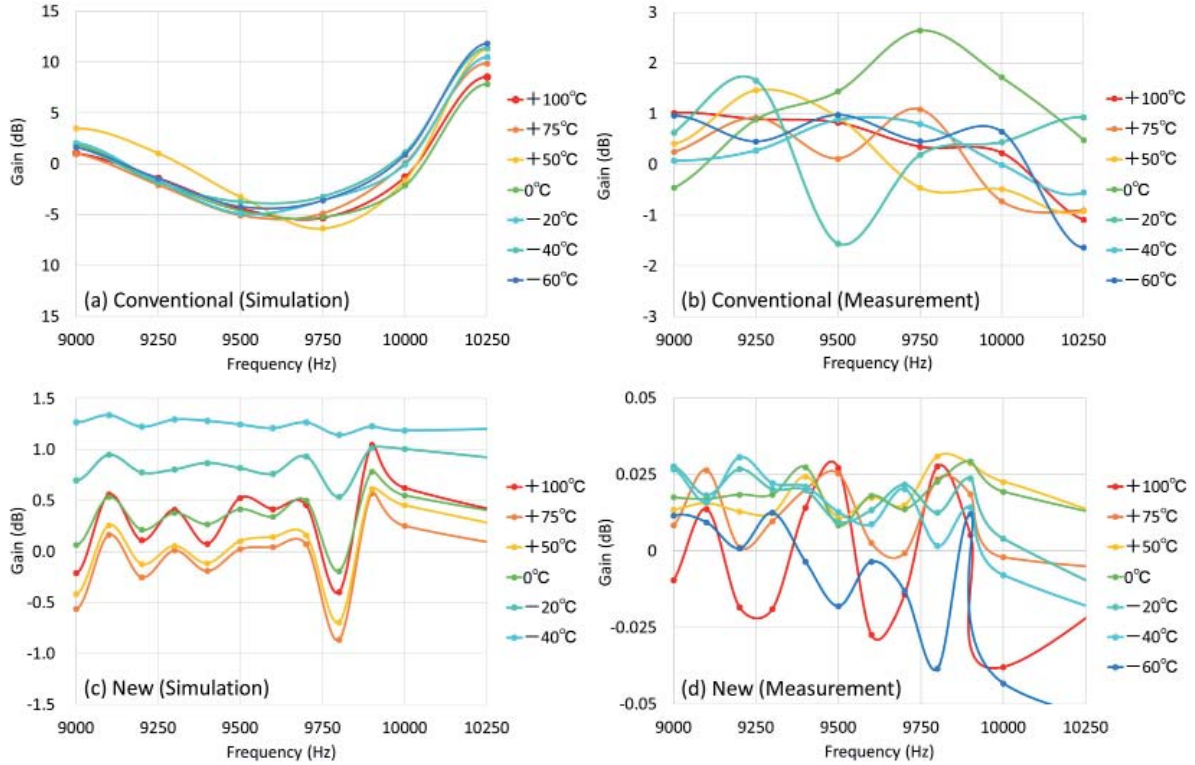

Figure 9. The simulated (a, c) and measured (b, d) temperature-dependence results for the conventional (top) and new (bottom) ASIC receivers.

was unchanged by the radiation tests due to the increased recombination rate of the larger amplifier. Gamma rays cause the transconductance, g_m, in Equation (3) of both ASIC receivers to decrease, generating interface states. A decrease in g_m leads to degraded output noise performance. However, in both receivers, output noise over 1 kHz was not affected by gamma rays. We selected a process (TSMC 0.25 μm CMOS) with a thinner gate-oxide film for both ASIC receivers to prevent generation of interface states. As shown in Figure 8, the conventional ASIC receiver was unable to tolerate radiation of 350 krad and over, while the new ASIC receiver showed no degradation of output noise performance following the radiation test. The new amplifier design with a CMOS surface area twice as large as that of the conventional amplifier effectively decreased the radiation absorbed dose and improved the radiation tolerance of the conventional ASIC receiver.

5. Stability in Thermal Variation

The gain response of the ASIC receiver was affected by ambient temperature variation, making measured plasma-wave amplitudes ambiguous. A constant gain with no temperature dependence was hence required. To evaluate the temperature dependence of both ASIC receivers, a *Tanner EDA* circuit simulator [15] was used. Figure 9 shows the temperature dependence relative to a +25° C reference point for the gain responses of both ASIC receivers. It should be noted that the range of the vertical axis for both receivers is different in Figure 9. The fluctuation for the new receiver was much smaller. As shown in the simulation results in Figure 9a, the conventional ASIC's temperature dependence was high due to the 2.0 dB pass-band ripple and the CMOS threshold voltage variation based on ambient temperature.

As shown in Figure 3, redesigning the switched-capacitor filter transfer function reduced the ripple from 2.0 dB to 0.8 dB. When the pass-band ripple in Figure 3 was shifted by a change in ambient temperature, the temperature dependence of the conventional ASIC receiver was greater than that of the new ASIC receiver. Reference currents should correspond to a threshold voltage variation of approximately ±10% from +25° C to −60° C and to +100° C. A bias resistance of 32 kΩ provided the reference currents of the conventional ASIC receiver.

We performed temperature simulations from −60° C to +100° C to evaluate the temperature-induced variation in the reference currents supplied by the bias-resistance and temperature-compensation circuit. From those simulations, the calculated rate of variation of the reference current from standard temperature at +25° C was approximately ±6% across the temperature range. We designed a temperature-compensation circuit without external bias resistance to supply reference currents depending on ambient temperatures [9]. The rate of variation of the reference current from the temperature-compensation circuit increased by approximately ±30% across the temperature range. Reference-current variation of ±30% across the range −60° C to +100° C corresponded with a 10% variation in threshold voltage due to ambient temperature.

Figure 10a. The temperature test setup for the conventional ASIC receiver.

Comparing the simulation results in Figures 9a and 9c, the temperature dependence of the new ASIC receiver with the temperature-compensation circuit improved significantly from ±15.0 dB to ±3.0 dB.

Figure 10 shows the temperature test setup for the conventional and new ASIC receivers. The temperature tests for the conventional and new ASIC receivers were conducted in ETAC FL420N (Kusumoto Chemicals, Ltd.) thermostatic chambers at Kanazawa University and MC-712 (ESPEC Corp.) at the National Institute of Technology, Ishikawa College, respectively. As per the temperature test results in Figures 9b and 9d, the temperature dependence of the new ASIC receiver drastically decreased to ±0.05 dB compared to the conventional ASIC receiver due to suppression of the pass-band ripple and compensation for temperature-induced variation in CMOS threshold voltage. These temperature test results indicated that the compensation circuit effectively reduced temperature dependence, minimizing the impact of wide temperature variations in space environments on the gain response of the new ASIC receiver.

6. Conclusion

We developed a rad-hard amplifier and a temperature-compensation circuit to improve the environmental tolerance of a conventional ASIC receiver. By replacing Gm-C filters with active low-pass filters, the new ASIC receiver's dynamic range expanded significantly from 1.5 Vpp to 2.7 Vpp, which was over 80% of the 3.3 V supply voltage. Because of this wide dynamic range and flat gain response from 1 Hz to 10 kHz with low pass-band ripple, the new ASIC receiver probes plasma waves without saturation. Based on the environmental test results, our new ASIC receiver demonstrated radiation tolerance of 350 krad or more and ultra-low temperature dependence

Figure 10b. The temperature test setup for the new ASIC receiver.

of ±0.05 dB variation in gain response in the range −60° C to +100° C.

The vibration and vacuum tests assuming the SS520-3 sounding rocket experiment were conducted to evaluate the robustness of the experimental ASIC receiver. The difference between the experimental receiver and the new ASIC receiver was the amplifiers comprising the switched-capacitor filter. During both the tests, the experimental receiver operated efficiently without any breakdowns. We consider the new ASIC receiver and the experimental receiver to be equally robust. Plasma waves have nonlinear temporal characteristics that are the key to understanding magnetospheric dynamics. Plasma-wave amplitude and phase information detected by the Arase (ERG) satellite [21, 22] contributed to the observation of the relationship between chorus waves and the auroral phenomena [23, 24]. The waveform receiver connected to the search-coil magnetometer of the Arase satellite covered the frequency range from 1 Hz to 20 kHz [22]. The new ASIC receiver operates over the same frequency range as the waveform receiver by inputting a 2 MHz clock. With its wide dynamic range and high environmental tolerance, our new ASIC receiver is therefore eminently suitable for obtaining accurate plasma-wave observations in high radiation environments and across wide temperature variations. The new ASIC receiver will contribute toward understanding the formation of radiation belts in harsh space environments.

7. Acknowledgments

This study was supported by Grant-in-Aid for Scientific Research (15H02136, 17H06140, and 17K06456) from the Japan Society for the Promotion of Science; by a research grant for Exploratory Research on Sustainable Humanosphere Science from Research Institute for Sustainable Humanosphere, Kyoto University; and a research grant from Sakigake project, Kanazawa University. This study was also supported by VLSI Design and Education Center, the University of Tokyo, with the collaboration of Cadence Design Systems, Inc., and Mentor Graphics Corporation. This study was also supported by Japan Atomic Energy Agency for the radiation simulation

by the *PHITS* code. The authors also thank Mr. I. Yoda of Radioisotope Research Center, Tokyo Institute of Technology, for his support and cooperation during the radiation tests. The authors also thank Prof. T. Fukami and Dr. R. Higashi of National Institute of Technology Ishikawa College, for their help during the temperature tests.

8. References

1. Y. Y. Shprits, R. B. Horne, A. C. Kellerman and A. Y. Drozdov, "The Dynamics of Van Allen Belts Revisited," *Nature Physics*, **14**, 1, February, 2018.

2. R. B. Horne, S. A. Glauert, N. P. Meredith, D. Boscher, V. Maget, D. Heynderickx, and D. Pitchford, "Space Weather Impacts on Satellites and Forecasting the Earth's Electron Radiation Belts with SPACECAST," *Space Weather*, **11**, January 2013, pp. 169-186.

3. G. Gustafsson, R. Boström, B. Holback, G. Holmgren, A. Lundgren, K. Stasiewicz, L. Åhlén, F. S. Mozer, D. Pankow, P. Harvey, P. Berg, R. Ulrich, A. Pedersen, R. Schmidt, A. Butler, A. W. C. Fransen, D. Klinge, M. Thomsen, C.-G. Fälthammar, P.-A. Lindqvist, S. Christenson, J. Holtet, B. Lybekk, T. A. Sten, P. Tanskanen, K. Lappalainen, and J. Wygant, "The Electric Field and Wave Experiment for the Cluster Mission," *Space Science Reviews*, **79**, January 1997, pp. 137-156.

4. V. Angelopoulos, "The THEMIS Mission," *Space Science Reviews*, December 2008.

5. R. B. Torbert, C. T. Russell, W. Magnes, R. E. Ergun, P.-A. Lindqvist, O. LeContel, H. Vaith, J. Macri, S. Myers, D. Rau, J. Needell, B. King, M. Granoff, M. Chutter, I. Dors, G. Olsson, Y. V. Khotyaintsev, A. Eriksson, C. A. Kletzing, S. Bounds, B. Anderson, W. Baumjohann, M. Steller, K. Bromund, Guan Le, R. Nakamura, R. J. Strangeway, H. K. Leinweber, S. Tucker, J. Westfall, D. Fischer, F. Plaschke, J. Porter, and K. Lappalainen, "The FIELDS Instrument Suite on MMS: Scientific Objectives, Measurements, and Data Products," *Space Science Reviews*, **199**, March 2016, pp. 105-135.

6. W. Magnes, M. Oberst, A. Valavanoglou, H. Hauer, C. Hagen, I. Jernej, H. Neubauer, W. Baumjohann, D. Pierce, J. Means, and P. Falkner, "Highly Integrated Front-End Electronics for Spaceborne Flux Gate Sensors," *Measurement Science and Technology*, **19**, September 2008.

7. A. Rhouni, G. Sou, P. Leroy, and C. Coillot, "Very Low 1/f Noise and Radiation Hardened CMOS Preamplifier for High-Sensitivity Search Coil Magnetometers," *IEEE Sensors Journal*, **13**, January, 2013, pp. 159-166.

8. M. Ozaki, S. Yagitani, H. Kojima, K. Takahashi, and A. Kitagawa, "Current-Sensitive CMOS Preamplifier for Investigating Space Plasma Waves by Magnetic Search Coils," *IEEE Sensors Journal*, **14**, February, 2014, pp. 421-429.

9. M. Ozaki, S. Yagitani, H. Kojima, K. Takahashi, H. Kouji, T. Zushi and Y. Tokunaga, "Development of an ASIC Preamplifier for Electromagnetic Sensor Probes for Monitoring Space Electromagnetic Environments," *Earth, Planets and Space*, **28**, May, 2016, pp. 68-91.

10. H. Kojima, H. Fukuhara, Y. Mizuochi, S. Yagitani, H. Ikeda, Y. Miyake, H. Usui, H. Iwai, Y. Takizawa, Y. Ueda, H. Yamakawa, "Miniaturization of Plasma Wave Receivers Onboard Scientific Satellites and Its Application to the Sensor Network System for Monitoring the Electromagnetic Environments in Space," *Advances in Geosciences*, **21**, 2010, pp. 461-481.

11. H. Fukuhara, H. Kojima, H. Ishii, S. Okada, and H. Yamakawa, "Tiny Waveform Receiver with a Dedicated System Chip for Observing Plasma Waves in Space," *Measurement Science and Technology*, **23**, September 2012.

12. T. Zushi, H. Kojima, K. Onishi, M. Ozaki, S. Yagitani, S. Shimizu, and H. Yamakawa, "Small Sensor Probe for Measuring Plasma Waves in Space," *Earth, Planets and Space*, **67**, August 2015, pp. 67-127.

13. O. Le Contel, P. Leroy, A. Roux, C. Coillot, D. Alison, A. Bouabdellah, L. Mirioni, L. Meslier, A. Galic, M. C. Vassal, R. B. Torbert, J. Needell, D. Rau, I. Dors, R. E. Ergun, J. Westfall, D. Summers, J. Wallace, W. Magnes, A. Valavanoglou, G. Olsson, M. Chutter, J. Macri, S. Myers, S. Turco, J. Nolin, D. Bodet, K. Rowe, M. Tanguy, B. de la Porte, "The Search-Coil Magnetometer for MMS," *Space Science Reviews*, **199**, March, 2016, pp. 257-282.

14. Y. Kasaba, K. Ishisaka, Y. Kasahara, T. Imachi, S. Yagitani, H. Kojima, S. Matsuda, M. Shoji, S. Kurita, T. Hori, A. Shinbori, M. Teramoto, Y. Miyoshi, T. Nakagawa, N. Takahashi, Y. Nishimura, A. Matsuoka, A. Kumamoto, F. Tsuchiya and R. Nomura, "Wire Probe Antenna (WPT) and Electric Field Detector (EFD) of Plasma Wave Experiment (PWE) Aboard the Arase Satellite: Specifications and Initial Evaluation Results," *Earth, Planets and Space*, **69**, December, 2017.

15. TannerEDA, "Mentor Graphics Japan Co., Ltd.," https://www.mentorg.co.jp/tannereda/, accessed on January 7, 2020.

16. R. Jacob Baker, *CMOS: Circuit Design, Layout, and Simulation (Third Edition)*, New York, IEEE Press, 2010.

17. P. E. Allen and D. R. Holberg, *CMOS Analog Circuit Design, Second Edition*, New York, Oxford Univ. Press, 2002.

18. R. M. Millan and D. N. Baker, "Acceleration of Particles to High Energies in Earth's Radiation Belts," *Space Science Reviews*, **173**, November 2012, pp. 103-131.

19. T. Sato, Y. Iwamoto, S. Hashimoto, T. Ogawa, T. Furuta, S. Abe, T. Kai, P. Tsai, N. Matsuda, H. Iwase, N. Shigyo, L. Sihver and K. Niita, "Features of Particle and Heavy Ion Transport code System (PHITS) Version 3.02," *J. Nucl. Sci. Technol*, **55**, 5, January, 2017, pp. 684-690.

20. T. R. Oldham and F. B. McLean, "Total Ionizing Dose Effects in MOS Oxides and Devices," *IEEE Trans. Nucl. Sci.*, **50**, 9, July, 2003.

21. M. Ozaki, S. Yagitani, Y. Kasahara, H. Kojima, Y. Kasaba, A. Kumamoto, F. Tsuchiya, S. Matsuda, A. Matsuoka, T Sasaki and T. Yumoto," Magnetic Search Coil (MSC) of Plasma Wave Experiment (PWE) Aboard the Arase (ERG) Satellite," *Earth, Planets and Space*, **70**, 4, May, 2018.

22. Y. Kasahara, Y. Kasaba, H. Kojima, S. Yagitani, K. Ishisaka, A. Kumamoto, F. Tsuchiya, M. Ozaki, S. Matsuda, T. Imachi, Y. Miyoshi, M. Hikishima, Y. Katoh, M. Ota, M. Shoji, A. Matsuoka and I. Shinohara, "The Plasma Wave Experiment (PWE) on Board the Arase (ERG) satellite," *Earth, Planets and Space*, **70**, 21, May, 2018.

23. M. Ozaki, K. Shiokawa, Y. Miyoshi, K. Hosokawa, S. Oyama, S. Yagitani, Y. Kasahara, Y. Kasaba, S. Matsuda, R. Kataoka, Y. Ebihara, Y. Ogawa, Y. Otsuka, S. Kurita, R. C. Moore, Y. M. Tanaka, M. Nosé, T. Nagatsuma, M. Connors, N. Nishitani, Y. Katoh, M. Hikishima, A. Kumamoto, F. Tsuchiya, A. Kadokura, T. Nishiyama, T. Inoue, K. Imamura, A. Matsuoka, I. Shinohara, "Microscopic Observations of Pulsating Aurora Associated with Chorus Element Structures: Coordinated Arase Satellite-PWING Observations," *Geophysical Research Letters*, **45**, 12, November, 2018. pp. 12,125-12,134.

24. M. Ozaki, Y. Miyoshi, K. Shiokawa, K. Hosokawa, S. Oyama, R. Kataoka, Y. Ebihara, Y. Ogawa, Y. Kasahara, S. Yagitani, Y. Kasaba, A. Kumamoto, F. Tsuchiya, S. Matsuda, Y. Katoh, M. Hikishima, S. Kurita, Y. Otsuka, R. C. Moore, Y. Tanaka, M. Nosé, T. Nagatsuma, N. Nishitani, A. Kadokura, M. Connors, T. Inoue, A. Matsuoka and I. Shinohara, "Visualization of Rapid Electron Precipitation via Chorus Element Wave–Particle Interactions," *Nature Communications*, **10**, 16, January, 2019.

Performance Improvement of Resonator-Coupled Wireless Power Transfer System Using Dual-Spiral Resonator with Angular Misalignments

Nur Syafiera Azreen Norodin and Masashi Hotta

Graduate School of Sciences and Technology for Innovation
Yamaguchi University
2-16-1 Tokiwadai, Ube, Yamaguchi, Japan
E-mail: b004wc@yamaguchi-u.ac.jp; hotta@yamaguchi-u.ac.jp

Abstract

The power transmission efficiency of a resonator-coupled wireless power transfer (RC-WPT) system with some angular misalignments is examined in this paper. In addition to conventional single-spiral resonators, the dual-spiral resonators which we have proposed are used in the RC-WPT system. It was confirmed that the power transmission efficiency of the RC-WPT system decreased with the increment of angular misalignments. However, it was shown that the decayed power transmission efficiency due to the angular misalignments could be recovered by adding the appropriate axial displacements between transmitting (Tx) and receiving (Rx) units.

1. Introduction

Wireless power transfer (WPT) systems have become widely employed due to their free access to the power supply. The most popular wireless power transfer system at this time is the electromagnetic-induction type, such as the Qi system used to charge mobile phones. However, that system requires careful positioning and is restricted to short-distance power transmission use. On the contrary, the resonator-coupled type of wireless power transfer (RC-WPT) system [1] has tremendous potential for the layout-free electric power supply for some electric appliances and/or IoT systems in the near future, due to its superiority of efficient power transmission for the middle-range distances [2-4].

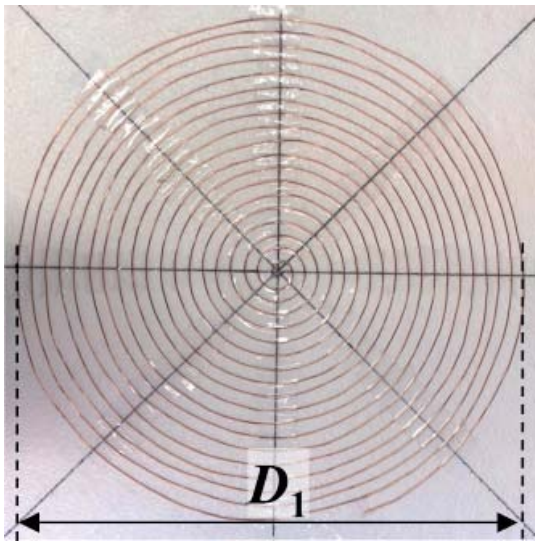

Figure 1a. A conventional single-spiral resonator with 10.0 mm-pitch winding.

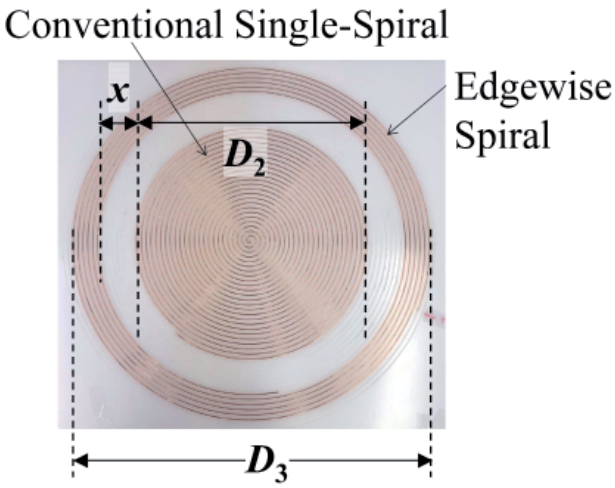

Figure 1b. A dual-spiral resonator with 5.0 mm-pitch winding.

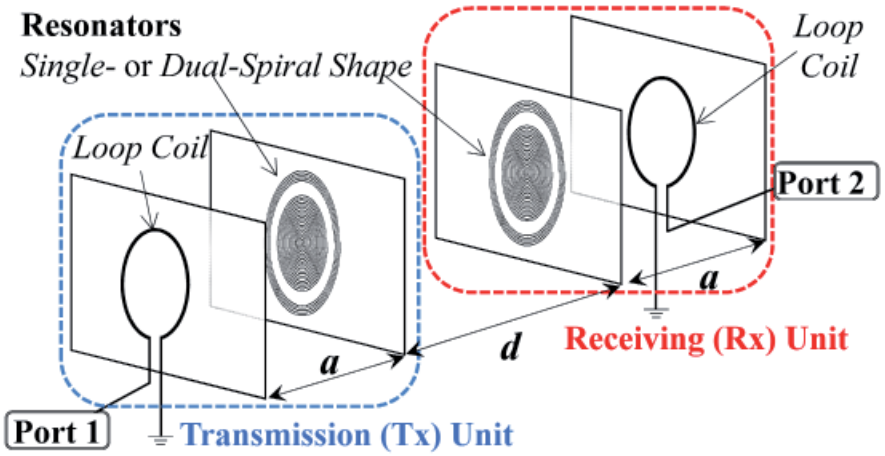

Figure 2. The schematic of the setup of the RC-WPT system.

In order to obtain good performance of an RC-WPT system, two types of spiral resonators have been used throughout this research, making a comparison between them. Up to now, the conventional single-spiral resonators, as shown in Figure 1a, were used for our RC-WPT system. In addition, to realize a widely applicable RC-WPT system, we have proposed the dual-spiral resonators presented in Figure 1b. These can avoid the influence of lossy objects that exist throughout the power transmission path [1, 5].

However, even if the RC-WPT system is used, the decay of transmission power caused by angular misalignments between transmitting (Tx) and receiving (Rx) units is inevitable. In this paper, the decay of the power transmission efficiency for the RC-WPT system with angular misalignments was investigated in detail. A way was found to recover that performance degradation by choosing appropriate positioning of the receiving units.

2. Configuration Setup of RC-WPT System

The schematic setup of our RC-WPT system is shown in Figure 1. Each transmitting and receiving unit consisted of a spiral resonator and a loop coil [6]. The loop coils worked as the power suppliers and receivers of this system, while the spiral resonators electromagnetically coupled between the transmitting and receiving units [3, 4]. Here, the distance between the spiral resonator and the loop coil was set as a [cm], and the distance between the spiral resonators was d [cm], which are also shown in Figure 2.

The loop coil was fabricated on Styrofoam boards using 1.0 mm diameter Cu wire with a loop diameter of 17.5 cm. The ends of the loop coils in the transmitting and receiving units were connected to ports 1 and 2 of vector network analyzer (VNA), respectively. For the initial position, the spiral resonators were facing each other with opposite winding directions, and their center axes coincided including the loop coils when the whole system was observed from the transmitting to the receiving unit [6, 7].

For the resonators in this paper, we used two types of spiral resonators: single-spiral and dual-spiral resonators. The single-spiral resonator was fabricated on Styrofoam boards with a thickness of 1.0 cm, with the 1.0 cm winding pitched spiral-shaped Cu wire, the diameter of which was 1.0 mm, as presented in Figure 1a. The whole diameter of the conventional single-spiral resonator, D_1, was 37.6 cm. For these conditions, the resonator frequency of that single-spiral resonator was just 10.0 MHz. This single-spiral resonator was a kind of spiral coil, so that it formed a strong magnetic field. This structure was of a planar type, so it would be a compact system towards the transmission direction.

Concerned with the resonator, we used dual-spiral resonators that were a combination of the conventional single-spiral and the edgewise-spiral resonators, as shown in Figure 1b. The dual-spiral resonators were fabricated by using polyethylene (PE) substrates with a thickness of 2.0 mm on which a 5.0 mm-pitched spiral-shape groove was drawn, and the 1.0 mm diameter Cu wire was embedded along there. The reason why the dual-spiral resonators were investigated was because it has been clarified that by using dual-spiral resonators, the power transmission efficiency of the RC-WPT system was made insensitive to lossy objects existing on the power transmission path, compared to an RC-WPT system with the conventional single-spiral resonators [1].

The dual-spiral resonators had two resonant points, since they were a combination of two different types of resonators, as mentioned above [5]. As can be seen in Figure 3, we call the resonant mode at the lower frequency *Mode* 1, and the other resonant mode *Mode* 2, respectively. In this study, we set the resonant frequency of *Mode* 1 as 10.0 MHz. For these conditions, the structural parameters of the dual-spiral resonator shown in Figure 2b were $D_2 = 24.1$ cm, $D_3 = 38.6$ cm, and $x = 5.0$ cm. Here, the resonant frequency of *Mode* 2 was 12.9 MHz.

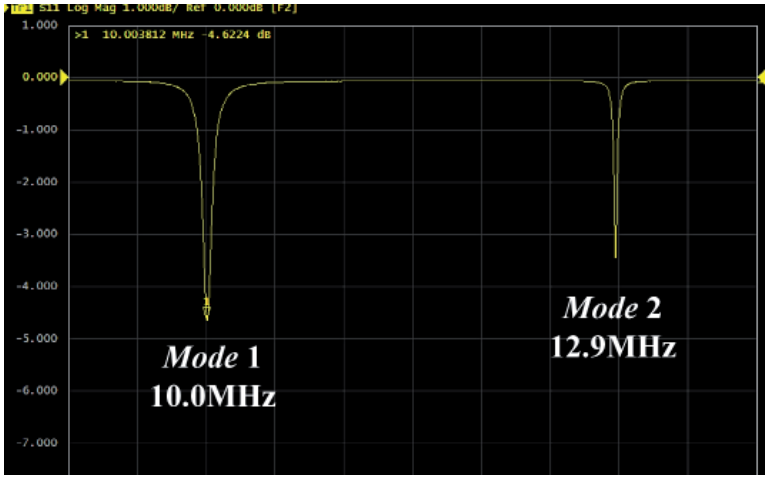

Figure 3. Two resonance points of the dual-spiral resonator.

3. Measurement of Power Transmission Efficiency for RC-WPT System

3.1 Unloaded *Q* of Dual-Spiral Resonator

At first, to investigate the properties of the single-spiral and dual-spiral resonators, the unloaded Q values, Q_u, which are proportional to the inverse of the losses dissipated in the resonator for *Mode* 1 and *Mode* 2 of the dual-spiral resonator as a function of the distance between the loop coil and resonator, a, are presented in Figure 4.

In each resonator, as the distance a is short, the value of unloaded Q becomes small. Here, the unloaded Q indicates the inverse of the loss for the resonator itself, which was isolated from the rest of the circuit. When the distance between the spiral resonator and the loop coil is too close, it might be affected by the interference effects from the loop coil.

From these results, the Q_u of the single-spiral resonator increased as the distance a became larger. It converged to the maximum value of 810 when the distance a was longer than 15.0 cm. The Q_u for *Mode* 1 increased as the distance a became larger. It converged to the maximum value of around 700 when the distance a was larger than 15.0 cm. To the contrary, the Q_u for *Mode* 2 showed almost the same characteristics when the distance a was shorter than 9.0 cm. However, it decreased when the distance a was larger than 9.0 cm, and could not be measured after the distance a was larger than 12.0 cm. The reason why this phenomenon for *Mode* 2 occurred has not yet been resolved. It could be made clear with the detailed inspection of the modal analysis for *Mode* 2.

3.2 Power Transmission Efficiency of RC-WPT System Without Some Misalignments

To evaluate the transmission efficiency of the RC-WPT system, we first found the sets of distances a and d

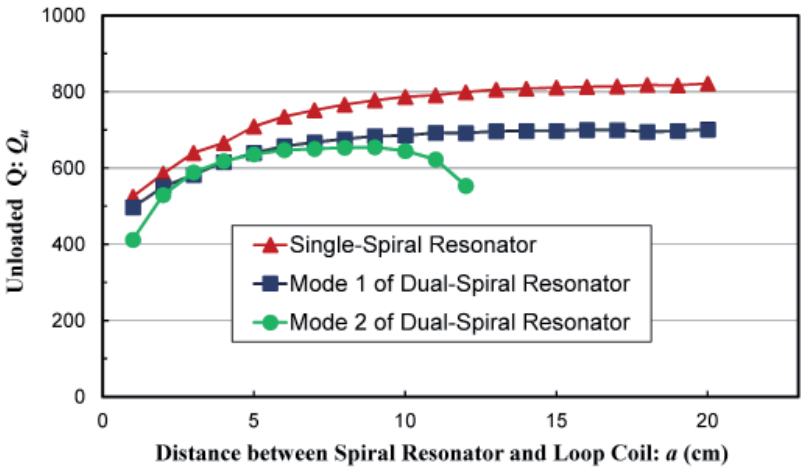

Figure 4. The measured unloaded *Q*.

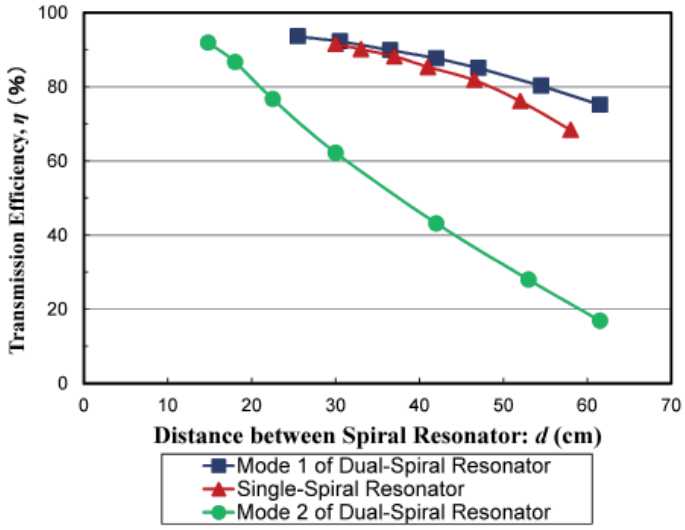

Figure 5. The results for the transmission efficiency of the fabricated RC-WPT system.

that satisfied the matching condition [7]. By choosing the set of *a* and *d* under the matching condition, after some fine adjustment of the distance *d* was carried out, the maximum power transmission efficiency could be measured. The measured results are shown in Figure 5.

From the experimental results, a comparison between the characteristics of the transmission efficiencies indicated that the transmission efficiency of the wireless power transfer system using *Mode* 1 of the dual-spiral resonator was larger than that of the system using the single-spiral and *Mode* 2 of the dual-spiral resonators. In addition, the RC-WPT system with the dual-spiral resonators had a wider transmittable range of *d* than that of the single-spiral resonator.

The system matching conditions for the RC-WPT system with the dual-spiral and the single-spiral resonators were different. Furthermore, the dual-spiral and the single-spiral resonators were kinds of coil type resonators, and the dual-spiral resonator more tightly confined the electric field to itself compared with the single-spiral resonator, as mentioned in Section 2. The near field of the dual-spiral resonator where the magnetic field dominantly performed would thus differ from that of the single-spiral resonator. At this time, the authors assume that these differences are the reasons why the transmission efficiency of the RC-WPT system with the dual-spiral resonators presented better performance than the system with single-spiral resonators.

3.3 Power Transmission Efficiency of RC-WPT System with Some Misalignments

To examine these circumstances, the structure of the RC-WPT system with angular misalignment was constructed, as shown in Figure 6a. The angular misalignment, θ [°], was defined by the angle between the loop coil's surface in the transmitting unit and the spiral resonator's surface in the receiving unit [6]. The receiving unit was rotated by θ on the transversely center axis of the spiral resonator in the receiving unit. In addition, when

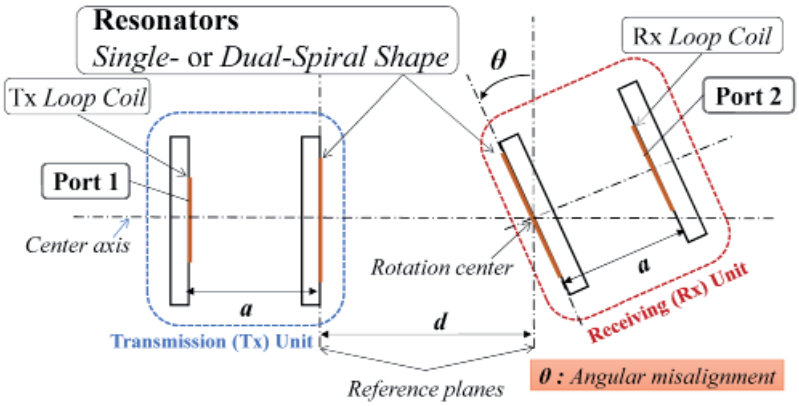

Figure 6a. A top view of the RC-WPT system with angular misalignments but no axial displacement, $c = 0$ cm.

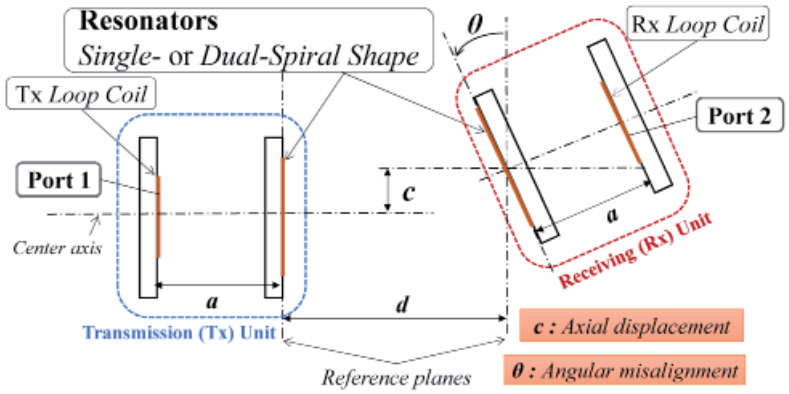

Figure 6b. A top view of the RC-WPT system with angular misalignments and axial displacements.

the spiral coils were observed from transmitting unit to receiving unit, the winding direction of the spiral resonator in the transmitting and receiving units was opposite to each other. The axial displacement between the transmitting and receiving units was set to be c [cm]. At first, Figure 6a shows the case for $c = 0$ cm.

As can be seen in Figure 6b, as the decay of power transmission efficiency due to the angular misalignments was investigated, to measure the characteristics of transmission efficiency against angular misalignments in the range of $0° \le \theta \le 60°$, the receiving unit was moved towards the reference line by the distance c.

Based on the system matching conditions described in [3], to get the maximum power transmission efficiency of the RC-WPT system the appropriate power transmission distance d should be chosen for the distance between the loop coil and spiral resonator a.

Figure 7 shows the power transmission efficiency of the RC-WPT system as a function of angular misalignments with the hollowed blue squares, □, for *Mode* 1 and the hollowed green circles, ○, for *Mode* 2, when $a = 7.0$ cm and $d = 61.5$ cm. However, the hollowed red triangles, △, for the single-spiral resonators presented the power transmission efficiency as a function of angular misalignments when $a = 7.0$ cm and $d = 58.0$ cm. The difference of d against the same a is due to the difference of matching conditions of each system since the type of resonators used were not the same. In this paper, we have presented the results of power transmission efficiency of RC-WPT system when $a = 7$ cm only. The results for other combinations of a and d were also examined, and it was confirmed that they had almost the same tendency and/or characteristics.

From the results in Figure 7, the power transmission efficiency of the RC-WPT system with *Mode* 1 was larger than the *Mode* 2 and single-spiral resonator cases. As the angular misalignments were increased, the power transmission efficiency of the RC-WPT system decayed in each case. It seemed that these decay of the power transmission efficiency of RC-WPT system was caused by the decrease of the overlapping rate between modal

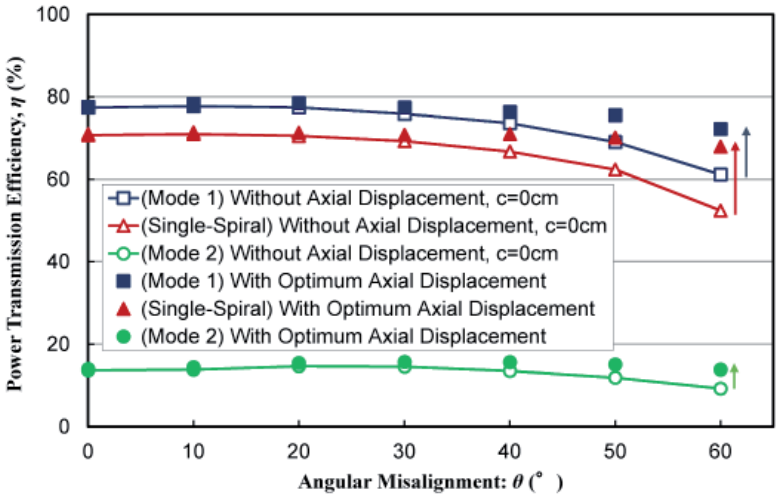

Figure 7. The recovered power transmission efficiency for the RC-WPT system with angular misalignment obtained by choosing the optimum axial displacement where $a = 7.0$ cm.

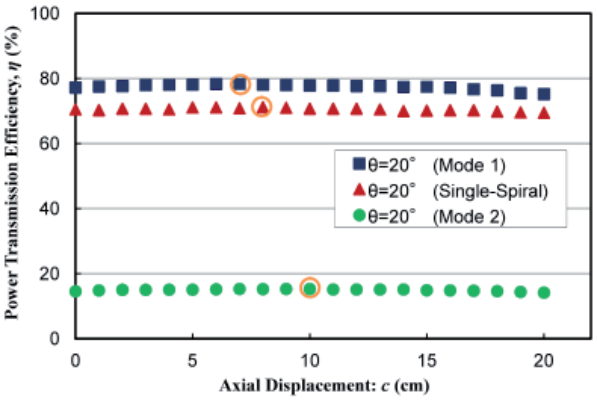

Figure 8a. The relationship between the transmission efficiency and the axial displacement in the case of angular misalignments, $\theta = 20°$.

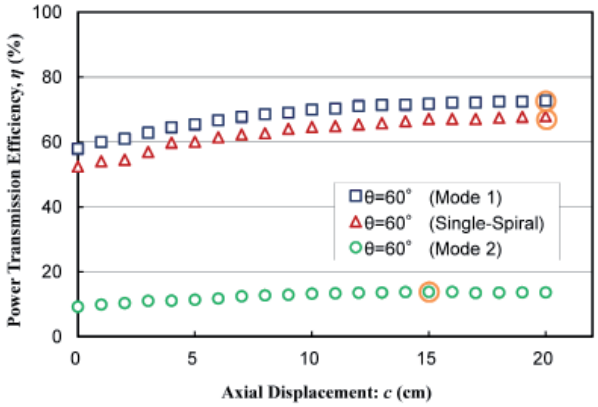

Figure 8b. The relationship between the transmission efficiency and the axial displacement in the case of angular misalignments, $\theta = 60°$.

profiles of the resonators in the transmitting and receiving units due to the tilted receiving unit.

Here, the decay of the power transmission efficiency caused by the angular misalignments could be recovered by adding an appropriate axial displacement. The power transmission efficiency was measured in the case that the receiving units with angular misalignments $\theta = 20°$ (presented in Figure 8a) and for $\theta = 60°$ (presented in Figure 8b) were shifted by a different axial displacement, c. Here, the hollowed orange circles, ○ show the axial displacement where the maximum transmission efficiency was obtained. The recovered power transmission efficiencies of the RC-WPT system for choosing the optimum axial displacement against each angular misalignment are also shown in Figure 7 with solid blue squares, ■, for *Mode* 1; with solid green circles, ●, for *Mode* 2 of the dual-spiral resonator; and the solid red triangles, ▲, for the single-spiral resonator. As can be seen in Figure 7, the recovery rate for the RC-WPT system with single-spiral resonators was much larger than that with the dual-spiral resonators. However, the power transmission efficiency for the RC-WPT system using *Mode* 1 of the dual-spiral resonators with a tilted receiving unit was higher than that of the single-spiral resonator. It is obvious that the proposed method for the improvement of the performance of the RC-WPT system with a tilted receiving unit would be effective for the wireless power transfer system with a wide variety of shapes of resonators. In addition, judging comprehensively from these results, the performance against the misalignment between transmitting and receiving units of the RC-WPT system with *Mode* 1 of the dual-spiral resonators is relatively better than the system with single-spiral resonators.

One of authors has presented the result that the transmission efficiency of the butt-joint between optical waveguides through an air gap and between single-mode and multi-mode waveguides greatly depends on the overlapping rate of their modal profile [8, 9]. From these results, the authors assume that by adding the appropriate axial displacement to the tilted receiving unit of the RC-WPT system, the rate of overlapping area between the modal profiles of the transmitting and receiving spiral resonators would become large, so that the decayed power transmission efficiency of the RC-WPT system could be recovered. To confirm these assumptions, we should investigate the modal shape of the spiral resonators in more detail by using an electromagnetic simulator.

4. Conclusions

The power transmission efficiency of the RC-WPT system with angular misalignments of *Mode* 1 was larger than that of the single-spiral and *Mode* 2 systems. In the case of no axial displacement, $c = 0$ cm, as the angular misalignments were increased, the power transmission efficiency of the RC-WPT system was decreased. However, we have experimentally shown that by adding appropriate axial displacement to the tilted receiving unit, the decay of the transmission efficiency of the RC-WPT system due to angular misalignment can be recovered. The recovery rate for *Mode* 1 is also much larger than that of the single-spiral and *Mode* 2 cases. As future research work, the modal properties of the *Mode* 1 and *Mode* 2 cases should be investigated in more detail.

5. Acknowledgements

The authors would like to thank the laboratory alumni, Mr. D. Sugita, who is currently with Sharp Cooperation, and Mr. Y. Goto, who is presently with Chugoku Electrical Safety Inspection Association, for their valuable discussions through their graduate research.

6. References

1. M. Hotta, Nur Syafiera Azreen Norodin, N. N. M. Zakaria, H. Onari, and T. Takegami, "Influence of Lossy Objects for Resonator-Coupled Type Wireless Power

Transfer System with Coplanar Dual-Spiral Resonators," Proceedings of 2018 Asia-Pacific Microwave Conference (Kyoto, Japan), WE1-C2-1, November 2018, pp. 40-42.

2. A. Kurs, A. Karalis, R. Moffatt, J. D. Joanopoulos, P. Fisher, and M. Soljacic, "Wireless Power Transfer via Strongly Coupled Magnetic Resonances," *Science*, **317**, July 2007, pp. 83-86.

3. I. Awai and T. Komori, "A simple Design of Resonator-coupled Wireless Power Transfer System," *IEEJ Transactions on Electronics, Information and Systems*, **130**, 12, December 2010, pp. 2198-2203.

4. M. Hotta, A. Nobu, T. Haruyama, T. Yuki, and M. Hano, "The Effect of Water and/or Dielectric Materials for Resonant Type Wireless Power Transfer System," *The Japanese Journal of the Institute of Industrial Applications Engineers*, **2**, 2, September 2014, pp. 23-31, DOI: 10.12792/jjiiae.002.02.002

5. X. Duan, K. Harada, H. Onari, and M. Hotta, "Fundamental Characteristics of Resonator-Coupled Type Wireless Power Transfer System by Using Planar Type Dual-Spiral Resonators," Proceedings of the 19th IEEE Hiroshima Section Student Symposium (Matsue, Japan), A1-7, December 2017, pp. 17-20.

6. Nur Syafiera Azreen Norodin, D. Sugita, M. Hotta, "Study on Performance of 10 MHz Resonator-Coupling Type Wireless Power Transfer System with Some Misalignments," Proceedings of the 19th IEEE Hiroshima Section Student Symposium (Matsue, Japan), A1-6, December 2017, pp. 13-16.

7. D. Sugita, M. Hotta, and M. Hano, "Transmission Characteristics for Resonator-Coupled Type Wireless Power Transfer System with Angular Misalignment," Proceedings of the 18th IEEE Hiroshima Section Student Symposium (Ube, Japan), B2-19, November 2016, pp. 290-293.

8. M. Hotta, M. Geshiro, K. Kanoh, and H. Kanetake, "Effects of Air Gaps Between Isotropic and Anisotropic Planar Waveguides," *IEICE Transactions on Electronics*, **E76-C**, 8, August 1993, pp. 1345-1349.

9. M. Hotta, M. Geshiro, and S. Sawa, "Application of Beam Propagation Method to Discontinuities of Weakly Guiding Structure," *IEICE Transactions on Electronics*, **E76-C**, 8, August 1993, pp. 1333-1338.

ULF Modulation of Energetic Electron Precipitation Observed by VLF/LF Radio Propagation

Takuya Miyashita[1], Hiroyo Ohya[1], Fuminori Tsuchiya[2], Asuka Hirai[2], Mitsunori Ozaki[3], Kazuo Shiokawa[4], Yoshizumi Miyoshi[4], Nozomu Nishitani[4], Mariko Teramoto[5] Martin Connors[6], Simon G. Shepherd[7], Yoshiya Kasahara[3], Atsushi Kumamoto[2], Masafumi Shoji[4], Iku Shinohara[8], Hiroyuki Nakata[1], and Toshiaki Takano[1]

[1]Graduate School of Engineering
Chiba University
1-33 Yayoi-cho, Inage-ku, Chiba 263-8522, Japan
E-mail: aeka2354@chiba-u.jp ohya@faculty.chiba-u.jp
nakata@faculty.chiba-u.jp takano@faculty.chiba-u.jp

[2]Graduate School of Science
Tohoku University
Aramaki-aza-aoba 6-3, Aoba, Sendai
Miyagi 980-8578, Japan
E-mail: tsuchiya@pparc.gp.tohoku.ac.jp hirai.a@pparc.gp.tohoku.ac.jp kumamoto@stpp.gp.tohoku.ac.jp

[3]Graduate School of Natural Science and Technology
Kanazawa University
Kakuma-machi, Kanazawa 920-1192, Japan
E-mail: ozaki@is.t.kanazawa-u.ac.jp kasahara@is.t.kanazawa-u.ac.jp

[4]Institute for Space-Earth Environmental Research (ISEE)
Nagoya University
Furo-cho, Chikusa-ku, Nagoya 464-8601 Japan
E-mail: shiokawa@nagoya-u.jp miyoshi@isee.nagoya-u.ac.jp nisitani@isee.nagoya-u.ac.jp masafumi.shoji@nagoya-u.jp

[5]Department of Space Systems Engineering Kyushu Institute of Technology
1-1 Sensui-cho, Tobata-ku, Kitakyushu-shi 804-8550, Japan
E-mail: teramoto.mariko418@mail.kyutech.jp

[6]Center for Science
Athabasca University
1 University Drive, Athabasca, AB T9S 3A3 Canada
E-mail: martinc@athabascau.ca

[7]Thayer School of Engineering
Dartmouth College
Hanover, NH 03755 New Hampshire, USA
E-mail: simon.g.shepherd@dartmouth.edu

[8]Institute of Space and Astronautical Science (ISAS)
Japan Aerospace Exploration Agency (JAXA)
Yoshinodai 3-1-1, Chuo-ku, Sagamihara, 252-5210 Japan
E-mail: iku@stp.isas.jaxa.jp

Abstract

We investigated the modulation of D-region signatures due to ultra-low-frequency (ULF) waves using very-low-frequency/low-frequency (VLF/LF) radio propagation. Three transmitters from the United States (NLK, NDK, and WWVB) were received at Athabasca (ATHA), Canada. We observed oscillations in intensities and phases on the NDK-ATHA and WWVB-ATHA paths with a period of 3 to 4 minutes, associated with ULF waves during a substorm at 05:25-05:45 UT on 4 June, 2017. This is the first observational report showing clear VLF/LF oscillations in the ULF range. The ground-based H-component magnetic-field variations and Doppler velocity observed by the SuperDARN HF radars showed the same periodic changes as seen in the VLF/LF oscillations, suggesting that energetic electron precipitation (EEP) over the WWVB-ATHA and NDK-ATHA paths was modulated by the ULF waves. Based on ground-based magnetic-field data, we concluded that the ULF wave corresponded to the Pi2 pulsations associated with the substorm, because the propagation direction of the wave was westward (66.4 km/s) from the pre-midnight sector, the magnetic variations at low latitudes were in-phase over wide longitudes, and the magnetic variations at ATHA slightly preceded those at low latitudes. A rising-tone chorus emission was observed in the frequency range of 5 kHz to 6 kHz at ATHA during the VLF/LF oscillations. Pitch-angle diffusion by the whistler-mode chorus wave is one possible mechanism accounting for the energetic electron precipitation.

1. Introduction

Energetic electron precipitation (EEP; >100 keV) from radiation belts to the lower ionosphere during substorms has been studied since the 1960s using very-low-frequency (VLF; 3 kHz to 30 kHz)/low-frequency (LF; 30 kHz to 300 kHz) radio waves and riometers (e.g., [1, 2]). Later, the effects of the D-region ionosphere on energetic electron precipitation were also studied via balloon-borne measurements of Bremsstrahlung X-rays [3] and incoherent scatter radar [4]. VLF/LF radio waves are most sensitive to the ionization of the D-region ionosphere, which is caused by energetic electron precipitation with energies typically >100 keV [5, 6]. During substorms, the intensity and phase of the VLF/LF waves largely vary at night, by ~30 dB and ~75°, respectively [7]. The low-latitude limit of particle precipitation is $L \sim 4.0$ [8].

Several studies have reported ionospheric modulations due to ultra-low-frequency (ULF) Pc5 modulation (period of 150 s to 600 s) [9, 10]. Pc5 modulation has been observed by GPS total electron content (TEC), high-frequency (HF) Doppler sounders, and SuperDARN HF radars [3, 11, 12]. Modification in the D-region ionosphere due to energetic electron precipitation has been reported based on riometer data and X-ray observations [10, 13]. Energetic electron precipitations associated with Pi2 pulsations (period of 40 s to 150 s) have also been reported [14]. Auroral precipitations and energetic particle fluxes near the equator in the nightside magnetosphere have been reported to occur due to Pi2

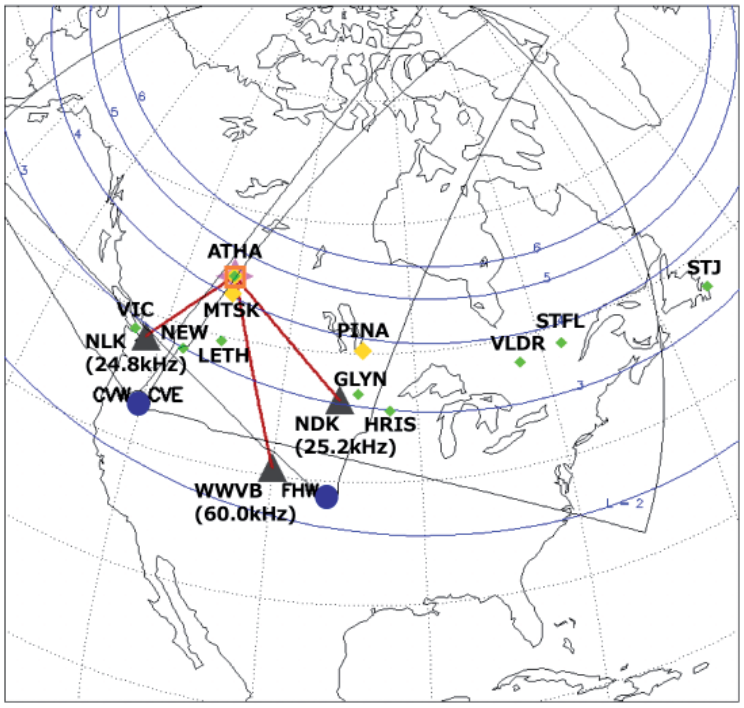

Figure 1. The location of the VLF/LF transmitters (black triangles), VLF/LF receiver (pink star), ground magnetometers (green diamonds), induction magnetometers (yellow diamonds), and SuperDARN HF radars (blue circles). The blue curves indicate the L-values.

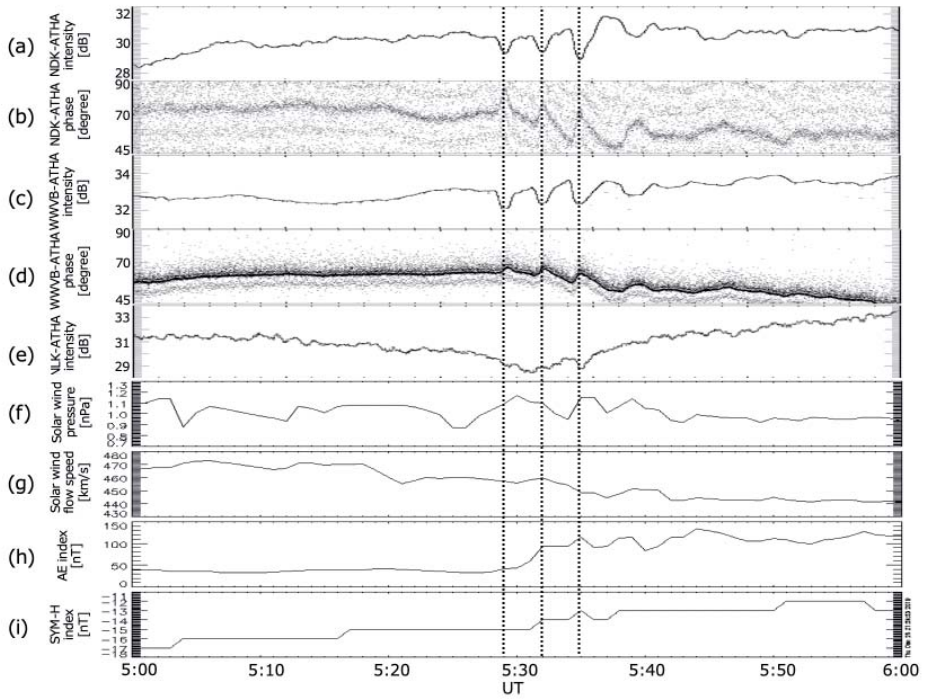

Figure 2. The periodic oscillations in intensities and phase of the VLF/LF transmitter signals in North America during the substorm of June 4, 2017: (a) NDK-ATHA intensity, (b) NDK-ATHA phase, (c) WWVB-ATHA intensity, (d) WWVB-ATHA phase, (e) NLK-ATHA intensity, (f) solar wind speed, (g) solar wind dynamic pressure, (h) AE index, and (i) SYM-H index.

modulation [15]. Precipitation of low-energy electrons (< 300 eV) was reported when a Pi2 pulsation with short periods (< 40 s) occurred [16].

Some candidate mechanisms have been proposed to account for ULF modulation of energetic electron precipitation. The periodic change in local magnetic field strength modulates the growth rate of whistler-mode chorus waves, and the associated rate of electron pitch angle scattering [17]. The electrons show variation in the strength of pitch-angle diffusion with the same period as that of the ULF pulsations. The amount of loss-cone filling is modulated, and precipitation can vary periodically. Electromagnetic ion cyclotron (EMIC) waves represent another candidate plasma wave that can cause pitch-angle scattering of energetic electron precipitation [18-20]. As ULF modulation of electromagnetic ion cyclotron waves has been reported [21], an electromagnetic ion cyclotron wave could modulate the energetic electron precipitation associated with ULF waves. An adiabatic effect has been proposed to explain ULF wave modulation [3]. The ULF wave affects the magnetic field configuration and size of the loss cone, leading to modulation of the energetic electron flux inside the loss cone without pitch-angle scattering. However, the mechanism underlying ULF modulation of energetic electron precipitations is not well understood.

VLF/LF transmitter signals provide a useful probe for monitoring the precipitation of energetic electrons with an energy of > 100 keV. However, ULF modulation of energetic electron precipitation using VLF/LF transmitter signals has not been reported to date. In this paper, we provide the first report on ULF modulation of energetic electron precipitations using VLF/LF transmitter signals.

2. Observations

Figure 1 shows the location of the VLF/LF transmitters and receiver used in this study. The black triangle, pink star, green diamond, yellow diamond, and blue circle indicate the location of the transmitters, receiver, fluxgate magnetometers, induction magnetometers, and SuperDARN HF radars, respectively. The three transmitters were NDK (frequency: 25.2 kHz, 46.37°N, 261.47°E, $L = 3.0$); WWVB (60.0 kHz, 40.67°N, 254.95°E, $L = 2.3$); and NLK (24.8 kHz, 48.20°N, 238.08°E, $L = 2.9$). One receiver at Athabasca (ATHA), Canada (54.6°N, 246.7°E, $L = 4.3$) was used. The receiver observed the intensity and phase of transmitter signals with a time resolution of 0.1 s. The intensity of the received radio signals was averaged over 30 s to improve the signal-to-noise ratio. The propagation distances of the NDK-ATHA, WWVB-ATHA, and NLK-ATHA paths were 1,386.8 km, 1,665.5 km, and 929.7 km, respectively. We used ground-based magnetometer data from ATHA and Lethbridge (LETH), Canada, which are operated by the THEMIS (Time History of Events and Macroscale Interactions during Substorms) ground-based observatory (GBO) [22, 23]. We used fluxgate magnetometers from Priddis (ROTH),

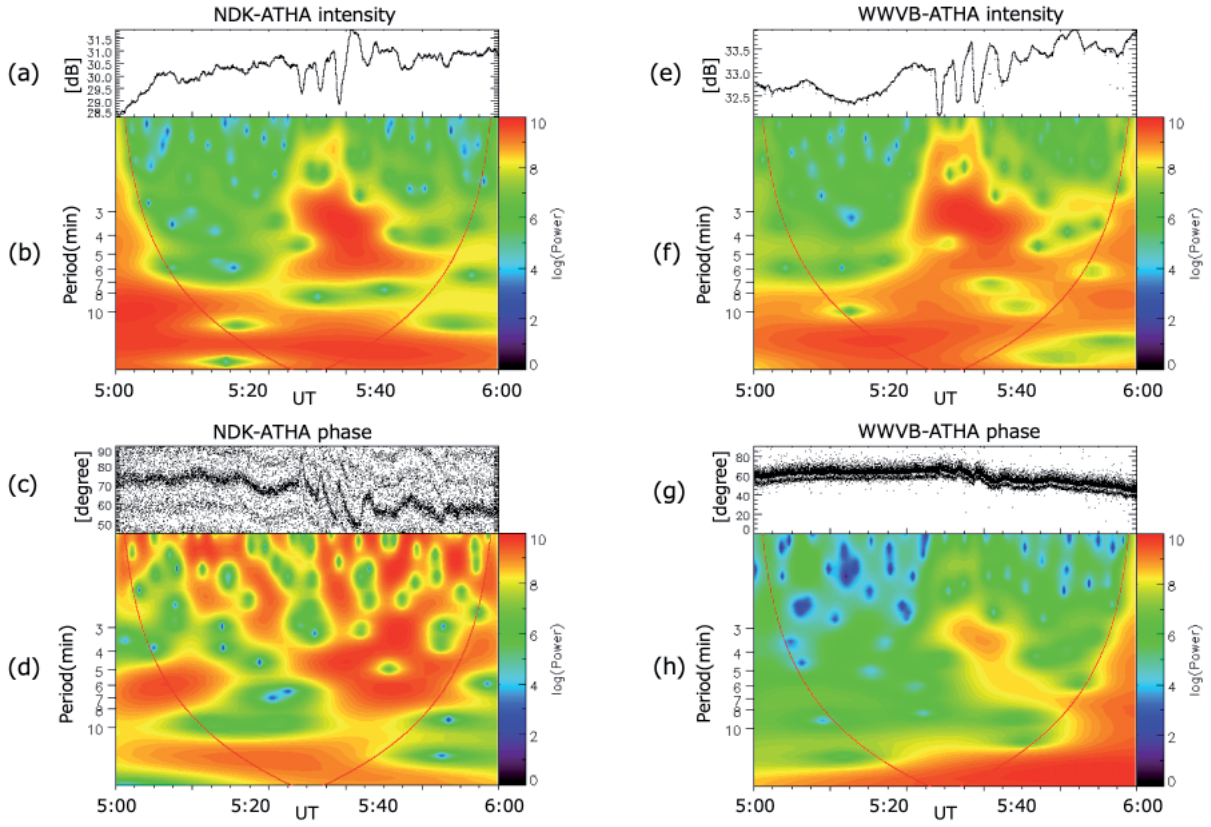

Figure 3. (a) The waveform of the NDK-ATHA intensity, (b) wavelet spectrum of (a), (c) waveform of the NDK-ATHA phase, (d) wavelet spectrum of (c), (e) waveform of the WWVB-ATHA intensity, (f) wavelet spectrum of (e), (g) waveform of the WWVB-ATHA phase, and (h) wavelet spectrum of (g) at 5:00–6:00 UT on June 4, 2017. The red curves in Figures 3b, 3d, 3f, and 3h indicate the COI.

which is operated by AUTUMN (Athabasca University THEMIS UCLA Magnetometer Network); Saint-Felicien (STFL), operated by AUTUMNX (Athabasca University THEMIS UCLA Magnetometer Network eXtension); Harris (HRIS), operated by the Falcon magnetometer project; Glyndon (GLYN), operated by McMAC (Mid-continent Magnetoseismic Chain); Victoria (VIC), operated by NRCan (Natural Resources Canada); and Colville National Forest outside of Newport (NEW), operated by the USGS (US Geological Survey). We used induction magnetometer data from ATHA, operated by the PWING (study of dynamical variation of Particles and Waves in the INner magnetosphere using Ground-based network observations) project and with a sampling frequency of 64 Hz [24]. Induction magnetometers at Pinawa (PINA) and Ministik Lake (MSTK), operated by CARISMA (Canadian Array for Realtime Investigations of Magnetic Activity) were also used to confirm the spatial extent of Pc1 waves [25]. The sampling frequency of the CARISMA data used in this study was 20 Hz. The SuperDARN is a network of HF radars located in the high- and mid-latitude regions of both hemispheres [26]. We used three radars to investigate the F-region ionosphere over the VLF/LF propagation paths, which were Christmas Valley East (CVE), Christmas Valley West (CVW), and the Fort Hays West (FHW) radars.

3. Results

A small substorm occurred from 05:25-05:50 UT on June 4, 2017. The auroral electrojet (AE) index began to increase from 5:25 UT and reached a maximum of 134 nT at 5:44 UT. Figure 2 shows periodic oscillations in the intensity and phase of the VLF/LF transmitter signals in North America during the substorm, the solar wind parameters, and geomagnetic indices: (a) NDK-ATHA intensity, (b) NDK-ATHA phase, (c) WWVB-ATHA intensity, (d) WWVB-ATHA phase, (e) NLK-ATHA intensity, (f) solar wind speed, (g) solar wind dynamic pressure, (h) AE index, and (i) SYM-H index. The phase data of the NLK-ATHA path was unavailable. Oscillations were clearly seen in the NDK-ATHA and WWVB-ATHA propagation paths (Figures 2a-2d) between 05:25-05:45 UT, but not on the NLK-ATHA path. The clear VLF/LF oscillations in the ULF range were identified for the first time with the VLF/LF transmitter signals. The intensity and phase of the oscillations were 1 dB to 2 dB and 3° to 20°, respectively. The solar wind speed and dynamic pressure (Figures 2f and 2g) showed some variations during the VLF/LF oscillations; however, they did not show similar periodicity. The oscillation was characterized by a simultaneous periodic decrease in VLF/LF intensity and VLF/LF phase advance. These features indicated periodic D-region ionization.

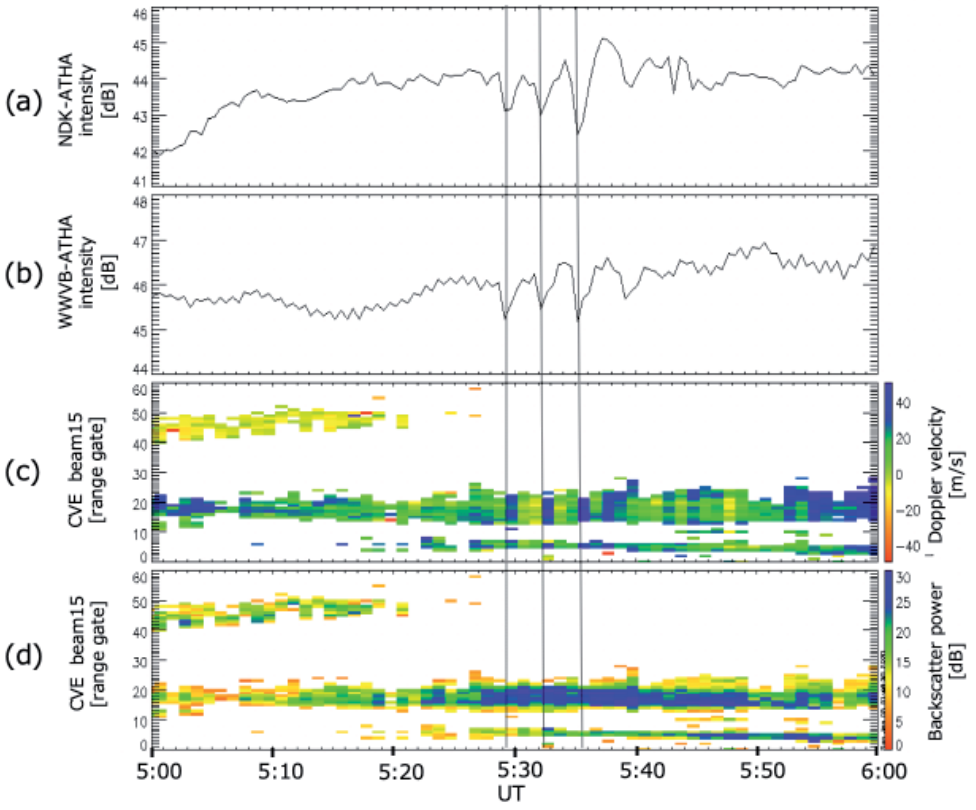

Figure 4. (a) The NDK-ATHA intensity, (b) WWVB-ATHA intensity, (c) LOS Doppler velocity (positive toward the radar) derived from SuperDARN HF radars (CVE), and (d) backscatter power derived by SuperDARN HF radars (CVE).

Figure 3 showed (a) the waveform of the NDK-ATHA intensity, (b) the wavelet spectrum of (a), (c) the waveform of the NDK-ATHA phase, (d) the wavelet spectrum of (c), (e) the waveform of the WWVB-ATHA intensity, (f) the wavelet spectrum of (e), (g) the waveform of the WWVB-ATHA phase, and (h) the wavelet spectrum of (g) between 5:00-6:00 UT. The red curves in Figures 3b, 3d, 3f, and 3h indicated the cone of influence (COI). The VLF/LF perturbations had a significant periodic component around 3 minutes to 4 minutes (broken red circles) for both paths between 05:25–05:45 UT.

Figure 4 shows (a) the NDK-ATHA intensity, (b) WWVB-ATHA intensity, (c) line-of-sight (LOS) Doppler velocity (positive toward the radar) derived from beam 15 of the SuperDARN HF radars (CVE), and (d) the backscatter power derived from beam 15 of the SuperDARN HF radars (CVE). The VLF/LF intensity decreased just before the Doppler velocity increased up to 60 m/s. The variations in Doppler velocity corresponded to periodic oscillations in the ionospheric electric field (periods of 3 to 4 minutes). Figure 5 shows the Doppler velocities against the radar beams from the CVE, CVW, and FHW radars near the VLF/LF paths at 05:35 UT, when the VLF/LF amplitude showed a local minimum. Positive and negative Doppler velocities were observed over the WWVB-ATHA path during the VLF/LF oscillations, which corresponded to changes in the ionospheric electric field.

4. Discussion

The most important issue to address in the present study is why the VLF/LF waves in the subauroral latitude region ($L = 3$ to 4) oscillated with a period of 3 to 4 minutes during the small substorm. Figure 6 shows the H-component of the ground-based magnetic-field variations (ΔB_H) at the same latitudes as the VLF/LF paths at $L = 3$ to 4. The bias components were subtracted from the observed magnetic field. From the top to the bottom panels, the magnetic data are shown from west to east in Figure 1. The local time at these stations at 05:35 UT ranged from 21:21 (VIC) to 26:04 (STJ), from west to east. The closest magnetometer to the WWVB-ATHA path was LETH, in the third panel. All of the magnetic data showed oscillations with a period of 3 to 4 minutes, which was the same as that of the VLF/LF waves. The ΔB_H pulsations at STJ (the bottom panel) were earlier (by 75 s) than those at VIC (the top panel), as shown by the two vertical dashed lines. The phase velocity was 66.4 km/s westward from midnight to dusk, based on the time difference in ΔB_H variations. The amplitude of the ΔB_H variations was largest at 5 nT near the VLF/LF paths (LETH, GLYN, and HRIS) in the pre-midnight sector, and was small (2 nT) away from the VLF/LF paths. The azimuthal wavenumber (m-number) was calculated to be -1.23 , -0.45 , -2.23 , and -1.45 for the magnetometers of VIC-NEW, NEW-LETH, GLYN-HRIS, and VLDR-STFL, respectively [27]. The westward propagation of the

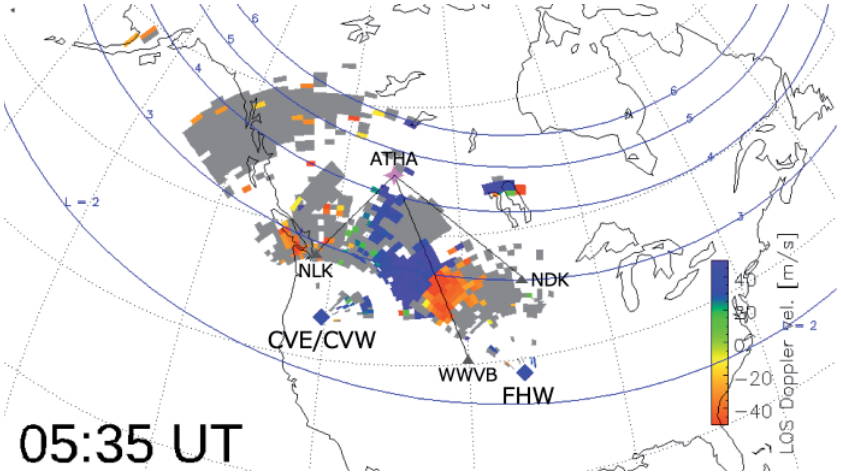

Figure 5. The Doppler velocities as a function of the radar beams from the CVE, CVW, and FHW radars near the VLF/LF paths during the VLF/LF oscillations at 05:35 UT on June 4, 2017.

ULF wave from midnight to dusk is not consistent with the drivers of the ULF in the dayside magnetopause, and suggests that this ULF wave constitutes Pi2 pulsations associated with the onset of a magnetospheric substorm from the nightside.

Figure 7 compares (a) the ΔB_H pulsations between ATHA and low-latitude sites ($L = 1$ to 2) in the wide longitudes, and (b) shows a location map. The red diamond, green diamond, and blue diamond markers indicate the locations of magnetometers that recorded negative-bay, positive-bay, and unclear periodic oscillations, respectively. All ΔB_H had pulsations with similar periods (3 to 4 minutes). The measured ΔB_H at low latitudes were in-phase, and the ΔB_H pulsations at ATHA slightly preceded those at the low-latitude stations. These magnetic data are consistent with the substorm as Pi2 (period of 40 to 150 s) signatures [28], because the propagation direction of the wave was westward (66.4 km/s) from midnight to dusk [29], ΔB_H pulsations at low latitudes in the wide longitudes were in-phase, and the amplitude of the ΔB_H pulsations in the pre-midnight sector was largest in the wide longitudes

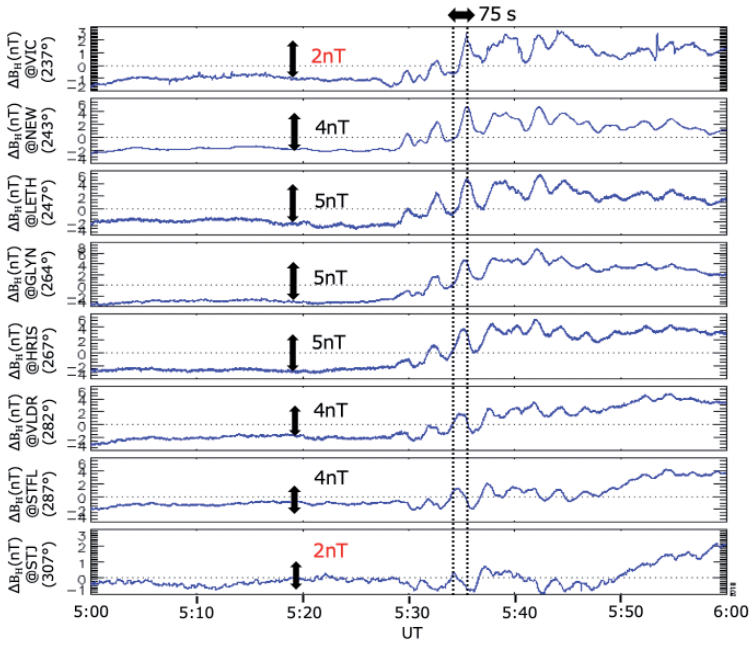

Figure 6. The H-component magnetic data from which the background levels were subtracted (ΔB_H), observed by ground-based magnetometers at the same latitudes with the VLF/LF paths ($L = 3 - 4$). The west-side to east-side magnetic data are shown from the top to the bottom panels (Figure 1).

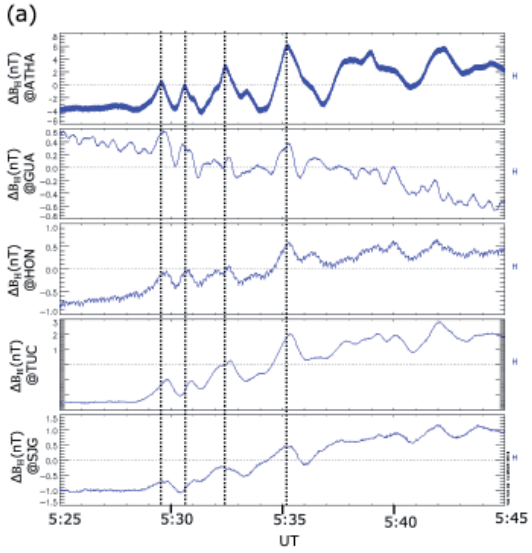

Figure 7a. A comparison of the ΔB_H pulsations between ATHA and low-latitude sites ($L = 1-2$) in the wide longitudes.

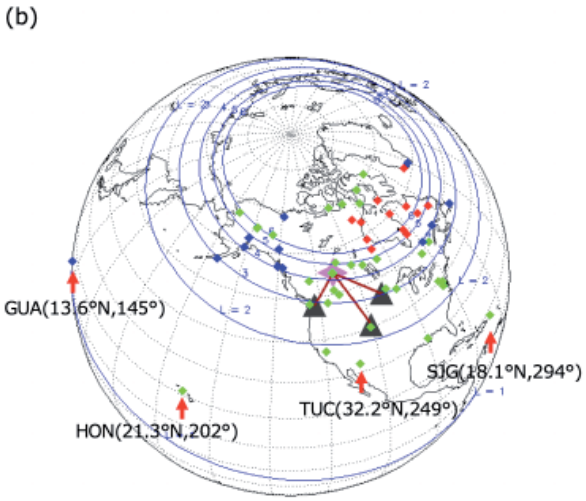

Figure 7b. The location map for Figure 7a. All of the ΔB_H had the same pulsations, with periods of 3 to 4 minutes.

[30-32]. If the origin is the solar wind dynamic pressure, the propagation direction should be eastward in the pre-midnight sector, which is opposite to these observations [33]. We thus conclude that the ULF oscillation shown in this study is the Pi2 pulsation associated with the observed substorm.

Some mechanisms have been proposed to account for the ULF modulation of energetic electron precipitation, as described in Section 1. Here, we discuss possible origins of the ULF modulation of the energetic electron precipitation during 05:25-05:45 UT. One possibility is the electromagnetic ion-cyclotron waves, which are excited near the magnetic equator by anisotropic ring current ions injected from the plasma sheet [34]. Electromagnetic ion cyclotron waves propagate along the magnetic field line to the Earth's surface, and are observed by ground magnetometers as Pc1 pulsations [35]. Correlations between Pc1 and energetic electron precipitations observed by VLF/LF transmitter signals [36, 37], and Pc1 and cosmic noise absorption (CNA) by a riometer [38] have been reported. We checked the appearance of Pc1 pulsations near the NDK-ATHA and WWVB-ATHA propagation paths by using induction magnetometers at ATHA, PINA, and MSTK. No Pc1 pulsation was found during 05:25-05:45 UT, and only bursts of broadband ELF waves associated with the substorm were observed. The electromagnetic ion cyclotron wave can thus be ruled out as a candidate source of the energetic electron precipitation modulations associated with ULF waves presented here. The other possible source was the lower-band chorus waves, which could cause pitch-angle scattering of both diffuse/pulsating auroral electrons [39-43] and more energetic electrons [44,4]. Energetic electron precipitations due to the chorus wave have been observed by VLF/LF transmitter signals [45] and riometers [46]. Figure 8 shows a dynamic spectrum in the VLF range observed at ATHA at 05:35 UT. The natural electromagnetic waves in the dynamic spectrum were observed by a loop antenna, similar to the antenna used in Syowa Station in Antarctica [47]. Rising-tone chorus emissions were found in the frequency range of 4.5 kHz to 6.5 kHz during the energetic electron precipitation. The typical duration, frequency bandwidth, and repetition period of the rising-tone emissions were 0.5 s, 1.0 kHz, and 0.5 s, respectively, similar to lower-band whistler-mode chorus waves [48, 49]. Using Tsyganenko 2001 and 2004 magnetic field models [50, 51], half of the electron gyrofrequency at the magnetic equator, the magnetic footprint of which is just above ATHA, was estimated to be ~4 kHz. If the observed rising-tone emissions were the lower band chorus waves excited at the magnetic equator, the source region was at a lower L-shell than ATHA, where half of the electron gyrofrequency was just above 6.5 kHz and the chorus waves propagated obliquely to the field line and reached the outer L-shell. Such an obliquely propagating whistler-mode wave could cause resonant electron pitch-angle scattering and precipitation of energetic electrons into the atmosphere [52]. On the other hand, considering the first-order cyclotron resonance condition, resonant energy greater than 100 keV can be achieved in the high latitude region [4]. Previous studies suggested the importance of whistler mode waves propagating along the magnetic field line under the presence of plasma ducts [44]. The plasma wave experiment onboard the Arase spacecraft [53-55] showed that the plasmapause location was $L = 5.4$ (MLT = 4, 6:52 UT). The source region of the rising-tone waves was well inside the plasmasphere. The excitation of the rising-tone waves inside the plasmasphere is another issue that remains to be investigated.

The periods of the VLF/LF oscillations were similar to those of the Doppler velocities derived from beam 15 of

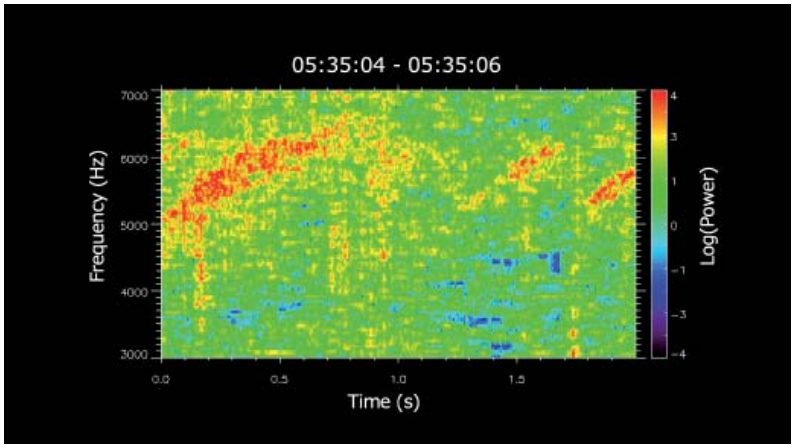

Figure 8. The dynamic spectrum of rising-tone chorus observed at ATHA during the VLF/LF oscillations at 05:35 UT on June 4, 2017.

the SuperDARN CVE radars, as seen in Figure 4. When the VLF/LF intensities decreased, the Doppler velocities became positive (toward the radar). If energetic electron precipitation occurs, the conductivity will increase and the VLF/LF intensity will decrease. This conductivity variation due to energetic electron precipitation may cause the Doppler velocity oscillation observed by the SuperDARN radar through polarization of the electric field. However, it is difficult to discuss the direction of this polarization electric field for the present event because we do not know the direction of the background ionospheric current. The other possible reason for the observed Doppler velocity oscillation is direct variation of the ionospheric electric field due to ULF pulsations [57, 58].

5. Conclusions

We have shown oscillations of VLF/LF transmitter signals (WWVB and NDK) observed at ATHA, Canada ($L = 4.3$), as signatures of energetic electron precipitation associated with Pi2 during a substorm at 05:25-05:45 UT on June 4, 2017. This is the first report of clear energetic electron precipitations modulated with Pi2 magnetic pulsation in the D-region ionosphere based on VLF/LF transmitter signals. Our conclusions can be summarized as follows:

1. The periods of the VLF/LF oscillations were 3 to 4 minutes based on wavelet analysis. The oscillation was characterized by a simultaneous periodic VLF/LF intensity decrease and VLF/LF phase advance. These features indicated periodic D-region ionization.

2. The solar wind speed and dynamic pressure did not show periodicity similar to the observed VLF/LF oscillations.

3. The Doppler velocity derived by the SuperDARN HF radars (the CVE radars) showed similar variation to the VLF/LF oscillations. Positive and negative Doppler velocities were seen over the WWVB-ATHA path during the VLF/LF oscillations, which corresponded to changes in the ionospheric electric field.

4. The ground-based ΔB_H at the same latitudes as the VLF/LF paths showed oscillations in the same periods as the VLF/LF oscillations over a wide longitude. The ΔB_H pulsations at the east-most site were earlier (by 75 s) than those at the west-most site, indicating propagation of the ULF waves with a longitudinal speed of 66.4 km/s from midnight to the dusk sector. The amplitude of the ΔB_H pulsations at the same longitudes as the VLF/LF paths in the pre-midnight sector was largest at 5 nT, and decreased at stations more remote from the VLF/LF paths.

5. The ΔB_H pulsations at low latitudes in the wide longitudes had the same periods as the VLF/LF oscillations, and were in-phase in all four magnetometers. The ΔB_H pulsations at ATHA slightly preceded those at the low-latitude stations. We concluded that the ULF oscillation shown in this study corresponded to the Pi2 pulsation associated with the observed substorm.

6. Rising-tone waves with a time scale of ~1 s were observed at ATHA in the frequency range of 5 kHz to 6 kHz during the VLF/LF oscillations. The characteristics of the rising-tone waves were similar to those of the whistler-mode chorus waves. Pitch-angle diffusion by chorus wave-particle interaction was one possible mechanism accounting for the energetic electron precipitation presented in this paper.

6. Acknowledgments

The VLF data (subionospheric propagation) used in this paper were accessed through the Planetary Plasma and Atmospheric Research Center (PPARC), Tohoku University (http://c.gp.tohoku.ac.jp/lf/). Solar wind data and geomagnetic indices were available through the OMNI database at (https://omiweb.gsfc.nasa.gov/). The ERG (Arase) satellite data were provided by the ERG Science Centre operated by the Institute of Space and Astronautical Science of the Japan Aerospace eXploration Agency (ISAS/JAXA) and ISEE, Nagoya University (https://

ergsc.isee.nagoya-u.ac.jp/index.shtml.en, [59]). PWE/HFA L2 ver01.01 was used to identify the plasmapause location. The ERG definitive orbit data (Level-2, ver. 02) were used to obtain the *L*-value of the satellite. The induction search coil magnetometer at ATHA was accessed through ISEE, Nagoya University, in facilities funded by the Canada Foundation for Innovation. The wideband VLF data (chorus waves) and search coil magnetometer data from the PWING project are available to the public from the ERG Science Center (https://ergsc.isee.nagoya-u.ac.jp/index.shtml.en). We thank I. R. Mann, D. K. Milling, and the rest of the CARISMA team for providing the induction search coil magnetometer data. CARISMA is operated by the University of Alberta and funded by the Canadian Space Agency. This work is supported by JSPS KAKENHI (15H05747, 15H05815, 16H06286). The Arase data were analyzed using the SPEDAS (the Space Physics Environment Data Analysis Software) framework [60] and ERG plug-in tools [59].

7. References

1. R. M. Thorne, and T. R. Larsen, "An investigation of relativistic electron precipitation events and their association with magnetospheric substorm activity," *Journal of Geophysical Research: Space Physics*, **81**, 31, 1976, pp. 5501-5506.

2. D. Jelly, and N. Brice, "Changes in Van Allen radiation associated with polar substorms," *Journal of Geophysical Research: Space Physics*, **72**, 1967, pp. 5919-5931.

3. T. Brito, L. Woodger, M. Hudson, and R. Millan, "Energetic radiation belt electron precipitation showing ULF modulation," *Geophysical Research Letters*, **39**, L22014, 2012.

4. Y. Miyoshi, S. Oyama, S. Saito, S. Kurita, H. Fujiwara, R. Kataoka, Y. Ebihara, C. Kletzing, G. Reeves, O. Santlik, M. Clilverd, C. J. Rodger, E. Turunen, and F. Tsuchiya, "Energetic electron precipitation associated with pulsating aurora: EISCAT and Van Allen Probe observations," *Journal of Geophysical Research: Space Physics*, **120**, 2015, pp. 2754-2766.

5. M. W. Chevalier, W. B. Peter, U. S. Inan, T. F. Bell, and M. Spasojevic, "Remote sensing of ionospheric disturbances associated with energetic particle precipitation using the South Pole VLF beacon," *Journal of Geophysical Research: Space Physics*, **112**, A11306, 2007.

6. C. J. Rodger, M. A. Clilverd, A. J. Kavanagh, C. E. J. Watt, P. T. Verronen, and T. Raita, "Contrasting the responses of three different ground-based instruments to energetic electron precipitation," *Radio Science*, **47**, RS2021, 2012.

7. M. A. Clilverd, C. J. Rodger, J. Brundell, J. Bahr, N. Cobbett, T. M.-Griffin, A. J. Kavanagh, A. Seppala, N. R. Thomson, R. H. W. Friedel, and F. W. Menk, "Energetic electron precipitation during substorm injection events: High-latitude fluxes and an unexpected midlatitude signature," *Journal of Geophysical Research: Space Physics*, **113**, A10311, 2008.

8. F. T. Berkey, V. M. Driatskiy, K. Henriksen, B. Hultqvist, D. H. Jelly, T. I. Shchuka, A. Theander, and J. Yliniemi, "A synoptic investigation particle precipitation dynamics for 60 substorms in IQSY (1964–1965) and IASY (1969)," *Planetary and Space Science*, **22**, 1974, pp. 255-307.

9. V. Belakhovsky, V. Pilipenko, D. Murr, and E. Kozlovsky, "Modulation of the ionosphere by Pc5 waves observed simultaneously by GPS/TEC and EISCAT," *Earth, Planets and Space*, **68**, 102, 2016.

10. J. Manninen, N. G. Kleimenova, O. V. Kozyreva, and T. Turunen, "Pc5 geomagnetic pulsations, pulsating particle precipitation, and VLF chorus: Case study on 24 November 2006," *Journal of Geophysical Research: Space Physics*, **115**, A00F14, 2010.

11. V. Pilipenko, V. Belakhovsky, D. Murr, E. Fedrov, and M. Engebretson, "Modulation of total electron content by ULF Pc5 waves," *Journal of Geophysical Research: Space Physics*, **119**, 2014, pp. 4358-4369.

12. X. Shi, J. M. Ruohoniemi, J. B. H. Baker, D. Lin, E. C. Bland, M. D. Hartinger, and W. A. Scales, "Survey of ionospheric Pc3-5 ULF wave signatures in SuperDARN high time resolution data," *Journal of Geophysical Research: Space Physics*, **123**, 2018, pp. 4215-4231.

13. T. Motoba, K. Takahashi, J. Gjerloev, S. Ohtani, and D.K. Milling, "The role of compressional Pc5 pulsations in modulating precipitation of energetic electrons," *Journal of Geophysical Research: Space Physics*, **118**, 2013, pp. 7728-7739.

14. A. Asnes, J. Stadsnes, J. Bjordal, N. Østgaard, D. L. Detrick, T. J. Rosenberg, and S. E. Haaland, "Pi2-pulsations observed in energetic electron precipitation and magnetic field in association with a substorm surge," *Annales Geophysicae*, **22**, 2004, pp. 2097-2105.

15. O. Saka, O. Watanabe, K. Okada, and D. N. Baker, "A slow mode wave as a possible source of Pi 2 and associated particle precipitation: a case study," *Annales Geophysicae*, **17**, 1999, pp. 674-681.

16. S. Tsunomura, T. Uwai, Y. Yamada, K. Hasegawa, F. Fukui, S. Toyodome, and M. Kuwashima, "Characteristics of geomagnetic variations associated with low latitude auroras," *Memoirs of the Kakioka magnetic observatory*, **24**, 1990, pp. 25-38.

17. F. V. Coroniti, and C. F. Kennel, "Electron precipitation pulsations," *Journal of Geophysical Research: Space Physics*, **75**, 1970, pp. 1279-1289.

18. D. Summers, and R. M. Thorne, "Relativistic electron pitch-angle scattering by electromagnetic ion cyclotron waves during geomagnetic storms," *Journal of Geophysical Research*, **108**, A4, 1143, 2003, doi:10.1029/2002JA009489.

19. Y. Omura, and Q. Zhao, "Relativistic electron microbursts due to nonlinear pitch angle scattering by EMIC triggered emissions," *Journal of Geophysical Research: Space Physics*, **118**, 2013, pp. 5008-5020.

20. Y. Miyoshi, K. Sakaguchi, K. Shiokawa, D. Evans, J. Albert, M. Conners, and V. Jordanova, "Precipitation of radiation belt electrons by EMIC waves, observed from ground and space," *Geophysical Research Letters*, **35**, L23101, 2008.

21. R. Rasinkangas, K. Mursula, G. Kremser, H. Singer, B. Fraser, A. Korth, and W. Hughes, "Simultaneous occurrence of Pc 5 and Pc 1 pulsations in the dawnside magnetosphere: CRRES observations," *Geophysical Monograph-American Geophysical Union*, **81**, 1994, pp. 417-424.

22. E. Donovan, S. B. Mende, B. Jackel, H. U. Frey, M. Syrjasuo, I. Voronkov, T. Trondsen, L. M. Peticolas, V. Angelopoulos, S. E. Harris, M. Greffen, and M. Connors, "The THEMIS all-sky imaging array – system design and initial results from the prototype imager," *Journal of Atmospheric and Solar-Terrestrial Physics*, **68**, 2006, pp. 1472-1487.

23. S. B. Mende, S. E. Harris, H. U. Frey, V. Angelopoulos, C. T. Russel, E. Donovan, B. Jackel, M. Greffen, and L. M. Peticolas, "The THEMIS array of ground-based observatories for the study of auroral substorms," *Space Science Review*, **141**, 2008, pp. 357-387.

24. K. Shiokawa et al., "Ground-based instruments of the PWING project to investigate dynamics of the inner magnetosphere at subauroral latitudes as a part of the ERG-ground coordinated observation network," *Earth, Planets and Space*, **69**, 160, 2017.

25. I. R. Mann, D. K. Milling, I. J. Rae, L. G. Ozeke, A. Kale, Z. C, Kale, K. R. Murphy, A. Parent, M. Usanova, D. M. Pahud, E.-A. Lee, V. Amalraj, D. D. Wallis, V. Angelopoulos, K.-H. Glassmeier, C. T. Russel, H.-U. Auster, and H. J. Singer, "The upgraded CARISMA magnetometer array in the THEMIS era," *Space Science Review*, **141**, 2008, pp. 413-451.

26. N. Nishitani, J. M. Ruohoniemi, M. Lester, J. B. H. Baker, A. V. Koustov, S. G. Shepherd, G. Chisham, T. Hori, E. G. Thomas, R. A. Makarevich, A. Marchaudon, P. Ponomarenko, J. A. Wild, S. E. Milan, W. A. Bristow, J. Devlin, E. Miller, R. A. Greenwald, T. Ogawa, and T. Kikuchi, "Review of the accomplishments of mid-latitude Super Dual Auroral Radar Network (SuperDARN) HF radars," *Progress in Earth and Planetary Science*, **6**, 27, 2019.

27. K. R. Murphy, A . R. Inglis, D. G. Sibeck, I. J. Rae, C. E. J. Watt, M. Silveira, F. Plaschke, S. G. Claudepierre, and R. Nakamura, "Determining the mode, frequency, and azimuthal wave number of ULF waves during a HSS and moderate geomagnetic storm," *Journal of Geophysical Research: Space Physics*, **123**, 2018, pp. 6457-6477.

28. T. Sakurai and T. Saito, "Magnetic pulsation Pi2 and substorm onset," *Planetary and Space Science*, **24**, 6, 1976, pp. 573-575.

29. T. Uozumi, K. Yumoto, H. Kawano, A. Yoshikawa, S. Ohtani, J. V. Olson, S.-I. Akasofu, S. I. Solovyev, E. F. Vershinin, K. Liou, and C.-I. Meng, "Propagation characteristics of Pi 2 magnetic pulsations observed at ground high latitudes," *Journal of Geophysical Research*, **109**, A08203, 2004.

30. T. Kitamura, O. Saka, M. Shimoizumi, H. Tachihara, T. Oguti, T. Araki, N. Sato, M. Ishitsuka, O. Veliz, and J. B. Nyobe, "Global Mode of Pit Waves in the Equatorial Region – Difference of Pit Mode Between High and Equatorial Latitudes," *Journal of Geomagnetism and Geoelectricity*, **40**, 1988, pp. 621-634.

31. M. Shinohara, K. Yumoto, A. Yoshikawa, O. Saka, S. I. Solovyev, E. F. Vershinin, N. B. Trivedi, J. M. Da Costa, and The 210°MM Magnetic Observation Group, "Wave characteristics of daytime and nighttime Pi2 pulsations at the equatorial and low latitudes," *Geophysical Research Letters*, **24**, 18, 1997, pp. 2279-2282.

32. M. Nose, K. Liou, and P. R. Sutcliffe, "Longitudinal dependence of characteristics of low-latitude Pi2 pulsations observed at Kakioka and Hermanus," *Earth Planets Space*, **58**, 2006, pp. 775-783.

33. R. L. Kessel, "Solar wind excitation of Pc5 fluctuations in the magnetosphere and on the ground," *Journal of Geophysical Research*, **113**, A04202, 2008.

34. J. M. Cornwall, "Cyclotron instabilities and electromagnetic emission in the ultra low frequency and very low frequency ranges," *Journal of Geophysical Research*, **70**, 1, 1965, pp. 61-69.

35. R. E. Erlandson, K. Mursula, and T. Bosinger, "Simultaneous ground-satellite observations of structured Pc-1 pulsations," Journal of Geophysical Research, 101, A12, 1996, pp. 27149-27156.

36. C. J. Rodger, T. Raita, M. A. Clilverd, A. Seppälä, S. Dietrich, N. R. Thomson, and T. Ulich, "Observations of relativistic electron precipitation from the radiation belts driven by EMIC waves," *Geophysical Research Letters*, **35**, L16106, 2008.

37. A. Hirai, F. Tsuchiya, T. Obara, Y. Kasaba, Y. Katoh, H. Misawa, K. Shiokawa, Y. Miyoshi, S. Kurita, S. Matsuda, M. Connors, T. Nagatsuma, K. Sakaguchi, Y. Kasahara, A. Kumamoto, A. Matsuoka, M. Shoji, I. Shinohara, J. M. Albert, "Temporal and spatial correspondence of Pc1/EMIC waves and relativistic electron precipitations observed with ground-based multi-instruments on 27 March 2017," *Geophysical Research Letters*, **45**, 2018, pp. 13182-13191.

38. M. Ozaki, K. Shiokawa, Y. Miyoshi, R. Kataoka, M. Connors, T. Inoue, S. Yagitani, Y. Ebihara, C.-W. Jun, R. Nomura, K. Sakaguchi, Y. Otsuka, H. A. Uchida, I. Schofield, and D. W. Danskin, "Discovery of 1 Hz range modulation of isolated proton aurora at subauroral latitudes," *Geophysical Research Letters*, **45**, 2018, pp.1209-1217, https://doi.org/10.1002/2017GL076486.

39. M. Ozaki, K. Shiokawa, Y. Miyoshi, K. Hosokawa, S. Oyama, S. Yagitani, S., Y. Kasahara, Y. Kasaba, S. Matsuda, R. Kataoka, Y. Ebihara, Y. Ogawa, Y. Otsuka, S. Kurita, R. C. Moore, Y.-M. Tanaka, M. Nosé, T. Nagatsuma, M. Connors, N. Nishitani, Y. Katoh, M. Hikishima, A. Kumamoto, F. Tsuchiya, A. Kadokura, T. Nishiyama, T. Inoue, K. Imamura, A. Matsuoka, and I. Shinohara, "Microscopic observations of pulsating aurora associated with chorus element structures: Coordinated Arase satellite-PWING observations," *Geophysical Research Letters*, **45**, 2018, pp. 12,125-12,134, https://doi.org/10.1029/2018GL079812.

40. M. Ozaki, Y. Miyoshi, K. Shiokawa, K. Hosokawa, S.-I. Oyama, R. Kataoka, Y. Ebihara, Y. Ogawa, Y. Kasahara, S. Yagitani, Y. Kasaba, A. Kumamoto, F. Tsuchiya, S. Matsuda, Y. Katoh, M. Hikishima, S. Kurita, Y. Otsuka, R. C. Moore, Y. Tanaka, M. Nosé, T. Nagatsuma, N. Nishitani, A. Kadokura, M. Connors, T. Inoue, A. Matsuoka, and I. Shinohara, "Visualization of rapid electron precipitation via chorus element wave-particle interactions," *Nature Communications*, **10**, 257, 2019.

41. Y. Miyoshi, Y. Katoh, T. Nishiyama, T. Sakanoi, K. Asamura, and M. Hirahara, "Time of flight analysis of pulsating aurora electrons, considering wave-particle interactions with propagating whistler mode waves," *Journal of Geophysical Research*, **115**, A10312, 2010.

42. Y. Miyoshi, S. Saito, K. Seki, T. Nishiyama, R. Kataoka, K. Asamura, Y. Katoh, Y, Ebihara, T. Sakanoi, M. Hirahara, S. Oyama, S. Kurita, and O. Santolik "Relation between fine structure of energy spectra for pulsating aurora electrons and frequency spectra of whistler mode chorus waves," *Journal of Geophysical Research: Space Physics*, **120**, 2015, pp. 7728-7736.

43. S. Kasahara, Y. Miyoshi, S. Yokota, T. Mitani, Y. Kasahara, S. Matsuda, A. Kumamoto, A. Matsuoka, Y. Kazama, H. U. Frey, V. Angelopoulos, S. Kurita, K. Seki, and I Shinohara, "Pulsating aurora from electron scattering by chorus waves," *Nature*, **554**, 2018, pp. 337-340.

44. R. B. Horne, and R. M. Thorne, "Relativistic electron acceleration and precipitation during resonant interactions with whistler-mode chorus," *Geophysical Research Letters*, **30**, 1527, 2003.

45. F. Tsuchiya, A. Hirai, T. Obara, H. Misawa, S. Kurita, Y. Miyoshi, K. Shiokawa, M. Connors, M. Ozaki, Y. Kasahara, A. Kumamoto, A. Kasaba, A. Matsuoka, M. Shoji, and I. Shinohara, "Energetic electron precipitation associated with pulsating aurora observed by VLF radio propagation during the recovery phase of a substorm on 27 March 2017," *Geophysical Research Letters*, **45**, 2018, pp. 651-660.

46. M. Grandin, A. Kero, N. Partamies, D. McKay, D. Whiter, A. Kozlovsky, and Y. Miyoshi, "Observation of pulsating aurora signatures in cosmic noise absorption data," *Geophysical Research Letters*, **44**, 2017, pp. 5292-5300.

47. M. Ozaki, S. Yagitani, I. Nagano, Y. Hata, H. Yamagishi, N. Sato, and A. Kadokura, "Localization of VLF ionospheric exit point by comparison of multipoint ground-based observation with full-wave analysis," *Polar Sci.*, **2**, 4, 2008, pp. 237-249.

48. S. Teng, X. Tao, Y. Xie, F. Zonca, L. Chen, W. B. Fang, and S. Wang, "Analysis of the duration of rising tone chorus elements," *Geophysical Research Letters*, **44**, 2017, pp. 12074-12082.

49. J.-H. Shue, Y. Nariyuki, Y. Katoh, S. Saito, Y. Kasahara, Y.-K Hsieh, S. Matsuda, Y. Goto, "A systematic study in characteristics of lower band rising-tone chorus elements," *Journal of Geophysical Research: Space Physics*, **124**, 2019, pp. 9003-9016.

50. N. A. Tsyganenko, "A model of magnetosphere with a dawn-dusk asymmetry: 2. Parameterization and fitting to observations," *Journal of Geophysical Research*, **107**, A8, 1176, 2002.

51. N. A. Tsyganenko, and M. I. Sitnov "Modeling the dynamics of the inner magnetosphere during strong geomagnetic storms," *Journal of Geophysical Research*, **110**, A3, 2005.

52. A. Artemyev, O. Agapitov, D. Mourenas, V. Krasnoselskikh, V. Shastun, and F. Mozer, "Oblique whistler-mode waves in the Earth's inner magnetosphere: Energy distribution, origins, and role in radiation belt dynamics," *Space Science Reviews*, **200**, 2016, pp. 261-355.

53. Y. Miyoshi, I. Shinohara,, T. Takashima, K. Asamura, N. Higashio, T. Mitani, S. Kasahara, S. Yokota, Y. Kazama, S.-Y. Wang, S. W. Tam, P. T. P Ho, Y. Kasahara, Y. Kasaba, S. Yagitani, A. Matsuoka, H. Kojima, H. Katoh, K. Shiokawa, and K. Seki, "Geospace Exploration Project ERG," *Earth, Planets and Space*, **70**, 101, 2018a.
54. A. Kumamoto, F. Tsuchiya, Y. Kasahara, Y. Kasaba, H. Kojima, S. Yagitani, K. Ishisaka, T. Imachi, M. Ozaki, S. Matsuda, M. Shoji, A. Matsuoka, Y. Katoh, Y. Miyoshi, and T. Obara, "High frequency analyzer (HFA) of plasma wave experiment (PWE) onboard the Arase spacecraft," *Earth, Planets and Space*, **70**, 82, 2018.

55. Y. Kasahara, Y. Kasaba, H. Kojima, S. Yagitani, K. Ishisaka, A. Kumamoto, F. Tsuchiya, M. Ozaki, S. Matsuda, T. Imachi, Y. Miyoshi, M. Hikishima, Y. Katoh, M. Ota, M. Shoji, A. Matsuoka, and I. Shinohara, "The plasma wave experiment (PWE) on board the Arase (ERG) satellite," *Earth, Planets and Space*, **70**, 86, 2018.

56. R. T. Tsunoda, "High-Latitude F Region Irregularities: A Review and Synthesis," *Reviews of Geophysics*, **26**, 4, 1988, pp. 719-760.

57. M. Teramoto, N. Nishitani, Y. Nishimura, and T. Nagatsuma, "Latitudinal dependence on the frequency of Pi2 pulsations near the plasmapause using THEMIS satellites and Asian-Oceanian SuperDARN radars," *Earth, Planets and Space*, **68**, 22, 2016.

58. M. Teramoto, N. Nishitani, V. Pilipenko, T. Ogawa, K. Shiokawa, T. Nagatsuma, A. Yoshikawa, D. Baishev, and K. T. Murata, "Pi2 pulsation simultaneously observed in the E and F region ionosphere with the SuperDARN Hokkaido radar," *Journal of Geophysical Research: Space Physics*, **119**, 2014, pp. 3444-3462.

59. Y. Miyoshi, T. Hori, M. Shoji, M. Teramoto, T. F. Chang, S. Matsuda, S. Kurita, T. Segawa, N. Umemura, K. Keika, Y. Miyashita, Y. Tanaka, N. Nishitani, T. Takashima, and I. Shinohara, "The ERG Science Center," *Earth, Planets and Space*, **70**, 96, 2018b.

60. V. Angelopoulos, P. Cruce, A. Drozdov, E. W. Grimes, N. Hatzigeorgiu, et al., "The space physics environment data analysis system (SPEDAS)," *Space Science Review*, **215**, 9, 2019.

Et Cetera

Tayfun Akgül
Istanbul Technical University
Dept. of Electronics and Communications Engineering
Telecommunications Division
80626 Maslak Istanbul, Turkey
Tel: +90 212 285 3605; Fax: +90 212 285 3565
E-mail: tayfunakgul@itu.edu.tr.

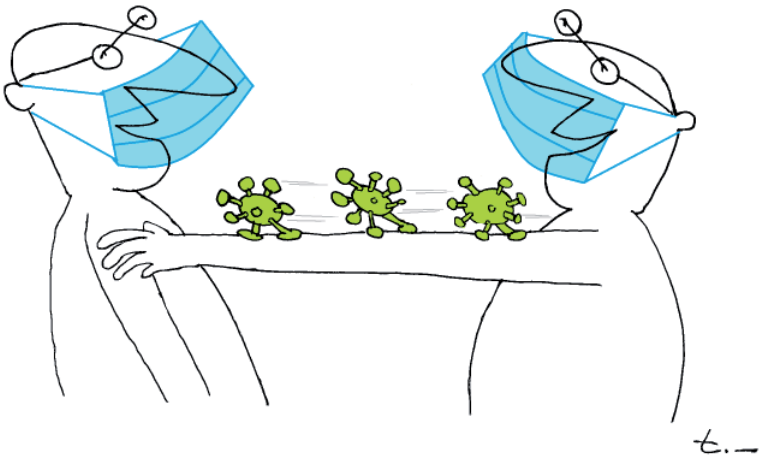

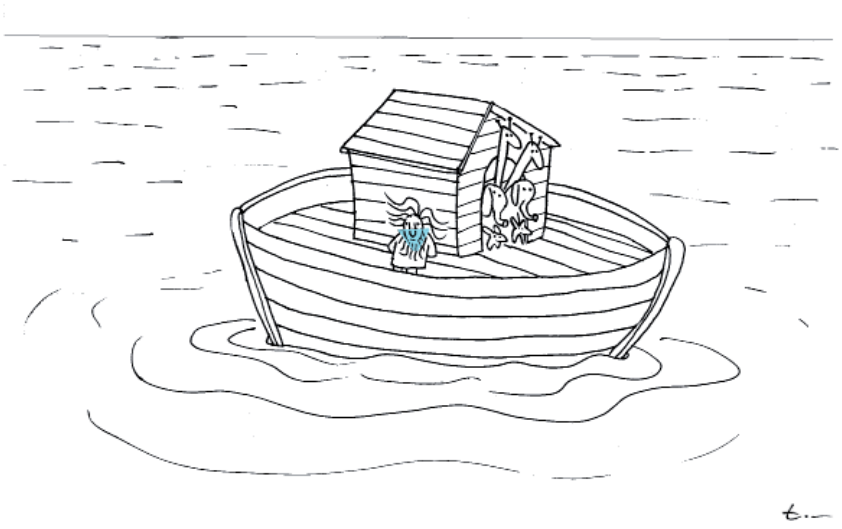

Book Review

George Trichopoulos
Electrical, Computer & Energy Engineering ISTB4 555D
Arizona State University
781 E Terrace Road, Tempe, AZ, 85287 USA
Tel: +1 614 364 2090
E-mail: gtrichop@asu.edu

Rocks, Radio and Radar: The Extraordinary Scientific, Social and Military Life of Elizabeth Alexander by Mary Harris, Singapore, World Scientific Publishing Co., 2019, ISBN 978-1-78634-664-3 (hardcover), ISBN 978-1-78634-666-7 (electronic).

This memoir of pioneering scientist and educator Frances Elizabeth Somerville Alexander is an excellent example of not only STEM research, but also interdisciplinary research in geology, physics, and electromagnetics. In the recent New Zealand government declassified World War II documents, Elizabeth was described as the world's first radio astronomer by the then director, Wayne Orchiston, of the Carter observatory in Wellington. Her life work straddled four continents in colonial England, including the countries of India, Singapore, Malaysia, New Zealand, Australia, and Nigeria. She was one of those forgotten world wartime revolutionary scientists that had to be resurfaced by her well-wishers rather than her colleagues or the respective engineering societies.

The author of the memoir is Elizabeth's daughter, who is an accomplished scientist. Dr. Mary Harris has done exquisitely detailed work in collecting and describing the socio-economic, cultural, political, and military history of the era based on Elizabeth's personal diary, scientific articles, unclassified government records, archived materials in government organizations, museums, and personal knowledge. I also believe that one of the major contributions of Elizabeth and Norman scientists is their overwhelming involvement in building and rebuilding the STEM educational institutions both in Singapore and Malaysia.

The book describes the detailed scientific work of Alexander, such as radio direction finding, Norfolk effect, and geological map of Singapore, etc. However, the book provides an amazing roadmap of the science and scientific laboratory activities and power struggle of the countries during the first and second world wars. It is also a window into the accomplished scientist lifestyle in colonial England, as well. Even though the scientists belonged to the middle class in England, they had very lavish and respectful social status in the colonies, such as India, Singapore, and Nigeria, etc. Working women or not, while living in Singapore, the English women didn't need to burden themselves with taking care of their children or household work. It was all taken care of by the servants and Ayahs. It is an account of English, Australian, and New Zealand scientists that were the privileged under colonialism. Job opportunity was endless for English scientists as long as they wanted to leave England. The book is also a good read on some relevant historical aspects of colonial England, such as the opium trade, indigo farming, etc., which economically benefited England and oppressed the natives. It provides a detailed description of the beginning of commercial intercontinental flights that included frequent overnight stops, and boat travel and other transportation of the time.

Alexander did have miserable war-time living as a single mother of three in New Zealand for three years, when she had to leave everything behind in Singapore, and her husband became a prisoner of war in Singapore. Those three years were also one of her most productive times as a professional. I believe that shows her strength and resilience the most as a woman scientist.

Even 100 years after Elizabeth was born, women in STEM research are still a minority. Unfortunately, even in the 21st century, they still have to go extra miles to survive and be recognized in the field. This book again proves that throughout history, life is different for women in any society if they belong to the privileged class. As a privileged class, opportunities for women were available for them to be successful. Overall, this is a very interesting book for not only scientists or historians, but for all readers that are interested in that era's lifestyle.

Niru K. Nahar
ElectroScience Laboratory
Dept. of Electrical and Computer Engineering
The Ohio State University
1330 Kinnear Rd, Columbus, OH 43212
E-mail: nahar.2@osu.edu

Özgür Ergül
Department of Electrical and Electronics Engineering
Middle East Technical University
TR-06800, Ankara, Turkey
E-mail: ozergul@metu.edu.tr

SOLBOX-19: Nano-Optical Diodes

Gökhan Karaova, Tuna Atmaz, and Özgür Ergül

Department of Electrical and Electronics Engineering
Middle East Technical University
TR-06800, Ankara, Turkey
E-mail: ozergul@metu.edu.tr

1. Introduction

The design and analysis of nano-optical structures involving nanoparticles has been discussed several times in previous issues of this column, e.g., see SOLBOX-08 [1] and SOLBOX-16 [2] for nano-optical couplers, and SOLBOX-13 [3] for nano-arrays. Given a grid of nanoparticles, the general aim is to reach a configuration by keeping/deleting nanoparticles such that the final structure operates as desired. In the case of nano-optical couplers, the designed configurations provide efficient transmission of electromagnetic waves through sharp bends and corners, while they also allow for diverse transmission options at junctions. Despite their geometric simplicity, such couplers can hence enable the construction of complex nano-optical networks. In the case of nano-arrays, similar nanoparticle configurations are used for beam shaping, particularly to obtain directional radiation from isotropic sources. On the other hand, in all these cases easy-to-define geometrical properties and design specifications turn out to be remarkably challenging computational problems. Using surface integral equations, the numbers of unknowns can be maintained at reasonable levels; however, large numbers of possible configurations make it impossible to test each candidate design to find the best design. For this reason, an in-house implementation of genetic algorithms was used in [1-3] to limit the number of simulations, while reaching satisfactory results. It was shown that successful coupler and array designs can be obtained via several thousands (instead of billions) of trials per optimization.

Combining a full-wave solver with genetic algorithms or similar heuristic optimization techniques is a well-known practice in computational electromagnetics, which leads to powerful tools for designing electromagnetic structures and systems. Freedom of choosing the cost function provides diverse design options to achieve unprecedented abilities in terms of scattering, radiation, reflection, and transmission. This is particularly important in the context of metallic nano-optical structures, where the plasmonic properties of metals result in surprisingly powerful and often unpredictable responses, leading to enhanced electromagnetic transmission and focusing. These responses are generally difficult to control and manipulate, making design procedures much more crucial in comparison to other sub-areas. In this issue of Solution Box (SOLBOX-19), the optimization mechanism used in [1-3] was employed to design challenging structures, namely nano-optical diodes, that had unidirectional transmission properties.

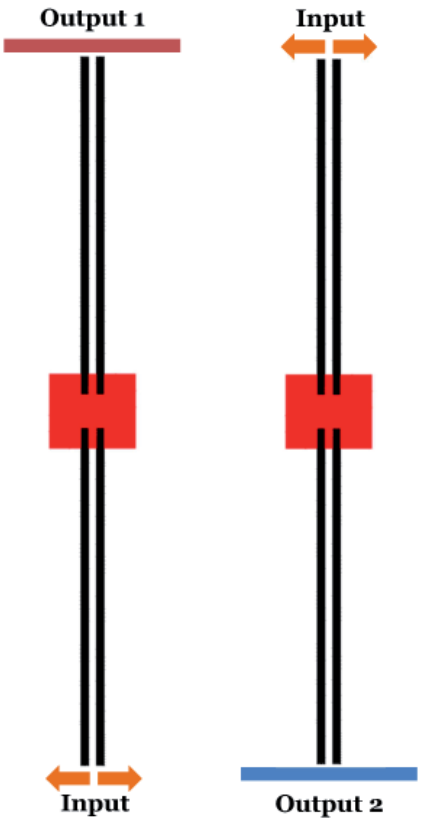

Figure 1. A general illustration of the inputs and outputs for the diode design problem. The diode was located between two nanowire segments that were not directly connected to each other.

This time, each optimization trial was a combination of two simultaneous full-wave simulations, which may be difficult to handle without using a heuristic algorithm. In addition to successful designs, numerical examples were shown to demonstrate sensitive characteristics of the designs. It should be emphasized that such unidirectional structures (via completely other approaches) were topics of much intensive research [4-8], as they may enable logic operations to build nano-optical circuits.

As for all problems considered so far in this column, alternative solutions to the presented design problems are welcome. Interested readers can send their solutions and results, as well as comments to share their experiences in computational electromagnetics. In addition to competitive simulations of the previous problems, readers can also submit their own interesting problems and sample solutions. This can be done to demonstrate either the effectiveness or the ineffectiveness of a method applied to a set of problems. Eventually, these experiences will be beneficial for all of us.

2. Problem SOLBOX-19

In SOLBOX-19, we considered steady-state electromagnetic transmission along pairs of Ag nanowires located in vacuum. Each nanowire had a 120 nm × 120 nm square cross section, while the surface-to-surface distance between the nanowires of a pair was set to 140 nm. The excitation was always a pair of Hertzian dipoles symmetrically located 200 nm away from the tips of the nanowire. In all simulations presented here, the frequency was fixed at 250 THz, whereas the constructed systems could operate in wide frequency bands of the optical regime. At 250 THz, the complex relative permittivity of Ag is $-60.8 + i4.31$, where i represents the imaginary unit. With this property, Ag nanowires are known to demonstrate excellent performance in transmitting electromagnetic power. The general optimization problem, which is simply illustrated in Figure 1, can be described as follows. Given two segments of nanowire pairs that are not physically connected (in the examples, a 660 nm gap exists between the tips), design a structure located between them that has a diode-like behavior to provide a unidirectional transmission ability. Specifically, the overall system should transmit the signal when it is excited from one side (the "on" state for Output 1), while it should not transmit (or poorly transmit, as much as possible) when it is excited from the other side (the "off" state for Output 2). For the examples presented below, each nanowire segment was assumed to have a length of 5 μm, so that an overall structure involving two segments and the designed component (diode) was slightly longer than 10 μm.

Similarly to the nanostructures considered in SOLBOX-8, SOLBOX-13, and SOLBOX-16, we considered grids of nano-cubes to design the desired diode components, while other options could be considered depending on the desired performance (in terms of on-off sensitivity, size, complexity, etc.) and application. Considering nano-cubes, the optimization problem could be described in more detail as follows: Given an 11 × 11 grid of nano-cubes (excluding those coinciding with nanowires), find which nano-cubes should be extracted or kept in order to obtain the best diode performance. Each nano-cube had 120 nm × 120 nm × 120 nm dimensions, while the surface-to-surface distance between them was fixed at 10 nm. The grid hence surrounded the tips of the nanowires from both two segments and filled the gap between them, but still without any physical contact (see examples below). To evaluate the performance of the candidate diode designs, alternative cost functions can be defined and used, again depending on the application. In any case, we were looking for both quantitative and qualitative data to demonstrate the effectiveness (or ineffectiveness) of the final designs.

3. Solution to Problem SOLBOX-19

3.1 Solution Summary

Solver type (e.g., Noncommercial, commercial): Noncommercial research-based code developed at CEMMETU, Ankara, Turkey

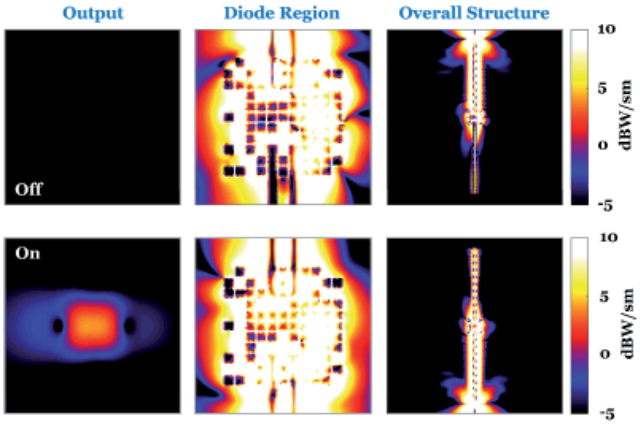

Figure 2. The results of an optimization to obtain unidirectional transmission characteristics. The designed diode structure consisted of 70 nano-cubes.

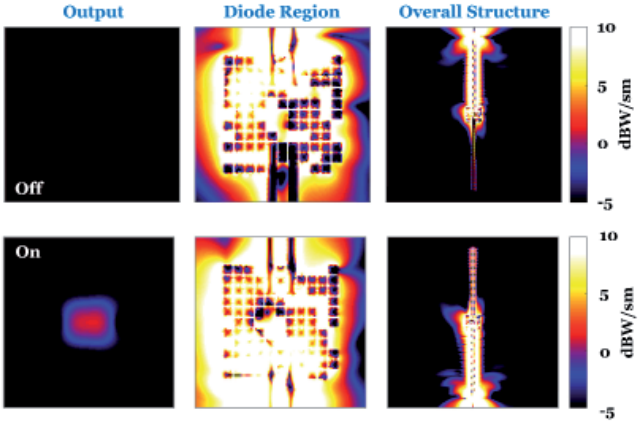

Figure 3. The results of an optimization to obtain unidirectional transmission characteristics. The designed diode structure consisted of 76 nano-cubes.

Solution core algorithm or method: Frequency-domain MLFMA + genetic algorithms
Programming language or environment (if applicable): *MATLAB +MEX*
Computer properties and resources used: 2.5 GHz Intel Xeon E5-2680v3 processors (using 32 cores)
Total time required to produce the results shown (categories: < 1 sec, < 10 sec, < 1 min, < 10 min, < 1 hour, < 10 hours, < 1 day, < 10 days, > 10 days): < 10 days per optimization, < 1 minute per problem, < 10 minutes for the problem in Figures 6 and Figure 7.

3.2 Short Description of the Numerical Solutions

The optimization problems described in SOLBOX-19 were considered and solved by using the mechanism presented in SOLBOX-08. In summary, the mechanism was an efficient combination of genetic algorithms and the Multilevel Fast Multipole algorithm (MLFMA) [9]. The in-house implementation of genetic algorithms involved improved operations such as success-based mutations and family elitism [10], while it was combined with MLFMA via dynamic accuracy control [11]. Using pools of 40 individuals, each optimization was carried out for a maximum of 200 generations, leading to total of $8000 \times 2 = 16,000$ simulations by MLFMA or its approximate form. The MLFMA solver was particularly designed for efficient analysis of plasmonic structures [12]. The main formulation was selected as the modified combined tangential formulation (MCTF) that provided both accurate and efficient solutions of homogeneous plasmonic objects [13]. The MCTF was discretized by using the conventional Rao-Wilton-Glisson (RWG) functions on triangular domains [14]. Using $\lambda/10$ triangles, where λ is the wavelength in vacuum, the number of unknowns was smaller than 20,000 for an optimization problem involving two nanowire segments. It should be noted that an extraction of a nano-cube corresponded to the deletion of the related rows and columns (corresponding to the RWG functions located on the extracted nano-cube) in the impedance matrix. For the large problem shown in the last example below (see Figures 6 and 7), the number of unknowns was approximately 70,000. MLFMA solutions were further accelerated via an inner-outer scheme [15], where approximate forms of MLFMA were used for preconditioning.

In the examples presented below, the success of a diode was defined based on the transmission characteristics in the "on" and "off" states. For this purpose, 900 nm × 900 nm output frames were defined at a 120 nm distance from the nanowire tips. A diode was then considered to be successful if (1) the overall output power was higher for the "on" state in comparison to the "off" state, (2) the power distribution at the output varied significantly for the "on" state, and (3) the power distribution at the output was uniform as much as possible for the "off" state. Depending on the application, only (1) could be used, while constraints (2) and (3) could be useful to avoid faults and misinterpretation of signals when the designed diode was used in more complex scenarios. For the visualization of the results, the absolute value of the complex power density was sampled in the output frames, as well as at various locations in the vicinities of the structures. Considering MLFMA simulations and near-zone power computations, any numerical result was estimated to have a maximum 1% error.

3.3 Results

Figures 2 and 3 present the results obtained from two different optimization trials. In each case, the power density was plotted in the output frames and in the diode region for both the "on" and "off" states. In addition, the corresponding power distributions are shown for the overall structure (again for both states). Snapshots of the diode region demonstrated complex interactions between the kept nano-cubes and nanowires. As was evident from the output and overall plots, the designed diodes involving 70 and 76 nano-cubes, respectively, provided quite unidirectional

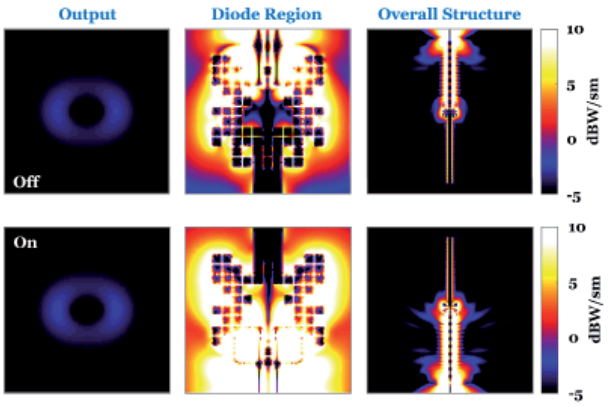

Figure 4. The results of an optimization to obtain unidirectional transmission characteristics. Vertical-line asymmetry was enforced in the diode design. The structure consisted of 61 nano-cubes.

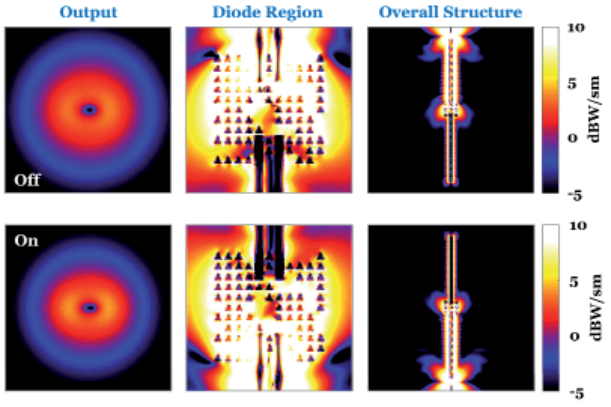

Figure 5. The power density distributions when the diode structure shown in Figure 3 consisted of nano-prisms instead of the original nano-cubes.

operations. Considering the diode in Figure 2, the mean/maximum power density values were −8.56 dB/−5.20 dB for the "off" state, while they were −4.26 dB/4.17 dB for the "on" state. Considering the diode in Figure 3, these values were −13.0 dB/−9.41 dB and −7.31 dB/1.20 dB, respectively, for the "off" and "on" states. Considering the peak power values, the on-off margins were hence 9.37 dB (for the diode in Figure 2) and 10.61 dB (for the diode in Figure 3). Visually, the results in Figure 2 and Figure 3 showed that both diodes provided non-detectable outputs in "off" states, while beam-like outputs were achieved in "on" states when using [−5,10] dB dynamic range.

Although not considered here, a detailed examination of the designed diodes showed that they achieved unidirectional operation thanks to their vertical-line asymmetry. Horizontal-line asymmetry was already expected before optimization trials (otherwise, the whole structure and its response would be perfectly bidirectional), whereas vertical-line asymmetry seemed to also be favored when genetic algorithms reach successful design candidates. To check this, another optimization was carried out by enforcing vertical-line symmetry, leading to the results depicted in Figure 4. In this figure, plots for the best design at the end of the optimization are shown, while we observed quite bidirectional operation with almost identical responses in the "on" and "off" states. Vertical-line asymmetry hence seemed to be crucial to obtain a unidirectional response from a diode.

While the diode designs such as shown in Figure 2 and Figure 3 provided quite successful performance in terms of unidirectional operation, they seemed to be sensitive to some geometrical properties. These were in fact commonly observed in similar coupler and array designs that involved metallic nanoparticles at optical frequencies [1-3]. Structures were generally robust against location and orientation errors, whereas geometries of nanoparticles often have large impacts on the performance of the designs. This must be considered carefully, especially if a design is to be fabricated, and fabrication errors tend to make significant variations in nanoparticle geometries. If possible, this type of uncertainty should be included the design stage, i.e., when the optimal structure is being found.

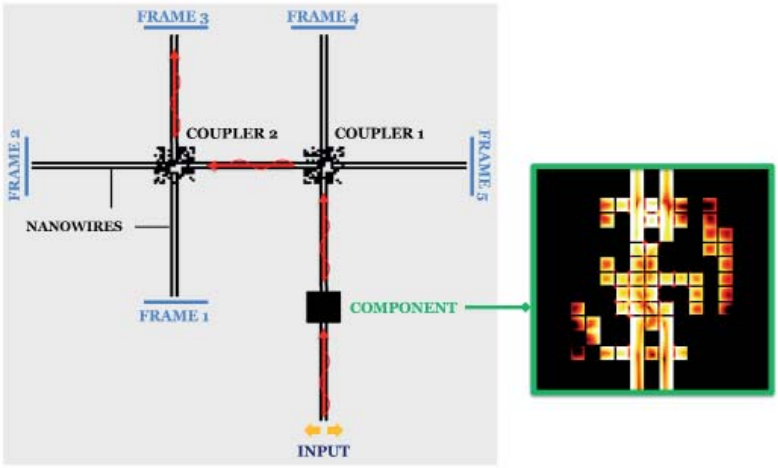

Figure 6. A nano-optical system involving nanowire segments and two couplers, as well as a diode to improve the transmission.

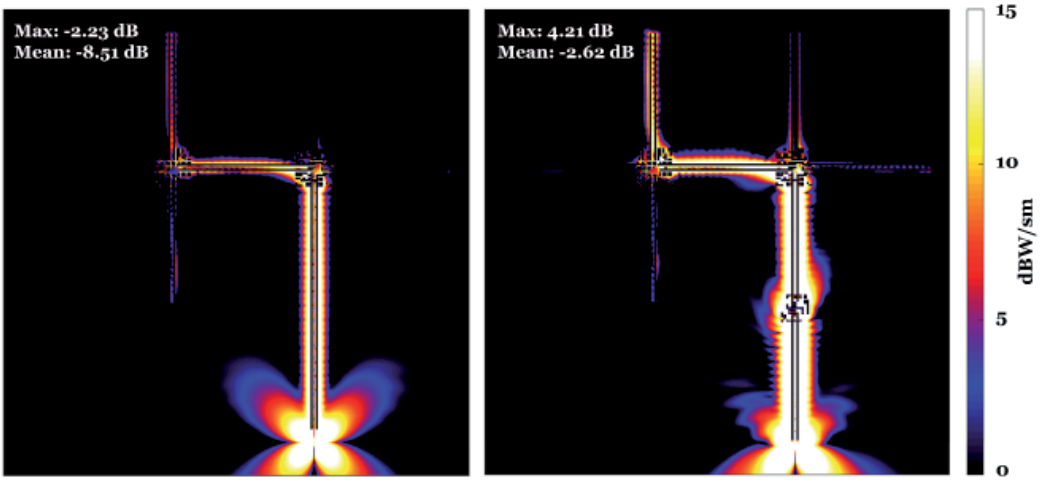

Figure 7. The power density distributions for the system in Figure 6 with (right) and without (left) the designed diode. When there was no diode, the related nanowire segments were directly connected to each other.

To demonstrate the effect of particle shape on the performance of a diode, we reconsidered the design in Figure 3, while the nano-cubes were replaced by nano-prisms with triangular cross sections. Investigating the results in Figure 5, particularly in comparison to those in Figure 3, we observed that the design completely lost its diode-like operation when the particle geometry was changed. Specifically, relatively high transmission was observed in both "on" and "off" states, with 4.17 dB and 3.61 dB peak power density values, respectively, at the corresponding outputs.

Finally, we present the results when a designed diode was used to improve the function of a larger system. Figure 6 presents the overall structure involving multiple nanowire segments connected via two couplers. The coupler designs were taken from [16], and with the given configurations, they provided efficient transmission to Frame 3. The diode (component) was used to improve the transmission on the input side. Specifically, it was designed to maximize/minimize the power transmission in the forward/backward direction, without considering any uniformity at its outputs. Figure 7 depicts the power density distributions with and without the diode. When the diode was not used, the reflected waves from the first coupler (as the coupler was not perfect) traveled back towards the input tips and radiated into vacuum. However, using the diode waves passing through the diode were trapped between the diode and the coupler, eventually leading to a more efficient overall transmission through the coupler. Considering the output frame (Frame 3 in Figure 6), the maximum power density was increased from −2.23 dB to 4.21 dB simply by integrating the diode into the system. It was remarkable that the diode was used between two unconnected nanowire segments, while it provided better results than the case when there was no discontinuity and the segments were directly connected.

4. References

1. A. Altınoklu and Ö. Ergül, "SOLBOX-08," *Radio Science Bulletin*, 362, September 2017, pp. 97-101.

2. A. Altınoklu and Ö. Ergül, "SOLBOX-16," *Radio Science Bulletin*, 369, June 2019, pp. 22-27.

3. A. Altınoklu and Ö. Ergül, "SOLBOX-13," *Radio Science Bulletin*, 367, September 2018, pp. 26-31.

4. R. M. Dickson and L. A. Lyon, "Unidirectional Plasmon Propagation in Metallic Nanowires," *J. Phys. Chem.*, **104**, 26, 2000, pp. 6095-6098.

5. Z. Li, S. Zhang, N. J. Halas, P. Nordlander, and H. Xu, "Coherent Modulation of Propagating Plasmons in Silver-Nanowire-Based Structures," *Small*, **7**, 5, 2011, pp. 593-596.

6. H. Wei, Z. Wang, X. Tian, M. Käll, and H. Xu, "Cascaded Logic Gates in Nanophotonic Plasmon Networks," *Nat. Comm.*, **2**, 387, 2011.

7. H. Wei, Z. Li, X. Tian, Z. Wang, F. Cong, N. Liu, S. Zhang, P. Nordlander, N. J. Halas, and H. Xu, "Quantum Dot-Based Local Field Imaging Reveals Plasmon-Based Interferometric Logic in Silver Nanowire Networks," *Nano Lett.*, **11**, 2, February 2011, pp. 471-475.

8. J. Xu, X. Zhuang, P. Guo, W. Huang, W. Hu, Q. Zhang, Q. Wan, X. Zhu, Z. Yang, L. Tong, X. Duan, and A. Pan, "Asymmetric Light Propagation in Composition-Graded Semiconductor Nanowires," *Sci. Rep.*, **2**, 820, November 2012.

9. Ö. Ergül and L. Gürel, *The Multilevel Fast Multipole Algorithm (MLFMA) for Solving Large-Scale Computational Electromagnetics Problems*, New York, Wiley-IEEE, 2014.

10. C. Önol and Ö. Ergül, "Optimizations of Patch Antenna Arrays Using Genetic Algorithms Supported by the Multilevel Fast Multipole Algorithm," *Radioengineering*, **23**, 4, December 2014, pp. 1005-1014.

11. C. Önol, B. Karaosmanoglu, and Ö. Ergül, "Efficient and Accurate Electromagnetic Optimizations Based on Approximate Forms of the Multilevel Fast Multipole Algorithm," *IEEE Antennas Wireless Propag. Lett.*, **15**, April 2016, pp. 1113-1115.

12. B. Karaosmanoğlu, A. Yılmaz, U. M. Gür, and Ö. Ergül, "Solutions of Plasmonic Structures Using the Multilevel Fast Multipole Algorithm," *Int. J. RF Microwave Comput.-Aided. Eng.*, **26**, 4, May 2016, pp. 335-341.

13. B. Karaosmanoğlu, A. Yılmaz, and Ö. Ergül, "Accurate and Efficient Analysis of Plasmonic Structures Using Surface Integral Equations," *IEEE Trans. Antennas Propag.*, **65**, 6, June 2017, pp. 3049-3057.

14. S. M. Rao, D. R. Wilton, and A. W. Glisson, "Electromagnetic Scattering by Surfaces of Arbitrary Shape," *IEEE Trans. Antennas Propag.*, **30**, 3, May 1982, pp. 409-418.

15. C. Önol, A. Üçüncü, and Ö. Ergül, "Efficient Multilayer Iterative Solutions of Electromagnetic Problems Using Approximate Forms of the Multilevel Fast Multipole Algorithm," *IEEE Antennas Wireless Propag. Lett.*, **16**, 2017, pp. 3253-3256.

16. G. Karaova, U. Tahan, T. Atmaz, and Ö. Ergül, "Design and Optimization of Nano-Optical Couplers for Controlling Transmission Between Electrically Isolated Nanowires," in Proc. Fifth International EMC Conference, 2019.

Commission E
(Electromagnetic Environment and Interference)

Announcement of a Commission E corner in the Radio Science Bulletin

Commission E announces a corner in the Radio Science Bulletin (RSB) showcasing latest research, news, updates and announcements from different geographical regions. Concise reports, editorially in line with the RSB and subsequent to a review process, would appear in this corner. The details along with an approximate length (maximum) is provided below.

- Updates on activities and latest developments from different geographical regions: Up to 2 paragraphs
- Short report or concise article on recent research and development (novel ideas, implementation, results) – 1 page including figures and plot
- Activities supporting the URSI flagship conferences, collaborations, Commission E promotion-related information – 1 page

The scope of URSI Commission-E includes (but is not restricted to) the following topics:

- Terrestrial and planetary noise of natural origin, seismic associated electromagnetic fields
- Man-made electromagnetic environment
- The composite noise environment
- The effects of noise on system performance
- The effects of natural and intentional emissions on equipment performance
- The scientific basis of noise and interference control, electromagnetic compatibility
- Spectrum management

Contributions can be sent to the following members:

Articles on recent research and development - Kaushal Buch (kdbuch@gmrt.ncra.tifr.res.in)

Updates from different geographical regions - Virginie Deniau (virginie.deniau@ifsttar.fr)

Conferences, collaborations, Comm-E related - Frank Gronwald (frank.gronwald@uni-siegen.de)

Randy L. Haupt
Colorado School of Mines
Brown Building 249
1510 Illinois Street, Golden, CO 80401 USA
Tel: +1 (303) 273 3721
E-mail: rhaupt@mines.edu

Amy J. Shockley
E-mail: aj4317@gmail.com

Reprioritization

About 25 years ago, my good friend Tim and I decided to cross-country ski to a cabin in the Colorado mountain backcountry. The cabin was located at about 3500 m above sea level, and was far from any roads. Tim was in charge of the United States "hot shot" crew that fought forest fires in Colorado, so he spent a lot of time outdoors in the wilderness, and was skilled at survival. I had just retired as the US Air Force Academy Nordic ski coach, and had gone through survival training a number of years earlier. The sun was shining and the snow was deep when we started out. We had a great time skiing and snowshoeing. We spent two days away from civilization, during which time the top priorities were to have fun, enjoy the outdoors, and get some challenging exercise. Worries such as our daughters will someday become teenagers were long forgotten.

On our last day, we woke up and went outside. Oh no! There were thick clouds on the horizon and the weather was changing fast. We scrambled to pack our things, strap into our skis, and took off down the mountain. The sun was brightly shining when we began, but the storm moved faster than us, and in a matter of minutes, we could no longer see each other in the whiteout. Our trip went from a fun experience to one of sheer terror, and taxed our Nordic skiing and survival skills. Over the course of a couple of minutes, our priorities abruptly changed. We no longer cared about exercise or the scenery, and instead focused on getting back to civilization and containing our panic. The storm effectively disrupted our plans and imposed new priorities. I'll spare you all of the details (although Tim did complete a 360° spinout over a small cliff before getting buried in a snow bank), but the story ends with us finding my car and stopping at our favorite pizza restaurant for a good, hearty meal before getting home.

Evaluating your bandwidth and then prioritizing your competing tasks in alignment with your ethics works most of the time. Start the week by evaluating tasks for the upcoming week, and through effective prioritization and capacity planning, define the timeline to get everything done. However, what happens if you become ill, or if your boss assigns you a new urgent project, or if a family member or friend needs help that requires a significant amount of your time? We do not live in a static world. It is ever-changing and evolving, and you can experience events that disrupt your plans, which requires yet one more skill in effective prioritization: reprioritization. Just think about how your priorities changed as the COVID-19 virus spread. We were unprepared and panic took over.

New information, opportunities, and trials intrude into our plans before we have fully processed the existing information and completed the current opportunities and challenges at hand. Adapting our tactics and evolving our schedule to accommodate changes provides a way to get through both mundane and challenging events. Taking a fluid approach to prioritization sounds overwhelming, and at times it can be. However, the fittest or best prepared are able to adapt to disruptions, and ultimately, to succeed.

Reprioritization requires the same ethics-based methodology used for prioritization. Simply evaluate how new tasks and events fit into the importance-urgency matrix, as well as how they compare to the previously identified items. Aligning your actions with your moral compass will then provide you the tools needed to discuss how you have reprioritized your time and efforts with stakeholders. Those impacted may be disappointed; however, as long as the decision aligns with the right allocation of your bandwidth, you can effectively manage any fallout by discussing your decision process.

Reprioritization requires a shift in mindset. Avoid getting upset or frustrated by new tasks and the need to de-prioritize previously prioritized items. Instead, approach the new challenges with curiosity. Curiosity leads to knowledge about the disruptor that in turn leads to effective decision making. An openness to change and a logical approach to reprioritization counters the disruptor's solicitation of an emotional response. Harnessing that emotional response, and instead learning about the disruptor and its overall impact, can often be empowering. However, also understanding what lies within your control and what lies beyond your control helps to reevaluate priorities.

In 1991, the IEEE AP-S Symposium was in Ontario, Canada. I had my plane tickets, registration, and hotel. The day before I was to leave, a water pipe in our house burst and flooded our first floor. I wisely cancelled my trip and paper presentation, even though I was looking forward to the event. While the trip had been fully planned and had clear professional benefits, it was still within my control and I was empowered to decide whether I would attend. The water pipe was out of my control. While getting upset would be an understandable response, instead accepting the disruptive event, its impact, and the fact that it required my immediate and full attention was necessary in effectively reprioritizing my time for that week.

Learning about new items as they arise, evaluating what is in your control, and constantly reprioritizing in alignment with your moral compass will empower you to fully optimize your capacity within your bandwidth. This approach to all aspects of your life will allow you to achieve the work-life balance you desire, and will allow you to take advantage of new opportunities as they arise. It will also make you better prepared for challenges that arise, such as the current COVID-19 pandemic. People and organizations were forced to reprioritize public health above all else. How did you and your organizations react to this disruptor? You are likely able to identify those who sought information, accepted the impact of the situation, and made defendable decisions, versus those who became overwhelmed with the need to adjust.

Last summer, my wife and I met Tim and his wife in Leadville, Colorado (population 2,762 at 3,094 m above sea level). We went for pizza at an eclectic restaurant, and reminisced about our great times together, including our ski trip. Tim was diagnosed with colon cancer in 1998, after we had both moved away from the community in which we became friends. We stayed in touch, and he is now cancer free, having even climbed up Mt. Kilimanjaro a few years ago. I remember that devastating news about his cancer diagnosis and his fight to survive. Tim has a strong moral compass and successfully reprioritized his life.

As we were strolling through downtown Leadville, my phone rang. It was my doctor. My colon-cancer test was positive. Now what? I was happy to have my wife, Tim, and his wife present when I got the news. I did not let that news ruin our time together – a higher priority right then. However, I started doing research immediately afterwards. How do I reprioritize my life now? I've been diabetic for 38 years: do I have the bandwidth to handle this new news? I knew that I must maintain my moral compass as I made plans to deal with an important disruptive priority that had suddenly appeared. Fortunately, there is a happy ending: the test was a false positive! No need to reprioritize – or is there?

Giuseppe Pelosi
Department of Information Engineering
University of Florence
Via di S. Marta, 3, 50139 Florence, Italy
E-mail: giuseppe.pelosi@unifi.it

Foreword

This issue presents a paper by Antonio Savini, Emeritus Professor at the University of Pavia, Italy, and Chair of the History activity Committee of the IEEE Italy Section. The paper originated at the time that was getting close to the anniversary of the discovery of thermoelectricity, credited to Thomas Johan Seebeck, Estonian scientist, in 1821. What is less widely known is that such credit is incorrect, since it has been recently proven that thermoelectricity was indeed first observed and reported by Alessandro Volta in 1787 [1] (based on previous investigations in Italian, dating to 2005). In this paper, Antonio Savini makes this point for the benefit of our wide community.

Reference

1. L. Anatychuk, J. Stockholm, G. Pastorino, "On the Discovery of Thermoelectricity by A. Volta," Proc. of the 8th European Conference on Thermoelectrics, Como, Italy, 2010, pp. 15-18.

The Early Experiments of Alessandro Volta and the Seebeck Effect

Antonio Savini

Research Centre for the History of
Electrical Technology
University of Pavia, Italy
E-mail: antonio.savini@unipv.it

Abstract

The early history of thermoelectricity is briefly reviewed, starting from the pioneering observations made by Alessandro Volta up to the work of Thomas J. Seebeck, to whom the effect of electric current generated by the difference of temperature in a metal chain is attributed.

1. Pioneering Observations Made by Alessandro Volta on Thermoelectricity

Stimulated by the booklet "De Viribus electricitatis in motu muscolari commentarius" by L. Galvani (1791), presented to him by B. Carminati, Professor of Anatomy at the University of Pavia, in 1792 Alessandro Volta started

Figure 1a. Luigi Galvani [Bologna, Italy, September 9, 1737 – Bologna, Italy, December 4, 1798].

Figure 1b. Alessandro Volta [Como, Italy, February 18, 1745 – Como, Italy, March 5, 1827].

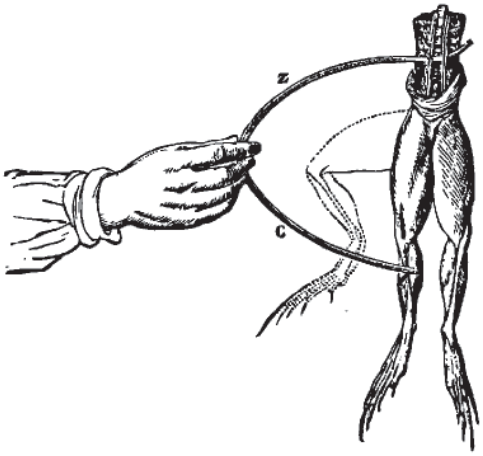

Figure 1c. Frog's legs used as a galvanoscope by both Galvani and Volta.

to investigate the so-called "animal electricity" using metallic arcs and frogs (Figure 1). He gradually came to the realization that the source of electricity was not in frogs (animal electricity) but in metals (metallic electricity), whereas frogs were merely "animal electrometers." He described his studies in many papers, and finally in a letter addressed to Anton Mario Vassalli, Professor at the University of Torino, on February 10, 1794 (Nuova Memoria sull'elettricità animale del Sig. Don Alessandro Volta) [1]:

> "Che pensa Ella della pretesa Elettricità Animale? Per me sono convinto da un pezzo che tutta l'azione procede originariamente dai metalli combacianti un corpo umido qualunque, o l'acqua stessa; in virtù del quale combaciamento viene spinto avanti il fluido elettrico in esso corpo umido od acqua dai metalli medesimi, da quale più da quale meno (più di tutti dal Zinco, meno quasi di tutti dall'Argento); onde indotta una comunicazione non interrotta di acconci conduttori è tratto esso fluido in un continuo giro...."
>
> "What do You think of the supposed Animal Electricity? I have been long convinced that all action is originated by metals in contact with any wet body or water itself; thanks to this contact the electric fluid is pushed forward to the wet body or water by metals themselves, more by some of them, less by others (more than others by Zinc, less than almost all others by Silver); then, having established a non-interrupted contact of suitable conductors, such a fluid is induced to a continuous circulation...." (translation from the original Italian)

As a result of a number of experiments using various material with differences at their ends (internal structure, thermal treatment, heat), in the same letter he described, as a side effect observed, what we can define as the first experiment of thermoelectricity:

"...Fatto dunque un arco di un grosso filo di ferro, crudo ed elastico, provava se intingendo i suoi due capi ne' due bicchieri d'acqua in cui pescava una rana puntualmente e di fresco preparata,...mi riuscisse di farla convellere e saltare....

...Or dunque trovato, con saggiarne molti, uno di tali archi di ferro, che non facesse nulla neppur da principio, ed altre volte aspettato che fosse indebolita la rana, e resa non più eccitabile da uno di quegli altri valevoli sulle prime a commuoverla (il che succede ben presto), tuffava nell'acqua bollente un capo di tal arco per qualche mezzo minuto, indi trattato fuori e senza dargli tempo di raffreddarsi, ritornava all'esperienza sopra i due bicchieri di acqua fresca: ed ecco che la rana a bagno si convelleva; e ciò anche due, tre, quattro volte ripetendo la prova; finché raffreddata per tali immersioni più o meno durevoli e ripetute...ritornava codesto arco inetto del tutto ad eccitare le convulsioni dell'animale...."

"…So, taken an arc of a thick iron wire, coarse and flexible, I tried to put its two ends into two glasses of water where two parts of a frog recently and conveniently prepared were immersed in order to observe contractions and jumping of the frog….

…After many e trials I took one of such iron arcs that had not reacted since the beginning and in other time after waiting that the frog became weak and no more sensitive to other arcs that first had been able to affect it (which soon happened), I immersed one end of the arc into boiling water for some half a minute then after removing it from there without letting it to cool down, I repeated the experiment with the two glasses of cold water; suddenly the frog started contracting; this happened two, three, four times until the arc, returned cold after repeated immersions, became unable of

Figure 2a. Johan Wilhelm Ritter [Samitz, Poland, December 16, 1776 – Munich, Germany, January 23, 1810].

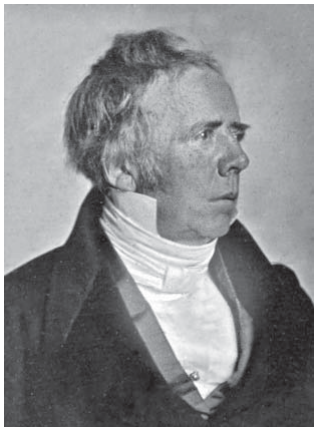

Figure 2b. Hans Christian Oersted (Rudkoebing, Denmark, August 4, 1777 – Copenhagen, Denmark, March 9, 1851).

Figure 2c. Thomas Johann Seebeck [Tallinn, Estonia, April 9, 1770 – Berlin, Germany, December 10, 1831]

exciting the animal's contractions…" (translation from the original Italian)

As Volta himself pointed out, the thermoelectric effect can be observed in an arc made of a single metal provided the material has some inhomogeneities between the ends. The effect is more pronounced if one uses a bimetallic arc.

It can be remarked that Volta just detected the phenomenon by rough instruments (frog, his own tongue), and did not perform detailed measurements of the phenomenon.

In all his investigations, Alessandro Volta was guided by the feeling that metals are motors of electricity. Throughout all the 1780s, he made experiments with conductors of different species, being convinced that an electromotive force (tension) originated from the contact of different conductors. Eventually in 1800, he communicated the invention of the artificial electric organ (the electric battery or pile): for the first time, a generator of continuous flux of electric charges was available.

Soon after the invention, scientists everywhere started to build and use batteries in order to investigate the effects of electric current. Johann W. Ritter, a German physicist, was among them. In 1801, he too observed thermoelectric currents (Figure 2).

2. Seebeck's Experiments

In 1820, Hans C. Oersted (Figure 2), when lecturing in electricity and magnetism at the University of Copenhagen, demonstrated the magnetic effect of electric current: a current flowing in a wire was able to deviate a magnetic needle placed nearby.

Attracted by Oersted's discovery, Thomas Johann Seebeck (Figure 2), an Estonian scientist and a member of the Berlin Academy, when studying magnetism on Earth, performed various experiments. In one of these, he connected two pieces of different metals in a circuit with a winding, over which he placed a magnetic needle. After heating one of the metals, he observed the deflection of the magnetic needle [2]:

> 12. Eine Wismuthscheibe wurde mit den beiden Enden einer Kupferspirale in Beruhnung gebracht, unter die geschlossen Kette eine Kalte unt auf dieselbe eine uber Lampe erwarmte Kupferscheibe gelegt. Es erfolge sopleich einer Declination, und dazu eine viel lebhaftere als bei den fruheren Versuchen. Die Magnetnodel innerhalb der Spirale machte eine Bewegung von 50° bis 60° und blieb bei 17° stehen,....
>
> 12. A bismuth disk was placed in contact with the ends of a copper winding and a copper disk was located under the closed chain; the copper disk was warmed over a lamp. A sudden deviation of the magnetic needle was observed, much more remarkable than the previous times. The needle within the winding rotated from 50° to 60° and remained at 17°....(translation from the original German)

In 1821, he reported this experiment to the Berlin Academy:

> Aus meinen Untersuchungen uber den Magnetismus der galvanischen Ketten in den Abhandlungen der Konigl. Akademie von 1820-1821 S. 289-346 hatte sich ergeben, dafs die Intensitaet des Magnetismus dieser ketten in geradem Verhaltnifs zu der Energie der durch den feuchten Leiter begrundeten chemischen Action stehe,....

From my research on the magnetism of the galvanic chains in the Proceedings of the Royal Academy of 1820-1821 p. 289-346 it has been concluded that the intensity of magnetism of these chains is in direct relation with the energy of the wet conductor based on the chemical action....(translation from the original German)

Seebeck emphasized the connection between heat and magnetism, a sort of thermos-magnetism. Actually, now one knows that the difference of temperature of the two metals produces an electromotive force that is responsible for the circulation of electric current, and eventually for the deviation of the magnetic needle.

In 1823, Oested himself reported Seebeck's discovery, and proposed to call it "thermoelectricity" [3]:

M. Seebeck, member de l'Acadèmie de Berlin, a découvert q'on peut établir un circuit électrique dans le metaux sans l'interposition d'aucun liquid. On établit le courant dans le circuit en troblant l'èquilibre de temperature. L'appareil pour faire voir cette action est fort simple: on peut le composer de deux arcs de mètaux diffèrences, par exemple, de cuivre et de bismuth soudès ensemble aux deux bouts, en sort qu'ils fassent en tout un circle....

Pour étanblir le courant, on chauffe l'anneau à l'un des deux endroits ou se touchent le deux metaux....

On ne peut dècouvrir ces courans électiques que par l'auguille aimantèe, sur laquelle ils exercent une influence très sensible il foudra sans doute dèsormais distinguer cette nouvelle classe de circuit électiques par une dènomination significative, et comme telle je propose l'expression de «circuits thermo-électriques» ou peut-etre «thermélectriques»: en meme temps ou pourrait distinguer le circuit galvanique par le nom circuit hydro-électrique ...."

Mr. Seebeck, a member of the Berlin Academy, has discovered that an electrical circuit can be established in materials without the interposition of any liquid. We establish the current in the circuit by adjusting the temperature equilibrium. The device to show this action is very simple: it can be composed of two arcs of different metals, for example, copper and bismuth welded together at the two ends, so that they make a whole circle....

To generate the current, we heat the ring in one of the two places where the two metals touch....

We can only discover these electric currents by the magnetic needle, over which they exert a very sensitive influence. It will undoubtedly be clear from now on to distinguish this new class of electric circuits by a significant denomination, and as such I propose the expression of «thermo-electric circuits» or perhaps «thermelectrics»: at the same time one could distinguish the galvanic circuit by the «name hydro-electric circuit»....

The discovery of thermoelectricity is normally attributed to T. J. Seebeck, while the original and fundamental observation made by Alessandro Volta is forgotten. However, in recent times the International Thermoelectric Academy recognized Alessandro Volta as the early discoverer of the thermoelectric effect [4]. As evidence of this, in 2005 a memorial plaque was therefore dedicated in Como, the birth place of Alessandro Volta.

3. Conclusion

In 2021, we will celebrate the two-hundredth anniversary of Seebeck's discovery. In this respect, it is necessary to remark that after him, investigations on thermoelectricity have not stopped and, in particular, in 1834 Jean-Charles A. Peltier, a French scientist, described the reverse effect, i.e. the cooling of a junction as electric current flows through it.

Even in recent times, scientists and technologists are studying new materials, including nano-engineered materials, in order to check the possibility of generating small voltages thanks to small differences in temperature, and also in the microscopic world [5, 6]. Harnessing wasted heat in the inorganic as well in the organic world is the main purpose of these investigations in progress.

4. References

1. A. Volta, "Nuova memoria sull'elettricità animale 1794-95" in *Le Opere di Alessandro Volta*, ed. naz. Vol. I, Hoepli, Milano, 1918, pp. 168-220.

2. T. J. Seebeck, "Magnetische Polarisation der Metalle und Erze durch Temperature-Differenz" in *Abhandlungen der Koniglichen Akademie der Wissenshsften zu Berlin aus den Jahren* 1822-23, p. 265.

3. C. Oersted, "Nouvelles experiences de M. Seebeck sur les actions èlectromagnetiques, *Annales de Chimie et de Physique*, 2nd series, 1823, pp. 199-201.

4. L. Anatychuk, J. Stockhom, and G. Pastorino, "On the Discovery of Thermoelectricity by A. Volta," Proc. 8th European Conference on Thermoelectrics, Como, 2010, pp. 115-18.

5. K. Uchida et al., "Observation of the Spin Seebeck Effect," *Nature*, **455**, 2008, pp. 778-781.

6. H. Kojima et al., "Universality of the Giant Seebeck Effect in Organic Small Molecules," *J. Materials Chemistry Frontiers*, **7**, 2018, pp. 1276-1283.

James C. Lin
University of Illinois at Chicago
851 South Morgan Street, M/C 154
Chicago, IL 60607 USA
E-mail: lin@uic.edu

The Covid-19 Pandemic and 5G Cellular Telecommunication Systems

Recently, there were several odd or unusual reports coming out of the UK about linking the coronavirus disease (COVID-19) pandemic to the rollout of 5G communication systems [1]. It sounded rather bizarre; even as a conspiracy theory, it did not make sense! While both 5G and COVID-19 are global phenomena happening at around the same time, it boggles the mind how the two got entangled. On second thought, it is not as shocking as it may seem upon first encounter!

By now (as I write this in early May 2020), the coronavirus has been established as a global pandemic with rapidly increasing case counts and fatalities worldwide [2]. The impact and interruptions of computer "viruses" on private citizen, commerce, corporation, and government operations and common lives have been widely publicized and recognized for quite some time, now. They have been slowly embedded into the public consciousness as an undesirable hi-tech affliction still in search of an effective remedy. Moreover, for a couple of years if not longer, various groups have been broadcasting and escalating politicized or overblown concerns about 5G security challenges and threats.

Aside from the array of socio-technical issues surrounding the 5G cellular mobile network and technology, the palpable politicization of 5G has caused bewilderment and consternation in its deployment. It has certainly impacted the pace with which investment decisions are being made: namely, to engage5G as a hare or tortoise.

The onset of coronavirus COVID-19, a complex and devastating global pandemic, on top of a public already jittery about computer viruses and 5G wireless cellular technology perhaps conjures up horrors in some people's minds of being attacked by pandemic viruses or malevolent cells, even the type associated with 5G cell phones. The script is not neoteric. Scapegoating has been a cultural norm in some quarters for no less than 2000 years.

The fact is that there is no link between the COVID-19 virus and 5G cell-phone technology or 5G communication base-station towers. These are totally different constructs: they are not even close. None of the conspiracy theories that try to link 5G and the coronavirus scientifically make any sense. The electromagnetic radiation from 5G devices and systems is not carrying the COVID-19 virus or any other microbial virus into which humans can come into contact, nor can infect anyone.

Proponents of 5G mobile technology hail 5G as a faster and more secure technology than its predecessors, 3G and 4G systems, which incidentally are not necessarily entirely secure, either. They can be just as vulnerable to attempts such as real-time location tracking and surveillance practices. However, there are 5G security concerns and issues that can be somewhat more complicated. A central vulnerability or key threat is that it may allow spying on users: not new, either. Nevertheless, this is a system architecture and technology or regulatory issue, but not a biological or health effect matter or challenge.

5G cellular mobile technology is a telecommunication platform that is multifaceted in radio-frequency (RF) engagement and varied in operational scope and performance. It includes an extremely wide range of multiple

RF bands. Its frequency coverage may be roughly separated into two ranges: the sub-6 GHz bands, and 24 GHz to 60 GHz frequencies that reach well into the millimeter-wave region. The frequency ranges have often been further divided into low-band 5G, mid-band 5G, and high-band 5G. Low-band 5G begins at about 400 MHz and often uses existing or previous 3G or 4G frequencies or newly opened frequencies to operate, which, for example, may overlap with the current 4G band. The mid-band 5G especially includes the frequencies around 3 GHz and 4 GHz. However, the primary 5G technological advances are associated with the high-band 5G, promising performance bandwidths as high as 20 GHz and multiple-input and multiple-output (MIMO), using 64 to 256 antennas at short distances, and offering performance up to 10 times that of the current 4G networks.

From the perspective of frequency allocation, 5G encompasses an enormous range, from 3 GHz to 60 GHz and beyond, in one giant skip from 4G. Even with current technological advances, the demand and performance challenges clearly vary immensely from the low to high bands. The anticipated performance bandwidth of 20 GHz obviously is not viable or supportable at low band. By design default or spectrum necessity, the bandwidth performance will only be accomplished by leapfrogging to the high-band 5G. For biological matters, it is not obvious whether the biological responses to high-band 5G radiations would be akin to earlier generations or low-band 5G radiations, given the distinctive characteristics of mm-wave and its interaction with the complex structure and composition of pertinent biological tissues.

In 2011, the World Health Organization's (WHO's) International Agency for Research on Cancer (IARC) classified exposure to RF radiation as a possible carcinogen to humans. The IARC had then evaluated available scientific studies and concluded that while evidence was incomplete and limited, especially regarding results from animal experiments, epidemiological studies of humans reported that increased risks for gliomas (a type of malignant brain cancer) and acoustic neuromas (or acoustic schwannomas – a non-malignant tumor of Schwann-cell-sheathed auditory nerves on the side of the brain) among heavy or long-term users of cellular mobile telephones are sufficiently strong to support a classification of being possibly cancer causing in humans for exposure to RF radiation [3, 4].

The classification of RF radiation as possibly carcinogenic to humans is third on the IARC groupings of carcinogenic risk to humans. The highest category is Group 1, which is reserved for agents that are found to be carcinogenic to humans. It is followed by Group 2A: probably carcinogenic to humans; 2B: possibly carcinogenic to humans; then Group 3: not classifiable as to its carcinogenicity to humans; and lastly, Group 4: probably not carcinogenic to humans.

Recently, the National Toxicology Program (NTP) of the US National Institute of Environmental Health Science (NIEHS) reported observations of two types of cancers in laboratory rats given life-long exposure to RF radiation used for 2G and 3G wireless cellular mobile telephone operations [5]. This was the largest health effect study ever undertaken by NIEHS/NTP. It concluded, among other observations, that there was statistically significant and "clear evidence" that the RF radiation had led to the development of malignant schwannoma (a rare form of tumor) in the heart of male rats. Further, there was "equivocal evidence" for the same schwannoma risk among female rats. NTP also noted that there were unusual patterns of cardiomyopathy, or damage to heart tissue, in both RF-exposed male and female rats when compared with concurrent control animals. In addition, based on statistical significance, the pathology findings showed indications of "some evidence" for RF-dependent carcinogenic activity in the brain of male rats, specifically glioma. However, the findings for female rats were deemed as providing only "equivocal evidence" for malignant gliomas when compared with concurrent controls [6, 7].

Note that the NTP uses five categories of evidence for carcinogenic activity to classify the strength of evidence observed in their reports: "clear evidence" and "some evidence" for positive findings; "equivocal evidence" for uncertain results; "no evidence" for no observable effects; and "inadequate study" for results that cannot be evaluated because of major experimental flaws.

Shortly after the NTP report, the Cesare Maltoni Cancer Research Center at the Ramazzini Institute in Bologna, Italy, published the final results from its comprehensive study on carcinogenicity in rats exposed (either lifelong or prenatal until death) to 2G/3G, 1800 MHz RF radiation [8]. The study involved whole-body exposure of male and female rats under plane-wave equivalent or far-zone exposure conditions. The authors estimated that the whole-body SARs were roughly 0.001 W/kg, 0.03 W/kg, and 0.1 W/kg during exposures of 19 h/day for approximately two years. A statistically significant increase in the rate of schwannomas in the hearts of male rats was detected for the highest RF exposure. Furthermore, an increase in the rate of heart Schwann cell hyperplasia was observed in exposed male and female rats at the highest RF exposure, although this was not statistically significant. An increase in the rate of gliomas was observed in exposed female rats at the highest exposure level, but it was not deemed statistically significant [9]. It is important to note that the recent NTP and Ramazzini RF exposure studies presented similar findings in heart schwannomas and brain gliomas. Two relatively well-conducted RF exposure studies employing the same strain of rats thus showed consistent results in significantly increased cancer risks.

More recently, an Advisory Group for IARC has recommended including re-evaluation of carcinogenicity of human exposure to RF radiation, with high priority, in their Monograph series [10].

As mentioned above, the 5G frequency domain is divided into low, mid, and high bands. The operating frequencies at low and mid bands can overlap with the current 4G band at 6 GHz or below. The biological effects of RF radiations at these lower-frequency bands are thus likely to be comparable to 2G, 3G or 4G. However, the scenarios of high band 5G, especially for 24 GHz to 60 GHz in the mm-wave region for high-capacity, short-range wireless data communications, are relatively recent new arrivals, and pose considerable challenge to health-risk assessment.

There is a paucity of data on permittivity and coupling such as reflection, transmission, and induced energy deposition in biological tissues in the mm-wave frequency band.

In principle, at mm-wave frequencies, the induced fields and energy deposition in biological medium can be determined in much the same manner as for RF if the permittivity of the relevant biological tissues at these frequencies is known. Although there were some earlier extrapolations based on Debye formulas and using complex dielectric permittivity of the skin at lower frequencies, some measurements for skin within the mm-wave range are available for humans [11] and rodents [12]. Note that skin tissue is not homogeneous but consists of multiple layers of stratum corneum, epidermis, and dermis. Moreover, it is differentiated according to body location: for example, forearm and palm skins have thin and thick stratum corneum, respectively.

It has been shown that the mm-wave permittivity of different skin layers may be described by the Debye equation with a single relaxation time [13]. Measured data for human skin in the frequency range of 37 GHz to 74 GHz showed that the measured results tended to be lower compared to earlier extrapolations. More importantly, at mm-wave frequencies, the permittivity of skin is governed by cutaneous free water content. Available information for 30 GHz to 90 GHz thus indicates that the behavior of relative permittivity follows that of the lower RF frequencies. Specifically, the real and imaginary parts of permittivity for skin decrease from 20 to 6 and 20 to 12, respectively.

The power reflection coefficients for frequencies from 37 GHz to 74 GHz decreased from 60% to 45% and 40% to 20% for skin on the forearm and palm, respectively. The power transmission coefficient for skin on the forearm showed an increase from 55% to 65%, respectively, between 30 GHz and 90 GHz. It is noteworthy that a thick stratum corneum in the palm causes an increase in transmission because of the layer-matching phenomenon at higher mm-wave frequencies. The penetration depth of a plane wave field decreases from 0.8 mm to 0.4 mm and 1.2 mm to 0.7 mm for skin on the forearm and palm, respectively, between 30 GHz and 90 GHz. Induced energy deposition increases with mm-W frequency. However, at the highest frequencies the energy deposition in the deeper regions inside the skin is lower because of the reduced penetration depth at these frequencies [14].

Studies on mm-wave interactions aimed both toward biological effects and medical applications began nearly 50 years ago, most notably in the former Soviet Union. A comprehensive review of research on biological effects of mm-waves from the former Soviet Union showed that at intensities of 100 W/m^2 or less, mm-wave can affect cell growth and proliferation, enzyme activity, genetic status, function of excitable membranes, peripheral receptors, and other biological systems [15].

A recently published review included 45 in vivo studies conducted using laboratory animals and other biological preparations, and 53 in vitro studies involving primary cells and cultured cell lines [16]. The review was based on published data from scientific papers written in English available through the end of 2018 using 6 GHz to 100 GHz as the RF source. However, because fewer studies were reported at 30 GHz or below and at frequencies higher than 90 GHz, the review mainly covered published studies conducted in the mm-wave frequency range from about 30 GHz to 65 GHz.

This industry-supported review noted that aside from the wide frequency ranges, the studies were diverse both in subjects and end points investigated. Biological effects were observed to occur both in vivo and in vitro for different biological endpoints studied. Indeed, the percentage of positive responses at non-thermal levels in most frequency groups was as high as 70%. (Higher mm-wave intensities, up to 200 W/m^2, did not seem to cause any greater responses.) For example, in the 53 in vitro studies involving primary cells ($n = 24$) or cell lines ($n = 29$), approximately 70% of the primary cell studies and 40% of the cell line investigations showed effects that were related to mm-wave exposure. However, the protocol applied for control of biological target or culture medium temperature during mm-wave exposure was unclear in a large fraction of these studies.

While many of these investigations with mm-wave exposures reported biological responses, there is inconsistency in the dependence of biological effects and mm-wave intensity used for exposure. The number of reported in vitro and in vivo laboratory investigations were also modest and diverse, considering the wide 5G mm-wave frequency domain. The jury on biological effects or health impact is still out on 5G. Moreover, there is a lack of ongoing controlled laboratory investigations. Simply put, the existing scientific data is inadequate for any reliable assessment or conclusion with confidence.

References

1. BBC, "Mast Fire Probe Amid 5G Coronavirus Claims," https://www.bbc.com/news/uk-england-52164358, April 4, 2020.

2. A. Schuchat, Public Health Response to the Initiation and Spread of Pandemic COVID-19 in the United States, February 24-April 21, 2020, *MMWR Morb Mortal Wkly Rep*. ePub: 1 May 2020, DOI: http://dx.doi.org/10.15585/mmwr.mm6918e2.

3. R. Baan, Y. Grosse, B. Lauby-Secretan, F. El Ghissassi, V. Bouvard, L. Benbrahim-Tallaa, N. Guha, F. Islami, L. Galichet, K. Straif, WHO International Agency for Research on Cancer Monograph Working Group, Carcinogenicity of Radiofrequency Electromagnetic Fields, *The Lancet Oncology*, **12**, 2011, pp. 624-626.

4. IARC Working Group on the Evaluation of Carcinogenic Risks to Humans, "Non-Ionizing Radiation, Part 2: Radiofrequency Electromagnetic Fields," *IARC Monogr. Eval. Carcinog. Risks Hum.*, **102**, 2, 2013, pp. 1-460.

5. The US National Toxicology Program, "Technical Report on the Toxicology and Carcinogenesis Studies in HSD: Sprague-Dawley SD Rats Exposed To Whole-Body Radio Frequency Radiation at a Frequency (900 MHz) and Modulations (GSM and CDMA) used by Cell Phones," NTP, Raleigh, NC, Tech. Rep. 595, 2018.

6. J. C. Lin, "Peer Review Conclusion of Clear Evidence of Cancer Risk from Cell Phone RF Radiation," *URSI Radio Science Bulletin*, 364, March 2018, pp. 75-78.

7. J. C. Lin, "Cancer Occurrences in Laboratory Rats from Exposure to RF and Microwave Radiation, "*IEEE J. Electromagn., RF Microw. Med. Biol. (J-ERM)*, **1**, 1, 2017, pp. 2-13.

8. L. Falcioni et al., "Report of Final Results Regarding Brain and Heart Tumors in Sprague-Dawley Rats Exposed From Prenatal life Until Natural Death to Mobile Phone Radiofrequency Field Representative of a 1.8 GHz GSM Base Station Environmental Emission," *Environ. Res.*, **165**, August 2018, pp. 496-503.

9. J. C. Lin, "What Must Not Be Neglected Are Overall Cancer Rates in Chronic Effects in NTP's Lifelong RF Exposure Study," *URSI Radio Science Bulletin*, 370, September 2019, pp. 70-73.

10. IARC, Priorities for Future IARC Monographs on the Evaluation of Carcinogenic Risks to Humans, *Lancet Oncol*., **20**, 2019, pp. 763-764.

11. S. I. Alekseev, M. C. Ziskin, "Human Skin Permittivity Determined by Millimeter Wave Reflection Measurements, *Bioelectromagnetics*, **28**, 2007, pp. 331-339.

12. S. I. Alekseev, A. A. RadzievskI, M. K. Logani, M. C. Ziskin, "Millimeter Wave Dosimetry of Human Skin," *Bioelectromagnetics*, **29**, 2008, pp. 65-70.

13. S. I. Alekseev, O. C. Gordiienko, M. C. Ziskin, "Reflection and Penetration Depth of Millimeter Waves in Murine Skin," *Bioelectromagnetics*, **29**, 2008, pp. 340-344.

14. J. C. Lin, *Electromagnetic Fields in Biological Systems*, Boca Raton, CRC Taylor/Francis, September 2011.

15. A. G. Pakhomov, Y. Akyel, O. N. Pakhomova, B. E. Stuck, M. R. Murphy, "Current State and Implications of Research on Biological Effects of Millimeter Waves: A Review of the Literature," *Bioelectromagnetics*, **19**, 1998, pp. 393-413.

16. M. Simkó, M. O. Mattsson, "5G Wireless Communication and Health Effects – A Pragmatic Review Based on Available Studies Regarding 6 to 100 GHz," *Int. J. Environ. Res. Public Health*, **16**, 18, September 2019, pp. 3406.

European School of Antennas 2021

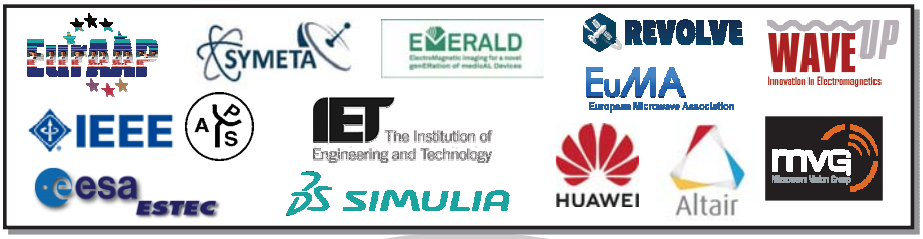

ESoA Board

ESoA Coordinator Prof. Stefano Maci
Dept. of Information Engineering and Mathematics
University of Siena, 53100 - Siena (Italy)
E-mail: macis@ing.unisi.it

www.esoa-web.org

http://www.facebook.com/europeanschoolofantennas

MICROWAVE IMAGING AND DIAGNOSTICS,
UMED-UNITN, Naples, February 1-5
Coordinators: A. Massa, T. Isernia, L. Crocco

ALL DIGITAL RADAR SYSTEM ENGINEERING,
KIT- Karlsruhe March 16-19, 2021
Coordinators: T. Zwick, M. Younis

COMPRESSIVE SENSING AS APPLIED TO ELECTROMAGNETICS
UNITN, Riva del Garda, March 22-26
Coordinators: A. Massa, G. Oliveri

LEAKY WAVES AND PERIODIC STRUCTURES FOR ANTENNA APPLICATIONS,
La Sapienza, Rome April 26-30 2021
Coordinator: F. Frezza

ADVANCED MATHEMATICS FOR ANTENNA ANALYSIS,
UNIZG Dubrovnik, 17-21 May
Coordinators: Z. Sipus, S. Maci

CHARACTERISTIC MODES: THEORY AND APPLICATIONS,
CTU, Prague 24-28 May,
Coordinators: M. Ferrando, P Hazdra

COMPACT ANTENNAS FOR SENSOR SYSTEMS, UPC – Barcelona, May 31-June 4, Coordinators : L. Jofre, A. Skrivervik

MOBILE RADIO PROPAGATION FOR 5G AND BEYOND
UNIBO, Cesenatico, June 7-11
Coordinators: , V. Degli Esposti, C. Oestges,T. Kürner

ANTENNA MEASUREMENTS,
UPM-MVG, Madrid, 14-18 June
Coordinators: M. Sierra, L. Foged

TERAHERTZ ANTENNA AND IMAGING SYSTEMS TuDelft – Delft, 21-25 June, Coordinators : A. Neto, N. Llombart . L. Jofre,

MILLIMETER WAVE ANTENNAS,
UR1 - Rennes, 28 June - 2 July
Coordinator: O. Lafond

Exploiting Symmetries in Artificial Materials for Antenna Applications
La Sorbonne, Paris, 13-16 September
G Valerio, E Martini, O Quevedo

ADVANCED COMPUTATIONAL EM,
POLITO, Torino, 20-24 September
Coordinators: F. Andriulli, G. Vecchi

ANTENNA SYNTHESIS,
UNINA, Capri, 11-15 October
Coordinator: A. Capozzoli

ACTIVE ANTENNAS
ESA-ESTEC , Nordwijk , 4-8 October
Coordinator: G. Toso, P. Angeletti

DISRUPTIVE ANTENNAS BASED ON EMERGING TECHNOLOGIES FOR NOVEL SATELLITE TELECOMMUNICATION SCHEME (REVOLVE)
TAS, Rennes, November 15-19
Coordinators: M. Ettorre, H. Legay

Asta Pellinen-Wannberg
Umeå University, Department of Physics and
Swedish Institute of Space Physics
S-90187 Umeå, Sweden
Tel: +46 90 786 7492
E-mail: asta.pellinen-wannberg@umu.se

Introduction by the Associate Editor

My engineering colleague, Karl-Arne Markström of the Swedish URSI committee, and I want to present an 80-year-old innovation for a very relevant application of today, made by two persons outside of the radio-science community. One of them can definitively be presented in "Women in Radio Science."

Some inventions have been made well ahead of their time and by the "wrong" people. Frequency-hopping spread spectrum is a very good example of this. Hedy Lamarr and George Antheil were professionals in show business, but they both had intellectual capacity, knowledge, and experiences that enabled them to think outside the box in order to be able to contribute to solve the problem of secret communications. Their still quite mechanical method, which is described below by Karl-Arne, required some advances in technology development in order to fulfill its potential in relation to Wi-Fi and Bluetooth applications of today.

Hedy Lamarr (Figure 1) was the artist's name of Hedwig Kiesler, born in Vienna in 1914. From when she was a young girl, she wanted to be an actress. She succeeded in her goal, becoming a famous movie star in Europe. Thanks to the #metoo movement, we recently have come to understand that young women are very vulnerable in the film industry. In the 1930s, a marriage hopefully gave some protection against such abuse. When she was very young, Hedy married Fritz Mandl, a rich arms manufacturer in Austria. While participating as a companion in Mandl's business meetings, she got a good insight into military technology.

In the late 1930s, Hedy moved to Hollywood, since her Jewish background made her life insecure in Europe. Both her professional and private life was spectacular in a way that we today would not react so much to. Hedy was also interested in science and technological development, which did not fit so well with the 1940s image of a female movie star, who was expected to concentrate on being attractive.

George Antheil was born in 1900 in an industrial district of Trenton, New Jersey. He was a vivid child and loved to play piano. He was very talented and became a popular concert pianist, composer, and author, active in Berlin, Paris, and Hollywood. He composed both symphonies and film music. The experiments for his most famous composition, "Ballet Mécanique," to synchronize many self-playing pianos gave him useful experience for the coming innovation.

Hedy Lamarr and George Antheil were not the most obvious inventors. They were both famous for something else: being hard-working people and having a good chemistry between them. Hedy was especially concerned about what was happening in her former homeland after

Figure 1. A photograph of Hedy Lamarr for the film, *The Heavenly Body*.

Hitler's takeover. From her time with arms dealer Mandl, she knew how torpedoes worked, and George had experience about the synchronization problem. When the need for secret communications became an urgent issue, Hedy and George started to brainstorm on how to solve the problem.

Their approach could be described as multidisciplinary, due to their different competences. They employed both a university professor in Electrical Engineering from Caltech, and the attorney firm of Lyon and Lyon, which specialized in patents, to produce a very competent patent for the "Secret Communication System" [1]. At the same time, they probably stepped into somebody else's territory.

Walters [1] referred to an event during the war where a commanding officer in the US Navy rejected the use of the patent and caricatures it when he learned who was behind it. To the contrary, some ten years later, when the US Navy contracted the design of a secure sonobuoy system from the Hoffman Corporation, a copy of the patent was provided. The person in charge at Hoffman assumed that "it was existing secret technology devised by some clever electrical engineer working under a Navy contract" [1].

Hedy passed away in the year 2000, and George in 1959, both unfortunately before the time when the full potential of their innovation could be realized. In 2014, they were inducted into the National Invertors Hall of Fame, which honors the people responsible for the great technological advances that make human, social, and economic progress possible.

Reference

1. R. Walters, *Spread Spectrum: Hedy Lamarr and the Mobile Phone*, www.robsbookshop.com, 2014.

The Invention by Hedy Lamarr and George Antheil of Frequency-Hopping Spread-Spectrum Secret Communications

Karl-Arne Markström

AFRY Digital Solutions AB
SE-169 99 Stockholm, Sweden
E-mail: karl-arne.markstrom@afry.com

Already before WW1, the general principles of using frequency agility to avoid detection and jamming had been proposed and actually used on a small scale. However, the limitations of the radio transmitters and receivers of the day made it impractical to implement systems that rapidly changed frequencies on a larger scale.

Remote-controlled flying bombs, torpedoes, and other unmanned craft were a common discussion topic in military circles during the pre-WW2 years, and some radical thinkers predicted their use in a coming war. However, a common concern was the relative ease of jamming or sending false remote-control signals to such weapons, which made the "Powers That Be" somewhat skeptical about their introduction and use. It was in this context that the invention by Lamarr and Antheil can be seen. When their application for US Patent 2,292,387, "Secret Communication System," was filed in June 1941, war had been raging in Europe for almost two years, and many saw it as only a matter of time before the United States was to be drawn into the conflict in one way or another.

Hedy Lamarr had befriended Howard Hughes, famous aviator and film mogul, who had a keen interest in technology and introduced her to commonly discussed matters of the day. It is very likely that she became part of discussions about "secret weapons," and she decided to make a contribution.

Here enters the musical – more specifically, pianist – background of George Antheil. The self-playing piano was an early example of a "programmable mechanism," somewhat in line with the punch-card-programmable Jacquard loom, and in a broader context, the Babbage "Analytical Engine." Punch cards had also been used for decades for accounting and tabulating-machine purposes.

They applied the principle behind the sequential generation of piano notes from a punched tape to the similar problem of generating and receiving radio frequencies in a pattern that was generated by hole patterns. In the proposed system, the number of frequencies in the table was 88, coincidentally the number of keys on a piano. This made it possible to transmit information that in their proposed system was encoded as audio tones of different frequencies, which in turn were sent and received using seemingly randomly selected carrier frequencies. A major problem in such a system was time synchronization. It is essential that the sequences at each end of the circuit accurately match each other for the whole duration of the mission. If the sequences start to drift apart, the transmissions soon become impossible to decode. In the system described in their patent application, the problem was addressed using a synchronization pulse between the transmitter and receiver at the start of the mission, and by then having accurately controlled speeds of the tape mechanisms at both ends of the circuit.

Unfortunately, the "state-of-the-art" of radio and electronics technology in 1941 did not make large-scale implementations of such systems practical, especially considering the reliability problems of vacuum-tube technologies on small and fast-moving platforms. It took until the introduction of solid-state technologies some 20 years later before their innovation could be implemented on a practical scale, starting with secure military communications. The abilities in counter-fading and narrow-band interference later made frequency-hopping spread spectrum (FHSS) one of the essential parts of high-capacity wireless data-transfer systems. Reliable synchronization was ultimately achieved by extracting the receiver's clock frequency and phase from the received data patterns.

The principles behind FHSS are remarkably unchanged from the 1941 invention, but it is the means and methods of their implementation that have changed. Current large-scale implementations include the Bluetooth and Wi-Fi signaling protocols, where frequency hopping is used to mitigate external and inter-system interference, and to avoid steady-state fading issues. The signaling scheme used in Wi-Fi (the original IEEE 802.11 specification) relies on dividing the spectrum in up to 14 overlapping channels in the 2400 MHz ISM band, spaced by 5 MHz, and to use a pseudo-random hop pattern to select the frequency to use at each instant. Use of forward error-correction (FEC) codes to detect and correct errors, and also retransmission of data (ARQ) that has been corrupted on another frequency that is not interfered with, makes the system quite resistant to narrow-band interference. A similar scheme is used in the Bluetooth standard.

IEEE RADIO 2019

The 2019 edition of the international conference, IEEE Radio and Antenna Days of the Indian Ocean (IEEE RADIO 2019), was hosted in Reunion Island for the second time. This seventh edition of the conference was held from September 23 to 26, 2019, at the Lux Resort & Hotel, Saint-Gilles Les Bain. The conference was managed by the Radio Society (Mauritius) and financially sponsored by the IEEE Antennas and Propagation Society (AP-S). Région Réunion financially supported the conference, and the Union Radio Scientifique Internationale (URSI) provided technical co-sponsorship. The Local Organizing Committee consisted of researchers from Centrale Supélec, France, the University of Mauritius, and the University of Reunion Island.

IEEE RADIO 2019 was attended by participants from about twenty different countries (Figure 1). The conference featured a tutorial on the design of radio amateur networks, followed by presentations of radio amateur activities in Mauritius and Reunion Island. Projects related to humanitarian activities were discussed during a special session organized by the IEEE Special Interest Group on Humanitarian Technology (SIGHT) Indian Ocean. Two workshops, open to all the participants of the conference, were organized in conjunction with the conference. The first workshop addressed measurements and simulations for industrial applications and development of standards. The second workshop was dedicated to the CARERC (Cartographie Electromagnétique par Réseaux de Capteurs) project that was undertaken by colleagues at the University of Reunion Island during past years. The regular sessions covered topics such antenna design, bioelectromagnetics, devices and circuits, wireless communication, and tracking systems. Three internationally recognized scientists delivered invited talks during the conference.

The oral presentations of students and young scientists were evaluated by a jury. A shield and a cash prize of 300 Euros were awarded to the best young scientist less than 36 years old. The presenters of the First, Second, and Third Best Student Papers were awarded shields and cash prizes of 300 Euros, 200 Euros, and 100 Euros, respectively (Figure 2). The AP-S sponsored Industrial Engineering Paper Award, consisting of a shield and a cash prize of 300 Euros, was presented to the author of the paper presenting the most innovative and significant contribution in terms of practical industrial engineering related to the fields of antennas, electromagnetics, and propagation.

Following the COVID-19 outbreak, the organizing committee decided to cancel the 2020 edition of the RADIO international conference.

Vikass Monebhurrun
General Chair, IEEE RADIO 2019
E-mail: vikass.monebhurrun@centralesupelec.fr

Figure 1. A group photo of RADIO 2019 attendees on Monday, September 23, 2019.

Figure 2. The recipients of the awards presented on Thursday, September 26, 2019.

URSI Accounts 2019

Introduction by the URSI Secretary General

URSI traditionally gets its income from the Member Committees contributing in line with their "unit of contribution" and in line with their impact in Council. Over the past few years, efforts have also been made to explore possible new resources from meetings through the creation of yearly URSI Flagship meetings. These Flagship meetings constitute, in a three-year cycle, the URSI General Assembly and Scientific Symposium (GASS), the Atlantic Radio Science Conference (AT-RASC) and the Asia-Pacific Radio Science Conference (AP-RASC). This has been very successful from a scientific point of view and encouraging from a financial point of view. The current worldwide travel restrictions in view of the COVID-19 pandemic will force URSI, just as other organizations, to re-consider the concept used for these meetings and conferences. Once considered as "to remain forever", these scientific conferences, being one of the cornerstones of URSI activities in bringing researchers, young scientists, and experts together in a multidisciplinary way from all over the world to interact, discuss and plan future activities, have now disappeared and have to be re-invented in a "corona-proof" concept.

URSI will need to be creative in setting up initiatives and further increase its efforts to stimulate and encourage interaction, collaboration and networking across different disciplines in the field of radio science. It can rely on some other initiatives already taken in the past, such as the establishment of the Individual Membership and a new publication, the *URSI Radio Science Letters*, which already successfully took off in its first year of operation. However, these initiatives consume part of the assets accumulated over many years. URSI has indeed accumulated substantial reserves in the past, allowing us to invest, but as the current pandemic illustrates, this should be handled with great care and cautiousness, to not compromise the long-term future of URSI.

As you may realize from the balance shown below, there seems to be a substantial increase in the assets of URSI comparing 2019 with the previous years. However, this is only the result of the fact that in the accounts the value booked is the value at the moment of purchase, not the market value. During 2019, some old investments were sold and reinvested, resulting in the fact that now in the accounts, the value of these assets has been actualized. The market value of all of the URSI investments is always included in this overview to clarify this situation, and from this overview in market value one realizes that the new initiatives taken have consumed some part of the URSI investments.

Besides the need to carefully take care of the financial aspect in running an organization such as URSI, it is also necessary to stress the tremendous amount of voluntary work done by all the URSI officers, Commission representatives and individuals within the URSI community supporting URSI. This commitment of our scientific community to URSI is crucial in the success of URSI and cannot be underestimated. It remains to be said that only thanks to this commitment, URSI is still in a financially healthy situation and able to perform its main objective: attracting researchers, with emphasis on young researchers, to careers in radio science, helping them successfully launch their careers, giving them the opportunity to present their work and facilitating their participation in a free exchange of scientific results in a worldwide community of radio scientists.

Prof. Peter Van Dale
Secretary General of URSI

BALANCE SHEET: 31 DECEMBER 2019

		EURO	EURO
ASSETS			
Installations, Machines & Equipment			1,316.91
Dollars			
BNP Paribas (USD)		118.98	
BNP paribas (CAD)		0.00	
			118.98
Euros			
Banque Degroof	0.00		
BNP Paribas zichtrekening	127,791.04		
BNP Paribas spaarrekening	692.87		
BNP Paribas portefeuillerekening (001-02)	117,415.44		
BNP Paribas portefeuillerekening (001-84)	0,57		
Paypal	691.32		
			246,591.24
Investments			
DPAM Bonds EMU (formerly Demeter Sicav Shares)	0.00		
Rorento Units	0.00		
DPAM MML MON (formerly Aqua Sicav)	0.00		
Bonds	1.068,197.46		
			1.068,197.46
673 Rorento units on behalf of van der Pol Fund	11,833.55		
			1.080,031.01
Petty Cash			208.39
Total Assets			1,328,266.53
Less Creditors			
IUCAF	36,783.12		
ISES	5,053.53		
			(41,836.65)
Balthasar van der Pol Medal Fund			(11,833.55)
Basu Medal Fund			(4,216.35)
Paid Remuneration			7,522.80
NET TOTAL OF URSI ASSETS			**1,277,902.78**

The net URSI Assets are represented by:	EURO	EURO
Closure of Secretariat		
Provision for Closure of Secretariat		120,000.00
Scientific Activities Fund		
Scientific Activities in 2019	60,000.00	
Routine Meetings in 2019	20,000.00	
Publications/Website in 2019	40,000.00	
Young Scientists in 2019	0.00	
Administration Fund in 2019	105,000.00	
I.C.S.U./I.S.C. Dues in 2019	6,000.00	
		231,000.00

Flagship Meetings		
GASS 2017 - Montreal	0.00	
GASS 2020 - Rome	180,000.00	
AT-RASC - Gran Canaria (2021)	60,000.00	
AP-RASC - Sydney (2022)	10,000.00	
Total allocated URSI Assets	601,000.00	
Unallocated Reserve Fund	676,902.78	
		1.277,902.78

Statement of Income and expenditure for the year ended 31 December 2019

I. INCOME

Contributions from National Members (year -1)	21,563.50	
Contributions from National Members (year)	189,725.00	
Contributions from National Members (year +1)	24,725.00	
Income General Assembly 2017/2020	1500.00	
Income AT-RASC 2015/2018	0.00	
Income AP-RASC 2019	0.00	
Support Conf Organization - ECIO	1500.00	
Support Conf. Organization - BSS	1000.00	
Support Conf Organization - Benelux Forum	2100.00	
Sales of Publications, Royalties	0.00	
Bank Interest	0.00	
Other Income	753.800.62	
Total Income		**995,914.12**

II. EXPENDITURE

A1) Scientific Activities		105,351.88
General Assembly 2014/2017	8,870.92	
Mid Term Meetings 2015	0.00	
AT-RASC	6,759.66	
AP-RASC	51,797.23	
Support Conf. Organization	9,611.79	
Scientific Meetings: Symposia/Colloquia	25,300.00	
Representation at Scientific Meetings	3,012.28	
Other	0.00	
A2) Routine Meetings		39.431.58
Bureau/Executive committee	39,431.58	
Other	0.00	
A3) Publications		33,641.84
B) Other Activities		5,897.00
Contribution to ICSU/I.S.C. (2019)	3,897.00	
Contribution to other ICSU bodies/I.S.C. bodies	2,000.00	
C) Administrative Expenses		221,349.24
Salaries, Related Charges	116,567.31	
General Office Expenses	2,096.23	
Travel and representation	3,971.52	
Insurances/Communication/Gifts	7,649.34	
Office Equipment	0.00	
Accountancy/Audit Fees	8,410.66	
Bank Charges/Taxes	81,377.26	
Depreciation	1,316.92	
Loss on Investments (realised/unrealised)		
Total Expenditure:		**405,671.54**

Excess of Expenditure over Income		590,242.58
Currency translation diff. (USD => EURO) - Bank Accounts		(1,669.26)
Currency translation diff. (USD => EURO) - Investments		0.00
Currency translation diff. (USD => EURO) - Others		0.00
Accumulated Balance at 1 January 2019		689,329.46
		1.277,902.78

Rates of exchange

January 1, 2019	1 USD = 0.8737 EUR	
December 31, 2019	1 USD = 0.8915 EUR	1 CAD = 0.6849 EUR

Balthasar van der Pol Fund

652 Robeco Global (formerly Rorento Shares) : market value on December 31	
(Aquisition Value: USD 14,175.00/EUR 11,833,55)	37,457.40

Book Value on December 31, 2019/2018/2017/2016	11,833.55

Market Value of investments on December 31, 2019-2014

DPAM EMU (formerly Demeter Sicav Shares)	0.00
Robeco Global (formerly Rorento Units) (1)	0.00
DPAM MML MON (formerly Aqua-Sicav)	0.00
Bonds	1.068,197.46
	1.068,197.46

Book Value on December 31, 2019/2018/2017/2016/2015/2014	1.080,031.01

(1) Including the 652 Rorento Shares of v d Pol Fund

APPENDIX : Detail of Income and Expenditure

I. INCOME

Other Income		
Young scientist support (Japan)	0.00	
Income bonds	753,800.62	
Other	0.00	
		753,800.62

II . EXPENDITURE

General Assembly 2017/2020		
Organisation	8,870.92	
Vanderpol Medal	0.00	
Basu Award	0.00	
President's Award	0.00	
Young scientists	0.00	
Expenses officials	0.00	
Support Commissions	0.00	
		8,870.92
AT-RASC		
Organisation	6,759.66	
Young Scientists	0.00	
Expenses Officials	0.00	
Support Commissions	0.00	
		6,759.66

AP-RASC		
Organisation	11,387.52	
Young Scientists	0.00	
Expenses Officials	15,076.11	
Support Commissions	25,333.60	
		51,797.23
Support Conference Organization		
ECOC	7,893.04	
Benelux Forum	1,718.75	
		9,611.79
Routine Meetings		
Board Meeting	39,431.58	
		39,431.58
Symposia/Colloquia/Working Groups		
Commission A	0.00	
Commission B	13,300.00	
Commission C	0.00	
Commission D	0.00	
Commission E	0.00	
Commission F	0.00	
Commission G	5,000.00	
Commission H	0.00	
Commission J	3,000.00	
Commission K	0.00	
Central Fund	0.00	
Central Fund (Student Award MC)	4,000.00	
		25,300.00
Contribution to other ICSU bodies		
IUCAF	2,000.00	
		2,000.00
Publications		
Publications/Website	33,641.84	
		33,641.84

THE CONFERENCE

EuCAP is Europe's largest and most significant antennas and propagation conference attracting more than 1400 participants from academia and industry, and more than 50 industrial exhibitors, from all over the world. It is a great forum for exchange of new technical-scientific achievements, for demonstrating state-of-the-art technology, and for establishing and strengthening professional networks.

The 2021 host country Germany has a strong antennas and propagation community both in academia and industry. Moreover, antennas and propagation play a central role in the current transition of Germany's strong automotive industry towards digitally connected cars and autonomous driving. Finally, many cellular operators and telecommunications equipment vendors have large branches and even headquarters in the host city Düsseldorf and the Rhine-Ruhr-Area, leading the development of 5G. Therefore, EuCAP 2021 will be a unique place to strengthen the link between the scientific antennas and propagation community and the automotive as well as the 5G industry.

INFORMATION FOR AUTHORS

Authors are invited to submit papers online with a minimum length of two and a maximum length of five A4 pages. The paper must contain enough information for the Technical Programme Committee and reviewers to assess the quality of the work in a single acceptance/ rejection review process. It will be possible to revise accepted papers in line with the reviewers' comments.

Submit your paper online at www.eucap2021.org no later than 16 October 2020. The submission requires an EDAS® account, which is free.

Presented papers will be included in IEEE Xplore, if the authors choose this option during the submission process. Compliance to the IEEE format is mandatory in this case.

IET AND EuMA

Authors can apply for publication in a special issue of either Microwaves, Antennas & Propagation (IET) or International Journal of Microwave and Wireless Technologies (EuMA) during the submission process.

IMPORTANT DATES

Deadline	16 October 2020
Notification	22 December 2020
Revised paper	5 February 2021

FIRM DEADLINE

For EuCAP 2021, there will be no extension of the paper submission deadline; late or updated submissions will not be accommodated after the deadline.

www.eucap2021.org

Organized by

Spupported by

URSI Conference Calendar

A detailed list of meetings is available on the URSI website at http://www.ursi.org/events.php

March 2020

URSI-France Workshop : Future Networks: 5G and beyond
Palaiseau, France, 11-13 March 2020
Contact: Prof. Alain Sibille, Telecom Paris, E-mail : alain.sibille@telecom-paris.fr
http://ursi-france.telecom-paristech.fr/evenements/journees-scientifiques/2020/2020-en.html

The 2020 e-Workshop on Instrumentation and Calibration in Radio Astronomy
will be held "virtually" on 26 March 2020
This will be an e-Workshop hosted at two sites (Stellenbosch, South Africa and Eindhoven, Netherlands), connected via video link. The aim of the workshop is to have a cost-effective way to give students the opportunity to present their work and make connections with an international audience.
Contact: Dr. Jacki Gilmore, E-mail : ackivdm@sun.ac.za

July 2020

2020 APS-URSI
2020 IEEE AP-S Symposium on Antennas and Propagation and CNC/USNC-URSI joint meeting
virtually held on 5-10 July 2020
Contact: General Chair: Ahmed Kishk, E-mail: ahmed.kishk@concordia.ca; General Co-Chairs: Lot Shafai, lot.shafai@umanitoba.ca , David G. Michelson, davem@ece.ubc.ca , Yahia M. M. Antar, antar-y@rmc.ca
https://2020apsursi.org/

August 2020

ICEAA - IEEE APWC 2020
The twenty-second edition of the International Conference on Electromagnetics in Advanced Applications
Honolulu, Hawaii, USA, originally 10-14 August 2020, is being postponed
Contact: Mrs. Manuela Trinchero SELENE Srl - Eventi e Congressi, Via Medici 23 10143 Torino, Italy, Tel: +39-011-7499601, Fax: +39-011-7499576, E-mail: iceaa@seleneweb.com or iceaa20@iceaa.polito.it ; Scientific Secretariat: Prof. Guido Lombardi, Politecnico di Torino, E-mail: iceaa20@iceaa-offshore.org
https://www.iceaa-offshore.org/j3

URSI GASS 2020
virtually held on 28 August – 4 September 2021
Contact: URSI Secretariat, Ghent University – INTEC, Technologiepark-Zwijnaarde 126, B-9052 Gent, Belgium, E-mail gass@ursi.org, Website: http://www.ursi2021.org, http://www.ursi.org/young_scientists.php#tab-section3 (link to all the Young Scientist abstracts and presentations) http://www.ursi.org/student_paper_competitions.php (link to the GASS 2020 Student Paper Competition with abstracts and list of finalists)

September 2020

URSI 2020 Spain
35th National Symposium of URSI in Spain
Malaga, Spain, 2-4 September 2020
Contact : https://www.conftool.net/ursi2020/index.php?page=browseSessions&print=export

NRSC2020 - 37th National Radio Science Conference
Annual meeting of the Egyptian URSI Committee
Cairo, Egypt, 8 - 10 September 2020
Contact: Prof. Rowayda A. Sadek, Secretary, URSI- Egypt National Radio Science Committee, Faculty of Computers and Information Technology, Helwan University, Helwan, Egypt, E-mail: Rowayda_sadek@yahoo.com , Rowayda_sadek@fci.helwan.edu.eg
https://nrsc2020.guc.edu.eg

6th A.P. Mitra Memorial Lecture
Online annual lecture event to remember Dr. A.P. Mitra
New Delhi, India, 16 September 2020
Contact: Dr. Amitava Sengupta, E-mail : sengupta53@yahoo.com, Website: https://indianradio.webex.com/indianradio/j.php?MTID=m177dbc74a693dbcfdf5910a28221e7b9

Kleinheubacher Tagung 2020
Annual meeting German URSI committee
Miltenberg, Germany, 28 - 30 September 2020
Contact: Prof. Dr. Madhu Chandra, Chair of High-Frequency Engineering and Electromagnetic Theory, Faculty of Electrical Engineering and Information Technology, Chemnitz University of Technology, E-Mail: kht2020@etit.tu-chemnitz.de, http://www.kh2020.de

Metamaterials 2020
Fourteenth International Congress on Artificial Materials for Novel Wave Phenomena
New York, NY, USA, 28 September – 3 October 2020 (in an online format)
Contact : E-mail: contact@metamorphose-vi.org
https://congress.metamorphose-vi.org/index.php/8-general-information/1-metamaterials-20161

November 2020

9th VERSIM workshop
Kyoto, Japan, 21-25 November 2020
Contact: Prof. Y. Omura, http://pcwave.rish.kyoto-u.ac.jp/versim/

December 2020

ECOC 2020
European Conference on Optical Communications
Brussels, Belgium, 6-10 December 2020
Contact: Prof. P. Van Daele, E-mail: E-mail: info@ecoc2020.org, Website : https://ecoco2020.org/

January 2021

USNC-URSI NRSM 2021
USNC-URSI National Radio Science Meeting
Virtual meeting on 4-9 January 2021
Contact: Dr. Sembiam R. Rengarajan, Department of ECE, California State University, Northridge, CA 91330-8346, USA, Fax: 818-677-7062, E-mail: srengarajan@csun.edu; Logistics: Christina Patarino, E-mail: christina.patarino@colorado.edu, Fax: 303-492-5959, Website: https://www.nrsmboulder.org/

EuMW 2021
European Microwave Week 2020
Utrecht, the Netherlands, 10-15 January 2021
Contact: E-mail: headquarters@eumwa.org, https://www.eumweek.com/

ISAP 2021
International Symposium on Antennas and Propagation
Osaka, Japan, 25-28 January 2021
Contact : Prof. Hiroyuki Arai: General Chair of ISAP 2020 Yokohama National University, Japan, ap_ac-isap2020@mail.ieice.org, Website: http://isap2020.org/

COSPAR 2021
43rd Scientific Assembly of the Committee on Space Research (COSPAR) and Associated Events
Sydney, Australia, 28 January – 4 February 2021
Contact : COSPAR Secretariat, 2 place Maurice Quentin, 75039 Paris Cedex 01, France, Tel: +33 1 44 76 75 10, Fax: +33 1 44 76 74 37, E-mail: cospar@cosparhq.cnes.fr http://www.cospar2021.org March

March 2021

EuCAP 2021
15th European Conference on Antennas and Propagation
Düsseldorf, Germany, 22 - 26 March 2021
Contact : Thomas Kürner, info@eucap2021.org, Website: https://www.eucap.org/conference/news-23092019

August 2021

URSI GASS 2021
Rome, Italy, August 28 -September 4, 2021
Contact: URSI Secretariat, Ghent University – INTEC, Technologiepark-Zwijnaarde 126, B-9052 Gent, Belgium, E-mail gass@ursi.org, Website: http://www.ursi2021.org/

October 2021

ISAP 2021
International Symposium on Antennas and Propagation
Taipei, Taiwan, 19-22 October 2021
Contact : http://www.isap2021.org/

May 2022

AT-RASC 2022
Third URSI Atlantic Radio Science Conference
Gran Canaria, Spain, 30 May - 4 June 2022
Contact: Prof. Peter Van Daele, URSI Secretariat, Ghent University – INTEC, Technologiepark-Zwijnaarde 126, B-9052 Gent, Belgium, E-mail: peter.vandaele@ugent.be http://www.at-rasc.com

August 2022

AP-RASC 2022
Asia-Pacific Radio Science Conference 2022
Sydney, Australia, 21-25 August 2022
Contact: URSI Secretariat, Ghent University – INTEC, Technologiepark-Zwijnaarde 126, B-9052 Gent, Belgium, E-mail: info@ursi.org

Information for Authors

Content

The *Radio Science Bulletin* is published four times per year by the Radio Science Press on behalf of URSI, the International Union of Radio Science. The content of the *Bulletin* falls into three categories: peer-reviewed scientific papers, correspondence items (short technical notes, letters to the editor, reports on meetings, and reviews), and general and administrative information issued by the URSI Secretariat. Scientific papers may be invited (such as papers in the *Reviews of Radio Science* series, from the Commissions of URSI) or contributed. Papers may include original contributions, but should preferably also be of a sufficiently tutorial or review nature to be of interest to a wide range of radio scientists. The *Radio Science Bulletin* is indexed and abstracted by INSPEC.

Scientific papers are subjected to peer review. The content should be original and should not duplicate information or material that has been previously published (if use is made of previously published material, this must be identified to the Editor at the time of submission). Submission of a manuscript constitutes an implicit statement by the author(s) that it has not been submitted, accepted for publication, published, or copyrighted elsewhere, unless stated differently by the author(s) at time of submission. Accepted material will not be returned unless requested by the author(s) at time of submission.

Submissions

Material submitted for publication in the scientific section of the *Bulletin* should be addressed to the Editor, whereas administrative material is handled directly with the Secretariat. Submission in electronic format according to the instructions below is preferred. There are typically no page charges for contributions following the guidelines. No free reprints are provided.

Style and Format

There are no set limits on the length of papers, but they typically range from three to 15 published pages including figures. The official languages of URSI are French and English: contributions in either language are acceptable. No specific style for the manuscript is required as the final layout of the material is done by the URSI Secretariat. Manuscripts should generally be prepared in one column for printing on one side of the paper, with as little use of automatic formatting features of word processors as possible. A complete style guide for the *Reviews of Radio Science* can be downloaded from http://www.ips.gov.au/IPSHosted/NCRS/reviews/. The style instructions in this can be followed for all other *Bulletin* contributions, as well. The name, affiliation, address, telephone and fax numbers, and e-mail address for all authors must be included with

All papers accepted for publication are subject to editing to provide uniformity of style and clarity of language. The publication schedule does not usually permit providing galleys to the author.

Figure captions should be on a separate page in proper style; see the above guide or any issue for examples. All lettering on figures must be of sufficient size to be at least 9 pt in size after reduction to column width. Each illustration should be identified on the back or at the bottom of the sheet with the figure number and name of author(s). If possible, the figures should also be provided in electronic format. TIF is preferred, although other formats are possible as well: please contact the Editor. Electronic versions of figures *must* be of sufficient resolution to permit good quality in print. As a rough guideline, when sized to column width, line art should have a minimum resolution of 300 dpi; color photographs should have a minimum resolution of 150 dpi with a color depth of 24 bits. 72 dpi images intended for the Web are generally *not* acceptable. Contact the Editor for further information.

Electronic Submission

A version of Microsoft *Word* is the preferred format for submissions. Submissions in versions of T_EX can be accepted in some circumstances: please contact the Editor before submitting. *A paper copy of all electronic submissions must be mailed to the Editor, including originals of all figures.* Please do *not* include figures in the same file as the text of a contribution. Electronic files can be send to the Editor in three ways: (1) By sending a floppy diskette or CD-R; (2) By attachment to an e-mail message to the Editor (the maximum size for attachments *after* MIME encoding is about 7 MB); (3) By e-mailing the Editor instructions for downloading the material from an ftp site.

Review Process

The review process usually requires about three months. Authors may be asked to modify the manuscript if it is not accepted in its original form. The elapsed time between receipt of a manuscript and publication is usually less than twelve months.

Copyright

Submission of a contribution to the *Radio Science Bulletin* will be interpreted as assignment and release of copyright and any and all other rights to the Radio Science Press, acting as agent and trustee for URSI. Submission for publication implicitly indicates the author(s) agreement with such assignment, and certification that publication will not violate any other copyrights or other rights associated with the submitted material.

Become An Individual Member of URSI

The URSI Board of Officers is pleased to announce the establishment of categories of individual membership of URSI. The purpose of individual membership of URSI is to secure professional recognition of individual radio scientists and to establish their better connection with the URSI Board of Officers, Scientific Commissions, and URSI Member Committees. Three categories of individual membership (URSI Corresponding Member, URSI Senior Member and URSI Fellow) have been established.

URSI Corresponding Membership is the first step into the URSI community and provides:

- Access to the proceedings of URSI Flagship Conferences via the Web site
- Notifications of new editions of URSI publications.

In addition, URSI Senior Members and URSI Fellows benefit from the following:

- Reduced registration fees at URSI Flagship Meetings.
- Reduced registration fees at some meetings organized by partnering organizations such as (but not limited to) IEEE AP-S and EuCAP.
- A page charge reduction from 175 USD to 150 USD for papers published in the URSI journal, *Radio Science Letters*.
- An invitation to receive their individual membership certificate at an URSI Flagship meeting.

Fellowship is by invitation only; Senior Membership can be by invitation or application. Corresponding Membership is a streamlined, instant process. Details, and an online application for URSI Senior Membership, are available at http://www.ursi.org/membership.php#tab-sectionA1.